CSIRO
AUSTRALIA

CRC SHM

A Comparison of Modelled Responses to Prescribed CO_2 Sources

P.J. Rayner and R.M. Law

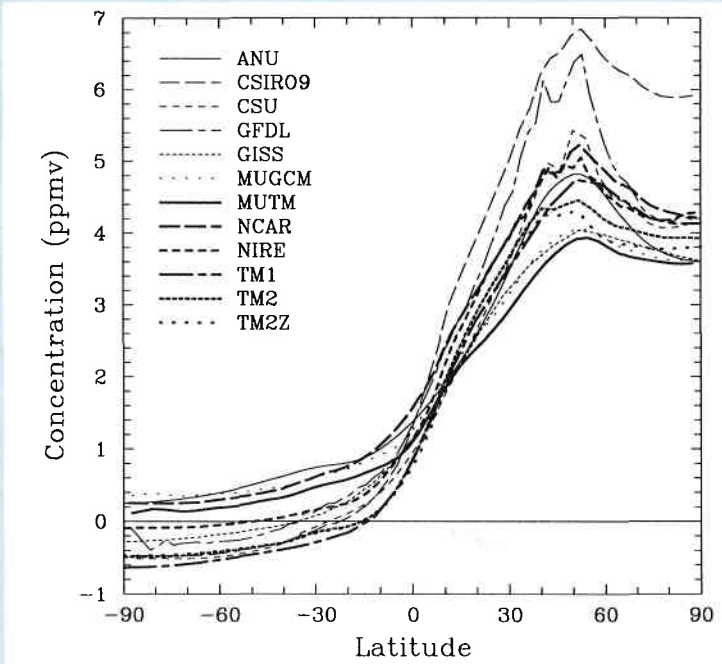

CSIRO DIVISION OF ATMOSPHERIC RESEARCH TECHNICAL PAPER NO. 36
COOPERATIVE RESEARCH CENTRE FOR SOUTHERN HEMISPHERE METEOROLOGY TECHNICAL REPORT NO. 1

CSIRO
AUSTRALIA

CRC SHM

A Comparison of Modelled Responses to Prescribed CO_2 Sources

P.J. Rayner and R.M. Law

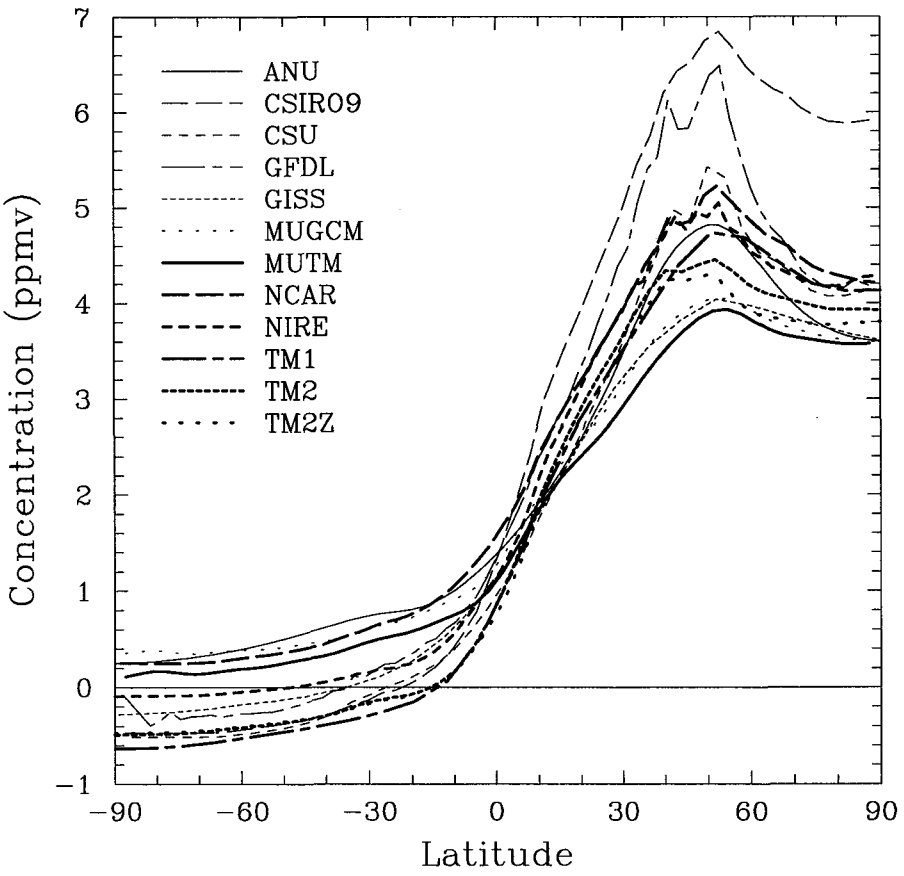

CSIRO DIVISION OF ATMOSPHERIC RESEARCH TECHNICAL PAPER NO. 36
COOPERATIVE RESEARCH CENTRE FOR SOUTHERN HEMISPHERE METEOROLOGY TECHNICAL REPORT NO. 1

National Library of Australia Cataloguing-in-Publication Entry

Rayner, Peter J.
A Comparison of Modelled Responses to Prescribed CO_2 Sources

Bibliography.
ISBN 0 643 05605 X

1. Atmospheric carbon dioxide - Mathematical models. 2. Carbon cycle (Biogeochemistry) - Mathematical models. I. Law, Rachel Mary. II. CSIRO. Division of Atmospheric Research. III. Cooperative Research Centre for Southern Hemisphere Meteorology. IV. Title. (Series : CSIRO Division of Atmospheric Research technical paper ; no. 36 (Series : Cooperative Research Centre for Southern Hemisphere Meteorology technical report ; no. 1).

Cover illustration: Zonal annual surface mean concentration in ppmv due to fossil fuel emissions for each of the participating models.

This study was carried out with support from the Australian Government Cooperative Research Centres Programme

A Comparison of Modelled Responses to Prescribed CO_2 Sources

P.J. Rayner and R.M. Law
Cooperative Research Centre for Southern Hemisphere Meteorology

Sources, model calculations and descriptions contributed by:

A.S. Denning[1], D. Erickson[2], I.Y. Fung[3], M. Heimann[4], R.M. Law[5], S.C. Piper[6], M. Ramonet[7], P.J. Rayner[5], S. Taguchi[8], J.A. Taylor[9], C.M. Trudinger[10], I.G. Watterson[10]

1. Department of Atmospheric Science, Colorado State University, Fort Collins, CO 80523, USA
2. National Center for Atmospheric Research, P.O. Box 3000, Boulder, CO 80307, USA
3. Centre for Earth and Ocean Research, University of Victoria, PO Box 1700, Mail-stop 4015, Vic. B.C., V8W2Y2, Canada
4. Max Planck Institut für Meteorologie, Bundesstrasse 55, D-20146 Hamburg, Germany
5. CRC for Southern Hemisphere Meteorology, Monash University, Wellington Rd, Clayton 3168, Australia
6. Scripps Institution of Oceanography A-020, La Jolla, CA 92093-0220, USA
7. Centre des Faibles Radioactivites, Laboratoire Mixte CNRS/CEA, Avenue de la Terrasse, F-91198 Gif-sur-Yvette Cedex, France
8. National Institute for Resources and Environment, Environmental Assessment Division, 16-3, Onogawa Tsukuba Ibaraki 305, Japan
9. CRES, Australian National University, GPO Box 4, Canberra 0200, Australia
10. CSIRO Division of Atmospheric Research, PMB 1, Mordialloc 3195, Australia

A Comparison of Modelled Responses to Prescribed CO_2 Sources

Contents

Figures

A Comparison of Modelled Responses to Prescribed CO_2 Sources

P.J. Rayner and R.M. Law

Abstract

This report presents a summary of results from the intercomparison of modelled tracer distributions resulting from a series of prescribed sources. The chosen sources are most relevant to simulation of the structure of atmospheric CO_2. The sources are representations of the annual mean input of CO_2 due to fossil fuel combustion and cement production and the seasonal fluxes associated with the action of terrestrial biota.

Twelve different three-dimensional atmospheric tracer transport models have been used in this intercomparison. The models include both online and offline types and use a variety of advection algorithms and sub-grid scale parameterisations. A range of model resolutions is also represented.

The modelled distributions show a large range of responses. For the fossil fuel source, the annual mean large-scale north-south gradient at the surface varies by a factor of two. This suggests a factor of two variation in the efficiency of interhemispheric exchange. In the upper troposphere zonal mean gradients within the northern hemisphere vary in sign.

For the terrestrial biotic source, the structure of the amplitude of the seasonal cycle of CO_2 concentration at the surface is largely conditioned by the position of the sources. The amplitudes, however, vary similarly to the fossil case. The annual mean response to the seasonal source also shows large differences in magnitude.

We discuss the implications of these results for carbon budget studies and suggest some methods for reducing the apparent large uncertainties.

1 Introduction

There is little doubt that a major source of uncertainty in predictions of future climate change is the evolution of atmospheric greenhouse gas concentrations. For CO_2 (the major contributor to the enhanced greenhouse effect), the situation is complicated by the integration of CO_2 in a wide range of biogeochemical processes. Changes in any of these processes, whether as a result of CO_2 changes, climate change or other (possibly anthropogenic) forcings could considerably alter the time evolution of CO_2 concentrations.

In order to assess any changes in the controlling processes for CO_2 concentration it is necessary to be able to quantify their present magnitude. It is also necessary to understand the controlling processes themselves and to this end there has been considerable effort in local flux measurements e.g. Wofsy et al. (1993) and Takahashi et al. (1993).

There is a limitation on how much information is available from local measurements. Many of the biogeochemical processes controlling CO_2 concentration are temporally noisy and spatially inhomogeneous so that direct measurement is liable to serious sampling bias. Many of the critical regions (e.g. the high latitudes of the southern ocean) are also remote from any convenient measurements.

What is available is a record of atmospheric CO_2 concentrations at a range of sites around the world. This record consists of measurements of CO_2 mixing ratio in air samples primarily from remote locations. The record commences with the measurements of C.D. Keeling in 1957 at South Pole and 1958 at Mauna Loa (Keeling et al., 1995). Spatial coverage increased

gradually through the 1960s and 1970s then more rapidly through the 1980s and early 1990s. The record of this "background" CO_2 concentration has already contributed greatly to our knowledge of the current carbon system. The first and most important point is that the record establishes incontrovertibly that CO_2 concentrations are increasing.

The record has a range of other uses too. In particular, its spatial structure contains information about the spatial structure of sources and sinks of CO_2. This spatial information has been used in a number of studies, e.g. Keeling et al. (1989), Tans et al. (1990), Enting and Mansbridge (1991), Law et al. (1992), Enting et al. (1993, 1995) to infer some details of the steady-state sources and sinks at some resolution. More recently, Conway et al. (1994) have used the spatial and temporal structure of the record to infer the time evolution and variability of the spatial structure of sources and sinks.

Each of these studies is dependent on some model of CO_2 transport in the atmosphere. These models are typically validated using trace gases such as krypton-85, CFCs and radon (e.g. Prather et al., 1987, Jacob et al., 1987, Heimann and Keeling, 1989, Jacob and Prather, 1990). However, there are limited observations of these gases and some uncertainties in their source distributions so that any model assessment is limited. The CO_2 budget studies listed above produce a range of results. It is important that we understand how much variation in model transport contributes to the variation in budgets produced and how much is due to other factors.

As an example, consider the conclusions of Enting and Mansbridge (1989) and Tans et al. (1990). These authors suggested that, contrary to previous orthodoxy, an important term for closing the global CO_2 budget might well be the northern hemisphere terrestrial biota. In the context of this work, it is important to recapitulate how Tans et al. in particular, arrived at their result. Their approach was to choose a number of sources broken into various regions. These sources were adjusted until the CO_2 distribution resulting from their combined effect closely matched that observed. Their chief finding was that in order to produce the observed interhemispheric gradient of CO_2 they needed to postulate a significant sink in the northern hemisphere. The southern ocean sink implied by air-sea CO_2 concentration differences was sufficient to close the global budget without invoking an extra sink but exacerbated the mismatch due to the gradient.

The above argument is important since it shows how inferences about the global tracer budget are drawn from knowledge of the spatial structure. Another way of restating the result of Tans et al. is that, based on the results of their transport model, they believe the atmosphere incapable of transporting the CO_2 resulting from fossil fuel burning in the northern hemisphere to the regions of the southern ocean which would absorb it. Thus the CO_2 must be absorbed nearer the source. Northern hemisphere air-sea flux measurements indicate an insufficient ocean sink so the northern biota is postulated by elimination.

It is worth noting that the above budget was only one of several possible budgets postulated by Tans et al. This variety showed among other things that the atmospheric spatial structure was not a very strong constraint on the net source distribution.

Keeling et al. (1989) used a slightly different approach. Rather than using external physical information such as air-sea flux measurements, they used the distribution of ^{13}C to check their proposed source-sink distributions originally obtained from fitting CO_2 distributions and globally constrained using a box diffusion model. The difference in isotopic signature between ocean and biospheric sinks of CO_2 enabled them to check the differentiation of these two sinks using observed isotopic composition.

On the basis of these observations they proposed quite a different budget, with the

predominant sink in the northern hemisphere oceans. It is likely that the different results produced by these two studies were due to the different external data sets used rather than to the different transport characteristics of the models used. A more extensive understanding of the comparable behaviour of these models, as produced by this intercomparison, should allow us to determine the relative importance of transport differences more readily.

In a similar study, Taylor (1989), used a different atmospheric tracer transport model to relate some proposed source functions to the observed CO_2 distribution. Unlike the previous study, Taylor did not require an extra northern hemisphere sink in order to match the observed zonal distribution. This difference is explicable in terms of the different transport characteristics of the models involved.

Several other aspects of the results of inversion studies are at wide variance in the same way as the annual mean results quoted in the previous paragraphs. In particular, there is considerable variety in the representation of the seasonality of sources and concentrations in the northern hemisphere, the location of the dominant forcing of the seasonal cycle, namely the terrestrial biota. These differences raise the natural question as to their cause. Put another way, to what extent are the varying source estimates consistent given observational uncertainties and model-model differences.

In the language of inverse theory, the current concentrations are related to past sources by a linear transport operator. Note that 'concentrations' may represent more than CO_2 concentrations as in the work of Enting et al. (1995).

Given the spatially sparse network of observations the information which can be gleaned about net sources is necessarily limited. One important task of researchers in the field of source estimation is to quantify not only the current best guess as to the source magnitudes and distributions but also the level of our ignorance. This is necessary not only for policy formation but also for pinpointing areas in which estimates can be feasibly improved.

The problem of error analysis in inverse calculations of CO_2 source estimates has been approached by a number of authors. Enting et al. (1993, 1995) in their Bayesian synthesis approach used prior estimates of sources and optimal fits to data to produce estimates of final source strengths. A product of such analysis is also the error estimates. Ciais et al. (1995) used a bootstrap approach in which the sources were estimated by randomly excluding various observations and uncertainties determined by the range of sources obtained.

In all this the transport operator is taken as certain. This is assumed out of necessity rather than confidence. In the case of atmospheric transport models there is as yet no computationally feasible way of characterizing uncertainty. An aim of this report is to provide one piece of data to this end.

In the next section, we outline the methodology and choice of experiments we undertook along with a brief description of the range of participating models. A summary of the characteristics of the actual models in the experiment is left for appendix C. Sections 3 and 4 present a broad range of the results of the two experiments. Section 5 presents discussion and some suggestions for reducing the uncertainties exposed. Appendix A lists the formal experimental specification and appendix B gives details of electronic access to the full set of results, specifications and inputs.

2 Method

Elucidating the variation of those aspects of atmospheric transport which impact the distribution of CO_2 poses several problems in experimental design. Foremost among these difficulties is a trade-off between the general description of transport characteristics and the direct comparison of carbon cycle responses. The first of these choices would require some experiments with idealized artificial tracers or alternatively some experiments with known sources and concentration profiles in an attempt to calibrate large-scale transport. This is likely to be of more direct interest to the tracer modelling community.

For the round of experiments described in this report we have chosen, instead, to follow the second line of inquiry outlined above. There are several reasons for this choice, some good and some merely historical. The primary reason was that the main aim of the study was to describe and perhaps quantify those variations in regional carbon budget estimates which were due to differences among atmospheric transport models. It was inconceivable that this process would not suggest further work in trying to understand and perhaps reduce these differences but we viewed this as a later step.

Another reason was the use of pre-existing experiments. Some of the models used in the comparison are computationally expensive to the extent that it would have been difficult for some workers to justify an extra run for our purposes. However the experiments we used are a very common part of regional carbon budget estimation.

A third guiding principle was simplicity. Many of the penetrative analyses of transport such as those outlined by Fung et al. (1983) or Plumb and Mahlman (1987) require significant modification of the transport model itself. Similarly, while a direct comparison of atmospheric transport arising from the current concentration profile of CO_2 would also be enlightening, it is also a non-trivial modification to many models. Such estimates have been made by, e.g. Law et al. (1992) but by few others. There are also conceptual difficulties in applying the limited (essentially one-dimensional) observed data to three-dimensional models.

Given the above we chose to base our comparison, like that of Prather (1992) for CFCs, on simple and realistic sources and sinks of the tracer, in this case CO_2, and under reasonably simple conditions. Since our experiment was never intended as a calibration, our requirements were simpler than those of Prather. The formal experimental specification may be found in Appendix A.

2.1 Models used

The basic task of a tracer transport model is to take a given large-scale flow field and a tracer source and produce a time-evolving tracer distribution subject to advection by the flow field and by closures to represent unresolved processes. Given this relatively simple statement of the problem the variety of available approaches is perhaps surprising. The aim of this tracer model intercomparison (hereafter referred to as TRANSCOM) was to remove one source of variation by using a common source field. Even this cannot be precisely achieved since a given source field will be aggregated or interpolated differently onto different model grids.

The flow fields differ primarily in whether they are generated by a GCM running concurrently with the tracer transport solution (a so-called online model) or whether the model uses pre-existing data (offline calculations). The offline models can also be subdivided according to the source of their data. Some models use data from previous GCM runs while others use analyzed flow fields and at various data frequencies. One model uses a statistical

representation of sub bi-monthly wind variability.

There is a plethora of methods for handling the numerics of explicit advection of the tracer by the flow field. To describe these in detail is far beyond the scope of this report. They can be broadly divided into the categories of spectral, finite-difference, semi-Lagrangian and fully Lagrangian. A review of many of these methods is given in Rood (1987). Many models use different schemes for horizontal and vertical advection. The impact of the advection scheme used is expected to be relatively small because of the smooth nature of the CO_2 field.

Subgrid scale processes may be treated either by closures in which the redistribution of tracer is inferred from properties of the large-scale flow or from externally provided information. In online models, for example, tracer may be redistributed by cumulus convection in the same way as water vapour (excluding the effects of precipitation of course). An offline model can use the same closure, a simpler one or statistics gathered from previous online experiments. TRANSCOM contains cases of all of these.

Models generally treat horizontal and vertical diffusion of tracers in the same way as for other model variables. This treatment will often be determined by the choice of advection scheme in the model.

Models may also differ in their treatment of the interaction between the atmosphere and the surface. While TRANSCOM experiments do not need to be concerned with processes of deposition, the rates of turbulent mixing of the tracer near the surface may have significant large-scale implications, particularly as the tracer source is at the surface. Models in TRANSCOM range from no special treatment of model layers in contact with the surface through to a prognostic calculation of the depth of the planetary boundary layer.

A summary of the major features of each of the participating models is given in Table 2.1.

2.2 Choice of sources

It is intuitively reasonable that the greatest differences in concentration due to transport alone should occur because of the interaction of transport with the largest sources. Also, since the differences noted in budget estimates in the first section occur in both annual mean and seasonal responses, two sensible choices for sources to use are those dominating the annual mean large-scale gradient and the seasonal cycle. These are, respectively, the input of CO_2 from the burning of fossil fuels and the seasonal cycle of terrestrial biota (Heimann et al., 1989, Keeling et al., 1989). However we note that the terrestrial biota only dominates the seasonal cycle in the northern extra-tropics with other sources of seasonality becoming important in the tropics and southern hemisphere. It is also noteworthy that, since this is not a calibration experiment the absolute accuracy of the sources is not particularly important. We will, however, make some comment on the sources where we might reasonably expect some agreement between modelled and observed concentrations.

The fossil fuel source we use was supplied by Fung and is that used in the work of Tans et al. (1990). It is based on country by country estimates derived by Marland et al. (1989). Fung distributed the country totals within each country according to population density. The data were provided to us on a $1^\circ \times 1^\circ$ grid (Fig. 2.1) and were then aggregated onto the grid for each model. Given different model resolutions, this aggregation causes considerable differences in the smoothness of the source field. However, the large scale structure of the input sources varies little from model to model.

The zonal mean of the fossil source used by a number of models is shown in Fig. 2.2a and the standard deviation of the source around each latitude is shown in Fig. 2.2b. The

Model	Modeller	Type	Horizontal Resolution	Vertical Resolution	Advection	Wind	Freq	Sub-grid scale				
								Hdiff	Vdiff	Conv	Turb	PBL
ANU	Taylor	Off	2.5°	7 pressure	lagrangian	ECMWF(80)	Stats	Y	Y	-	-	-
CSIRO9	Watterson	On	3°×5.6°	9 sigma	semi-lag	-	-	-	-	Y	Y	-
CSU	Denning	On	4°×5°	17 sigma	2nd order	-	-	-	-	Y	Y	Y
GFDL	Rayner	Off	265 km	11 sigma	2,4 order	GFDL GCM	6 hr	Y	Y	-	-	-
GISS	Trudinger	Off	8°×10°	9 sigma	slopes	GISS GCM	4 hr	Y	-	Y	-	-
MUGCM	Law	On	R21	9 sigma	spectral	-	-	Y	Y	Y	-	-
MUTM	Law	Off	R21	9 sigma	spectral	MU GCM	24 hr	Y	Y	Y	-	-
NCAR	Erickson	On	2.8°	18 sigma	semi-lag	-	-	-	Y	Y	-	Y
NIRE	Taguchi	Off	2.5°	15 sigma	semi-lag	ECMWF(92)	6 hr	-	-	-	-	Y
TM1	Piper	Off	8°×10°	9 sigma	slopes	ECMWF(79)	12 hr	Y	-	Y	-	-
TM2	Heimann	Off	4°×5°	9 sigma	slopes	ECMWF(86)	12 hr	-	Y	Y	-	-
TM2Z	Ramonet	Off	2.5°	9 sigma	slopes	ECMWF(90)	12 hr	-	Y	Y	-	-

Table 2.1: Summary of model details and acronyms. The year of ECMWF wind analyses used is given by the number in brackets. Note that the list of sub-grid processes contains some overlap but is based on the modeller's choice of terminology. The processes are horizontal and vertical diffusion, convection, turbulent mixing and planetary boundary layer formulations. More details are available in Appendix C.

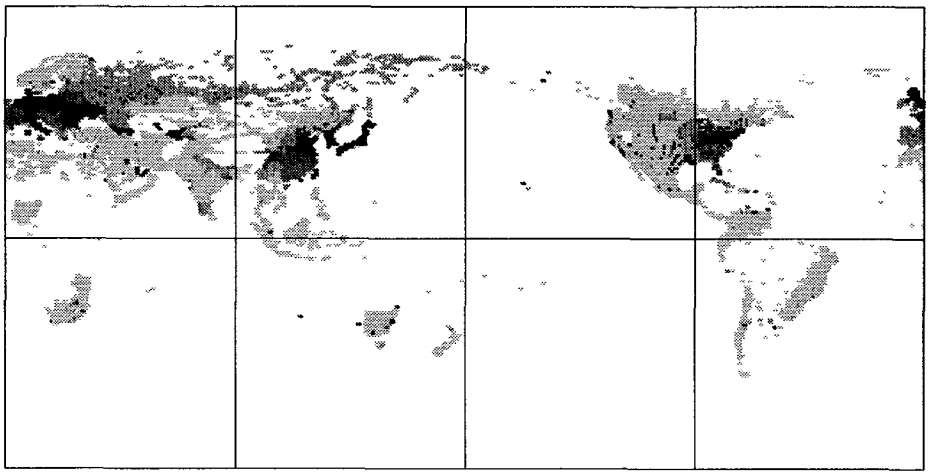

Fig 2.1: Fossil emissions in $gCm^{-2}yr^{-1}$. Each $1° \times 1°$ square is shaded. The darker greys indicate higher emissions. The values used to determine the grey shade are 1, 50, 100, 200, 500, 1000 and 5000 $gCm^{-2}yr^{-1}$.

model acronyms used in the figure key are listed in Table 2.1. It is apparent that the lower resolution (GISS) and spectral (MU) models are unable to resolve the 40°N maximum and 47°N minimum emissions. The standard deviations are also poorly represented around 40°N. The fossil fuel source is specified constant in time. The most important details of the fossil fuel source are an overall magnitude of 5.3 $GtCyr^{-1}$ with the majority of this occurring in the northern midlatitudes. 77% of the source lies between 30°N and 60°N and 96% of the source is north of the equator.

The vegetation source was taken from the satellite-derived estimates of Fung et al. (1987). Fung et al. used satellite microwave radiometer data to calculate the normalized difference vegetation index (NDVI) as a measure of photosynthesis. This provides the seasonality of photosynthesis. The other two terms in the terrestrial biotic flux, the soil respiration and net primary productivity, were supplied from field measurements and a previously calculated global distribution. Exponential and linear relationships between NDVI and photosynthetic uptake were tested using the GISS model. The exponential relationship resulted in better agreement with observed seasonal cycles. We use here the sources based on the exponential relationship.

The terrestrial biotic source has an annual mean of zero everywhere. However, the terrestrial biotic source does exhibit much larger instantaneous values than the fossil fuel source at some times and places. Indeed the gross or absolute magnitude of the flux, (the sum of all fluxes of one sign), yields a flux of 12.9 $GtCyr^{-1}$. Figs. 2.3 and 2.4 show two different views of the terrestrial biotic flux used in these experiments. Fig. 2.3 shows the peak to peak (ptp) amplitude, the difference between the largest positive monthly mean flux and the largest negative monthly mean flux. This indicates the regions of peak seasonality, principally through the north of the Eurasian and American continents, China, India and tropical Africa. Fig. 2.4 shows a time latitude plot of the zonal mean source. The largest seasonal sources occur in the northern midlatitudes. The flux is small during winter increasing to a maximum positive flux in May. A second maximum positive flux occurs in October. The positive fluxes

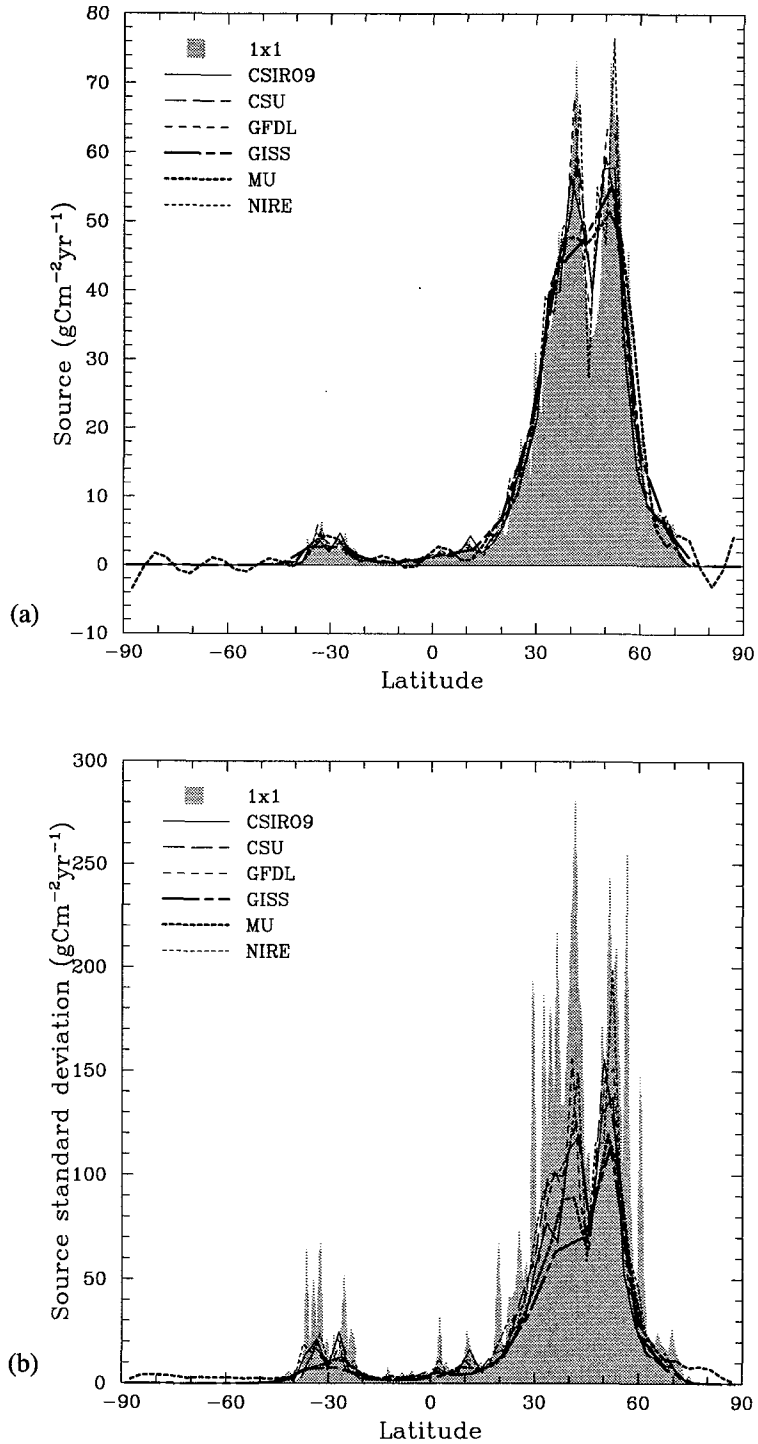

Fig. 2.2: (a) Zonal mean fossil emissions and (b) standard deviation of fossil emissions at each latitude for the models listed in the key. The result for the orginal 1x1 degree emissions has been emphasised by shading the area below the values for this dataset.

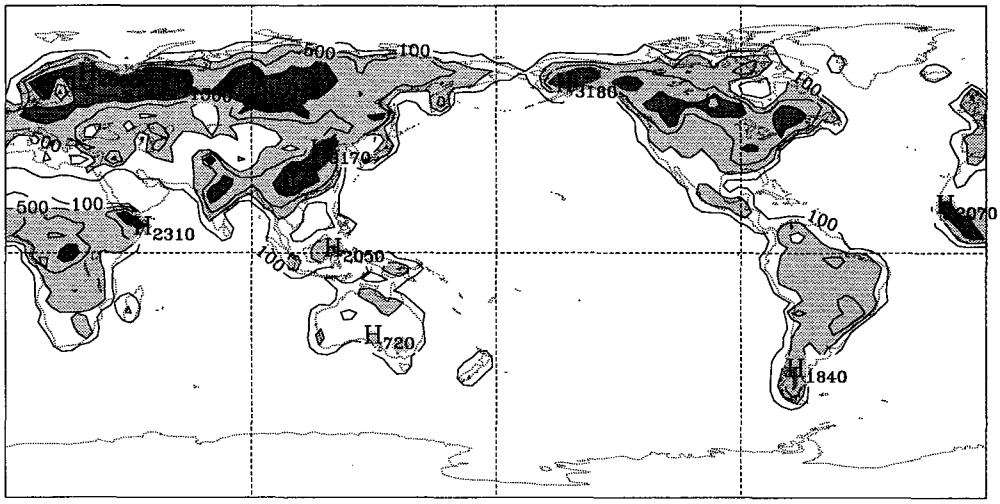

Fig. 2.3: Peak-to-peak amplitude of the seasonal biosphere source. The contours are 100, 500, 1000, 1500, 2000 and 2500 $gCm^{-2}yr^{-1}$. Values greater than 500 and 1500 $gCm^{-2}yr^{-1}$ are shaded in light and dark grey respectively.

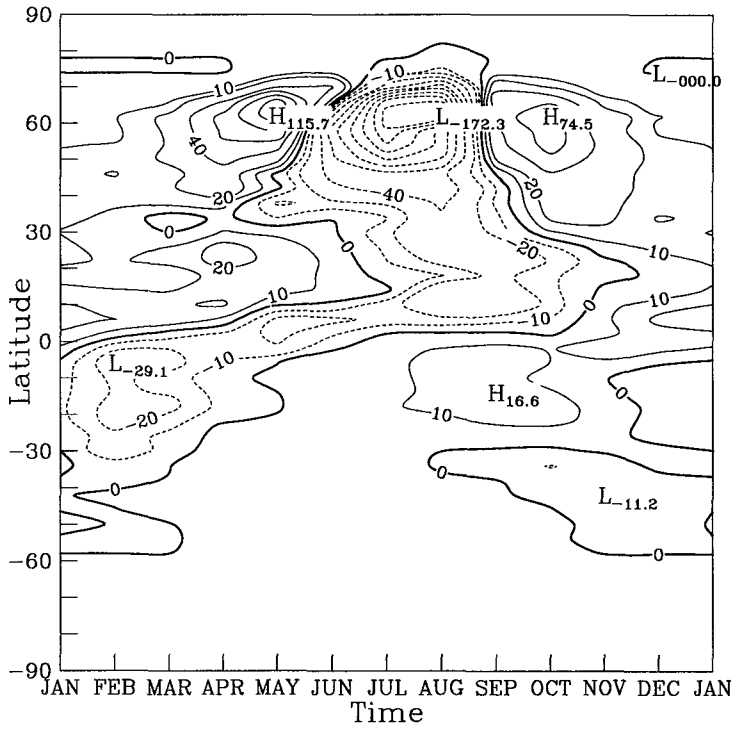

Fig. 2.4: Zonal monthly mean biosphere source. The contour interval is 20 $gCm^{-2}yr^{-1}$ and the -10 and 10 contours are also shown.

indicate periods when respiration dominates and are balanced by a larger and shorter-lived negative spike during the peak growing season of summer. At other latitudes the fluxes are smaller and more sinusoidal in nature. The phase in the southern hemisphere is opposite to that in the northern hemisphere.

While these sources were chosen because of their relevance to the observed CO_2 distribution, it is interesting to ask how well they elucidate the character of large-scale transport. The fact that both sources have most activity in the northern hemisphere is one apparent limitation since there is most likely considerable difference in atmospheric transport within the two hemispheres.

A more serious limitation of the two sources chosen is that they are both contained mainly in the midlatitudes. These experiments provide no information as to the response to tropical sources. They also are located entirely over land so provide no information on the possible response to oceanic sources. The rapidity of mixing in the midlatitudes means this last point may be less important although seasonal shifts in the location of convection from land to ocean may have an impact.

2.3 Equilibrium requirements

Most attempts to infer carbon sources from CO_2 spatial structure have assumed, often implicitly, that CO_2 sources are in equilibrium with CO_2 gradients e.g. Keeling et al. (1989), Tans et al. (1990), Law et al. (1992), Enting et al. (1993, 1995). This has often led to some difficulty as discussed, for example, by Enting et al. (1995). Tans et al. (1989) and Conway et al. (1994) relax this condition by using a two-dimensional model and the time series of CO_2 observations from various stations. They assume that differences in inferred sources sprang from differences in CO_2 distributions since there was no interannual variability in the transport forcing.

In this report we focus on tracers with an infinite lifetime. In such cases the information returned from the temporal behaviour of a model is its relaxation time towards equilibrium. This is mainly a function of its large-scale mixing rates which will also be revealed by its response at equilibrium.

Given the interpretative difficulties of time-varying experiments and the little extra information provided by such experiments, we chose to limit this study to the equilibrium response. Given that interhemispheric mixing times for the large-scale tropospheric response differ considerably among models but are usually between 0.6 and 1.5 years, a reasonable requirement was that data be provided from at least the fourth year of the model run.

The requirement of equilibrium also skirts some potential problems in experimental specification such as the need for an initial state. Using only equilibrium responses does not allow direct comparison with the non-equilibrium observational record. We were not intending these experiments as model calibrations and additionally many of the models use climatologies generated by atmospheric GCMs rather than analyzed flows. Hence, to the extent that interannual variability in transport is important, these models could not be realistically compared with any particular observational snapshot.

2.4 Choice of fields

The trade-off between the general description of tracer transport and the specifics of the carbon cycle to which we alluded in an earlier section reappears when considering which

fields to archive and display for a model comparison. Here, again, we are also guided by the need to keep the demands on participating modellers at a feasible level. Also, the data had to be statistical in nature, i.e. some kind of average. This immediately precludes some types of analysis which might be very interesting in such a comparison.

We requested two types of data from TRANSCOM participants: horizontal fields and meridional cross-sections. The horizontal fields were monthly averages of the tracer mixing ratio at the surface, 500 hPa and 200 hPa. We chose the averaging period based on its use in various inversion studies and its use in data sets of observations.

The surface was an obvious choice for the comparison since surface data from models are used for inversion studies. The 500 hPa level was chosen as representative of the midtroposphere. The 200 hPa level was chosen firstly to represent the upper troposphere and because there are some observational data available at this level (Nakazawa et al., 1991). Almost all the models in TRANSCOM are run on σ coordinates so participants interpolated their data to the required pressure surfaces.

For almost all models, the surface was the bottom model layer. This is the layer into which surface sources were injected. Three models contained an explicit formulation for the planetary boundary layer. These participants supplied these PBL data.

The cross-section data were the monthly mean zonal mean mixing ratios at each model level and latitude. While these data could not be directly compared one against another (since each model used different configurations of levels) the data did allow consistent calculation of various vertical integrals. These data also allowed us to investigate the vertical propagation of seasonal signals such as the biotic source. Not all participants were able to supply cross-section data.

All data have been archived in a common format. This format is described as part of the experimental specification in appendix A.

2.5 Normalization

In a comparison such as TRANSCOM we are interested in differences in the structure of modelled fields. These can be masked by systematic differences. To reduce this we required all archived fields to be normalized. Normalization removes the effect of the initial condition (assuming that the distribution is in equilibrium with the source and transport characteristics) and also the amount of time spent in spinning up the model before the data are sampled. Normalization also corrects for drift in the global mean caused by slight differences in global mean source strength. These result from differences in interpolation from the supplied source field to the model grids.

Several choices of normalization were available. We chose to use the global mean mixing ratio for January. Ideally this is pressure-weighted so that it represents the total tracer mass. A test of normalizing with and without pressure weighting on one set of results shows the difference to be insignificant. After normalizing, the January cross-section for each experiment for each model has a global mean of zero.

3 Fossil experiment results

Our presentation of the fossil experiment results focusses on the annual mean. The fossil source is constant in time and so any seasonality in the results is due to transport alone. While this may be of some interest, it was not considered to be a major feature of the fossil experiment and is not presented here. We will however make some brief comments on the fossil seasonality in the context of the biosphere experiment in section 4. We present first the annual mean surface results, followed by those at 500 and 200 hPa and finally the vertical structure.

3.1 Surface

3.1.1 Zonal, hemispheric and global annual means

Fig. 3.1 shows the zonal annual mean at the surface for the fossil experiment while Table 3.1 gives the associated global and hemispheric annual means. The difference between the hemispheric means is also given. This will be referred to as the interhemispheric difference (or IHD). All models produce a similar CO_2 gradient through the southern hemisphere but differ substantially in the northern hemisphere. This is emphasised in the IHD data which range from 2.3 to 4.7 ppmv. The models produce maximum concentrations around 50°N which span approximately 3 ppmv although this range can be reduced by almost half if the CSIRO9 and GFDL results are excluded. Given that a number of the other models have been calibrated using krypton-85, it is likely that this smaller range is more realistic. It is also

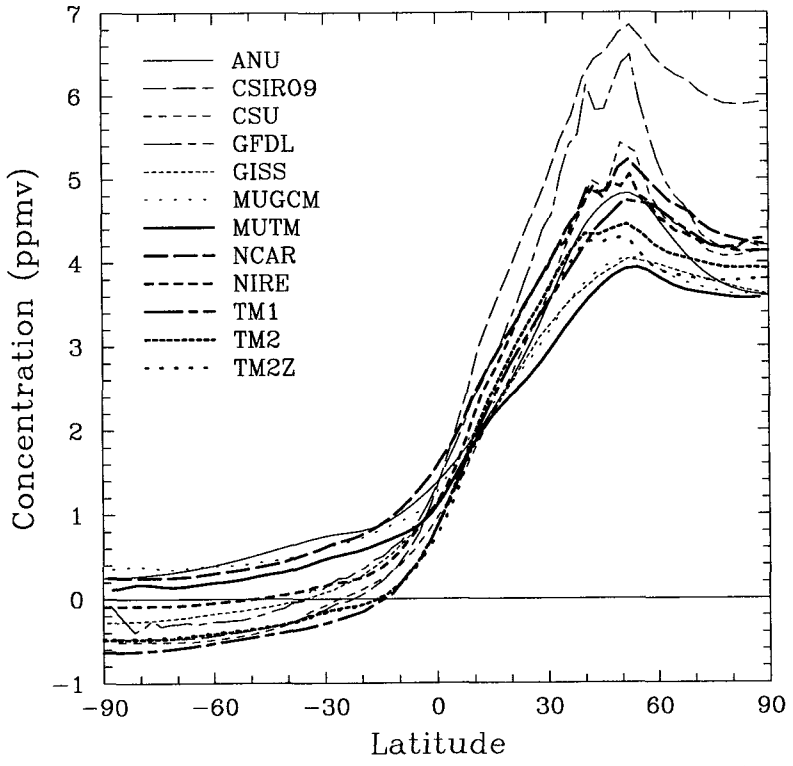

Fig. 3.1: Zonal annual surface mean concentration in ppmv due to fossil emissions.

Model	Global mean	SH mean	NH mean	IHD
ANU	2.01	0.73	3.29	2.56
CSIRO9	2.36	–0.00	4.72	4.72
CSU	1.68	–0.03	3.39	3.42
GFDL	2.19	0.25	4.14	3.89
GISS	1.58	0.19	2.97	2.78
MUGCM	1.82	0.65	2.30	2.35
MUTM	1.66	0.49	2.83	2.35
NCAR	2.20	0.68	3.72	3.05
NIRE	1.91	0.25	3.56	3.31
TM1	1.55	–0.20	3.29	3.49
TM2	1.58	–0.11	3.26	3.36
TM2Z	1.51	–0.11	3.12	3.23

Table 3.1: Global and hemispheric surface mean concentration in ppmv.

worth noting that the NIRE and TM models which are run with analysed winds give very similar interhemispheric differences (3.2–3.5 ppmv).

In the northern hemisphere the CSIRO9 and MUTM models give concentrations at the extremes of the range shown here. To try to understand this difference, the fossil experiment was repeated using MUTM forced with winds from the CSIRO9 GCM. The results suggest that approximately half of the original difference between these models may be explained by the large-scale advection and the other half by the sub-grid scale parameterisation.

The global means at the surface range from 1.5 to 2.4 ppmv. This range is related to differences in vertical transport between models, probably largely due to the different sub-grid scale parameterisations employed. Experiments with MUTM suggest that differences in vertical velocities play only a minor role in the troposphere.

3.1.2 Maps

The annual mean CO_2 distributions at the surface are shown in Fig. 3.2. All models agree that the highest concentrations occur over Europe, North East America and the China-Japan region (usually in that order). This is to be expected as the largest fossil sources are in these regions. There is also reasonable agreement on the longitudinal variations of concentration in areas more remote from the sources, for example across the northern ocean basins. Major differences do, however, occur in the magnitudes of the high concentration features. For example, the European maximum ranges from 6.3 ppmv in the GISS model to 25.2 ppmv in the GFDL model. There is some evidence that the larger concentrations occur in those models with higher resolution (e.g. GFDL, NCAR and NIRE). This would result from the ability to resolve smaller scale features both in the concentration and source fields. For example the maximum value in the GISS fossil source distribution is 515 $gCm^{-2}yr^{-1}$ compared to 912 $gCm^{-2}yr^{-1}$ for the GFDL source distribution.

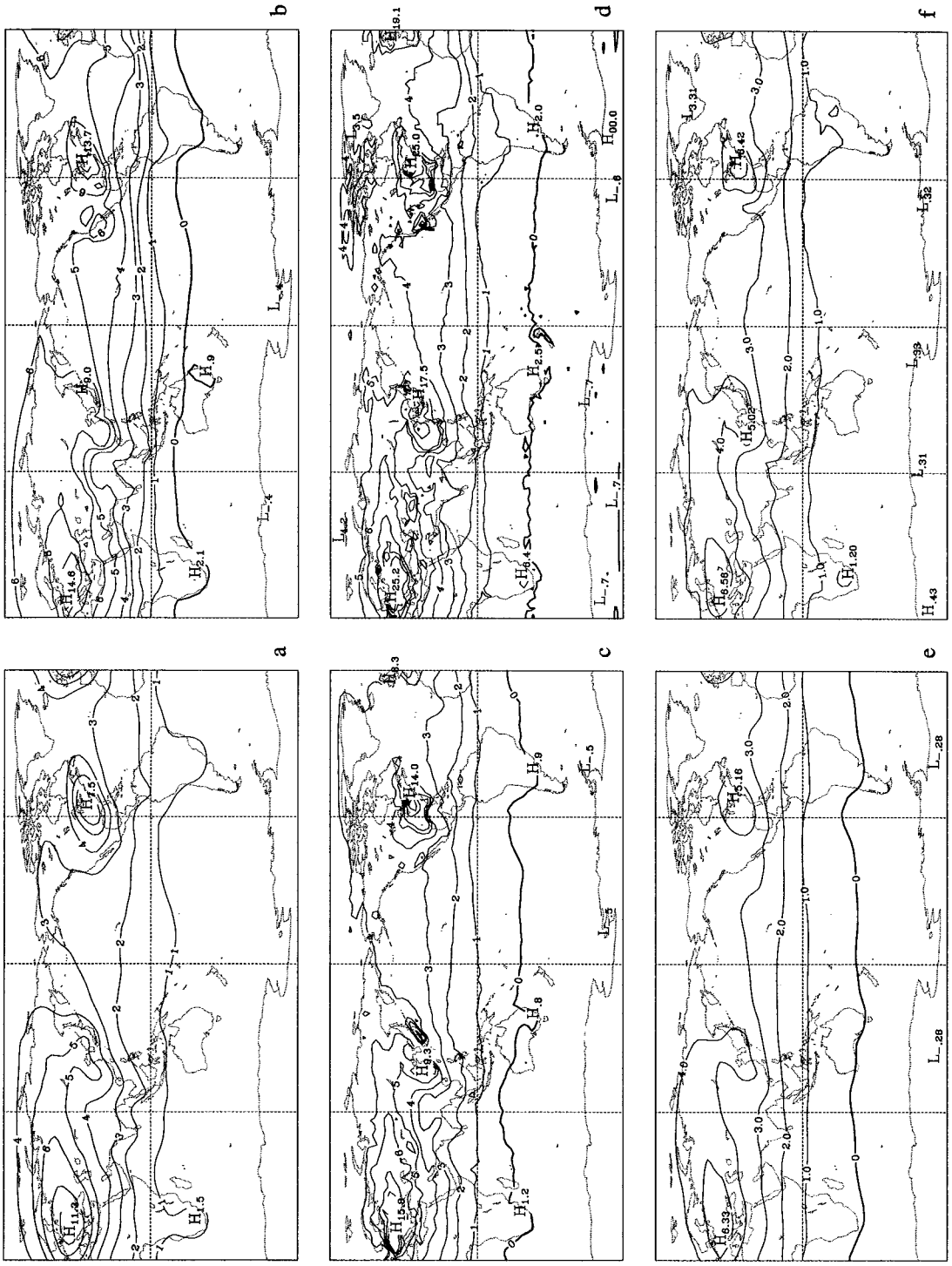

Fig. 3.2: Surface annual mean concentration for the fossil case for (a) ANU, (b) CSIRO9, (c) CSU, (d) GFDL, (e) GISS, (f) MUGCM. The contours are 0, 1, 2, 3, 4, 5, 6, 8, 10, 12, 16, 20, 24 ppmv.

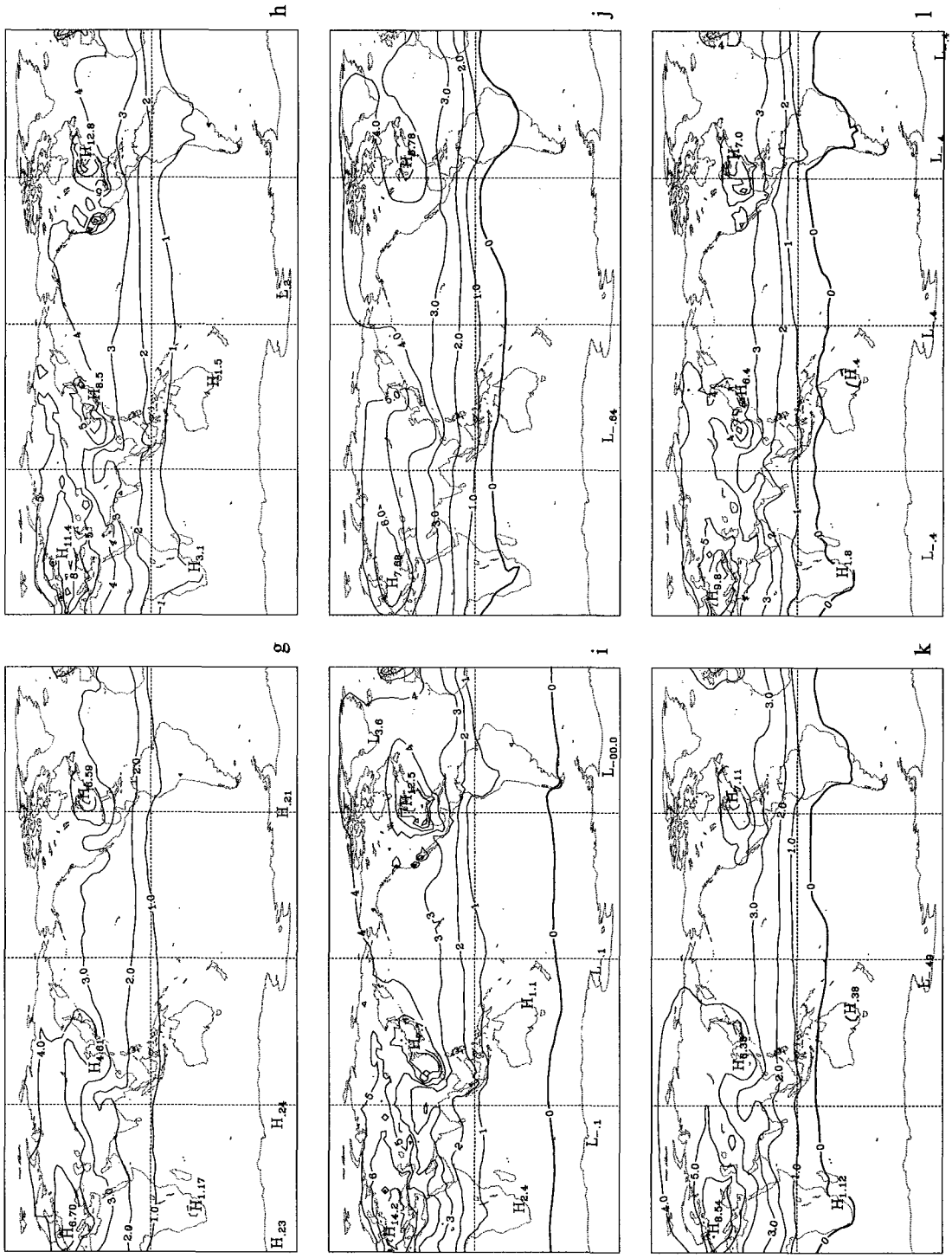

Fig. 3.2: Surface annual mean concentration for the fossil case for (g) MUTM, (h) NCAR, (i) NIRE, (j) TM1, (k) TM2, (l) TM2Z. The contours are 0, 1, 2, 3, 4, 5, 6, 8, 10, 12, 16, 20, 24 ppmv.

3.2 500 hPa

3.2.1 Zonal, hemispheric and global annual means

At 500 hPa, the zonal mean concentration shows a more uniform increase from south to north than at the surface (Fig. 3.3). There is also less variability between models; there is a smaller range of global means than at the surface (Table 3.2) and at all latitudes, almost all model zonal mean concentrations are within 1 ppmv. However the range of interhemispheric differences remains high (0.9–2.8 ppmv) as models with a low southern hemisphere mean tend to have a high northern hemisphere mean and vice versa.

Model	Global mean	SH mean	NH mean	IHD
ANU	1.07	0.62	1.52	0.90
CSIRO9	1.65	0.26	3.05	2.78
CSU	1.26	0.31	2.21	1.90
GFDL	1.64	0.63	2.65	2.02
GISS	1.40	0.32	2.49	2.17
MUGCM	1.62	0.89	2.34	1.45
MUTM	1.46	0.66	2.26	1.59
NCAR	1.83	1.01	2.64	1.63
NIRE	1.32	0.45	2.19	1.73
TM1	1.25	0.01	2.49	2.49
TM2	1.27	0.09	2.45	2.37
TM2Z	1.27	0.07	2.47	2.40

Table 3.2: Global and hemispheric mean concentration at 500 hPa in ppmv.

3.2.2 Surface to 500 hPa difference

The difference between the zonal mean concentration at the surface and 500 hPa is plotted in Fig. 3.4. This gives some indication of the vertical CO_2 gradient through the lower troposphere. There is generally good qualitative agreement between models but a large range in the magnitude of vertical differences, particularly in the northern hemisphere. All models, except ANU, give a region of increasing concentration with height between the equator and at least 50°S. The increase with height is largest around 10–20°S and is associated with high concentration air from the northern hemisphere which is transported southwards in the upper troposphere. In the northern hemisphere, maximum surface to 500 hPa differences occur between 40 and 60°N and range from 0.7–3.0 ppmv. The largest vertical differences occur for those models with the largest surface concentrations at these latitudes. The ANU model appears to have a larger vertical difference than would be expected based on its surface concentrations.

3.2.3 Maps

The 500 hPa distributions (Fig. 3.5) are much more zonally uniform than at the surface. Apart from very small regions in the CSIRO9, CSU and GFDL results, the concentrations are within ±0.5 ppmv of the zonal mean. The maximum values range from 2.1(3.5 without ANU)– 4.7 ppmv and tend to occur over Eurasia.

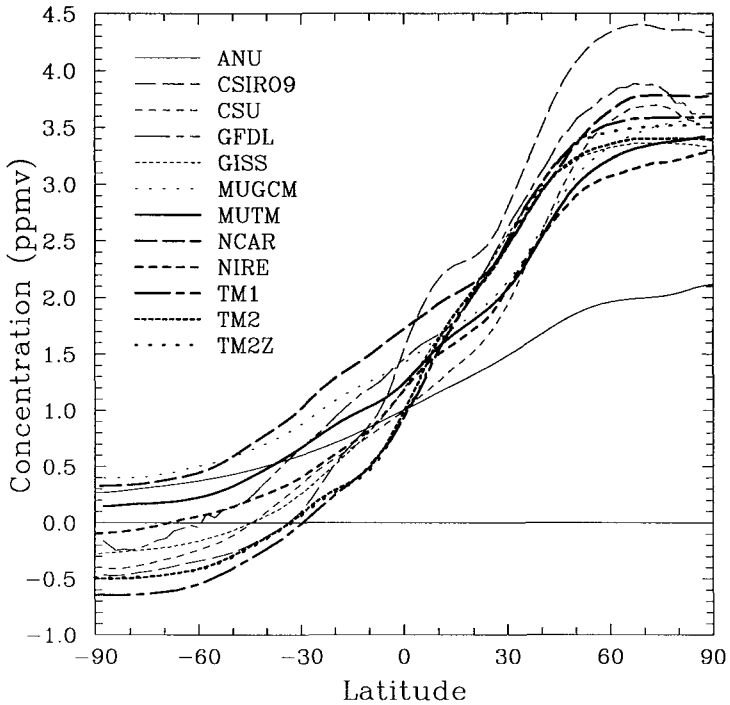

Fig. 3.3: Zonal annual 500 hPa mean concentration for the fossil case in ppmv.

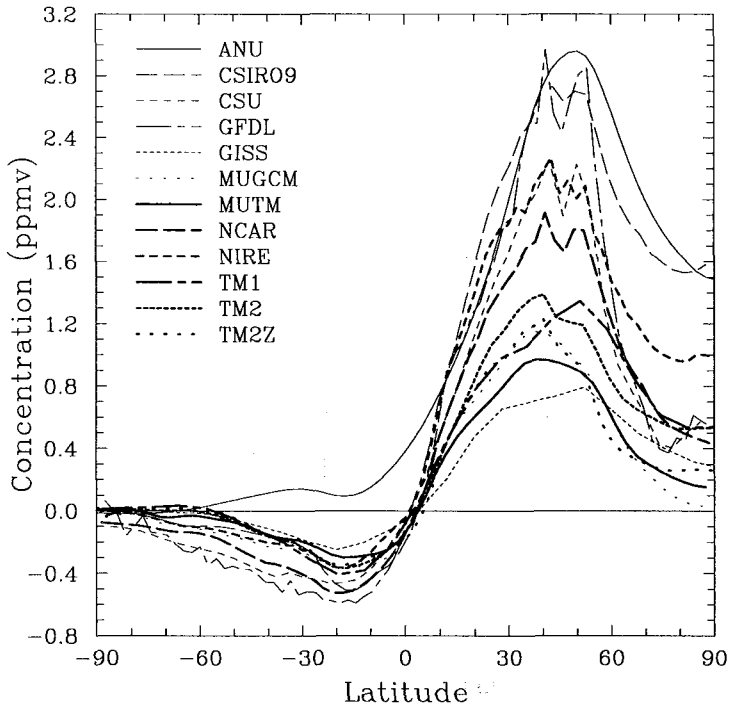

Fig. 3.4: Difference between the zonal annual surface and 500 hPa mean concentrations for the fossil case in ppmv.

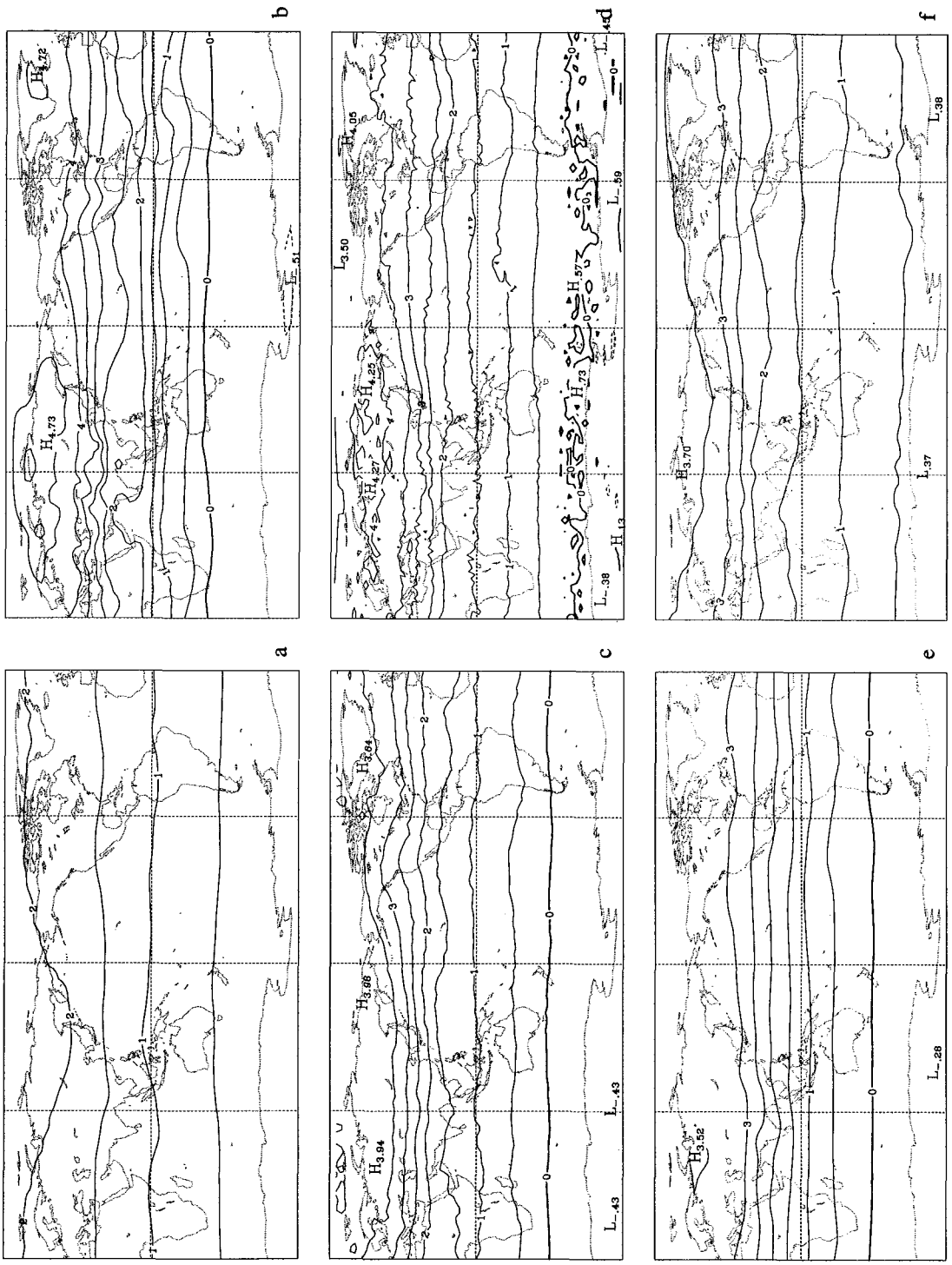

Fig. 3.5: 500 hPa annual mean concentration for the fossil case for (a) ANU, (b) CSIRO9, (c) CSU, (d) GFDL, (e) GISS, (f) MUGCM. The contour interval is 0.5 ppmv.

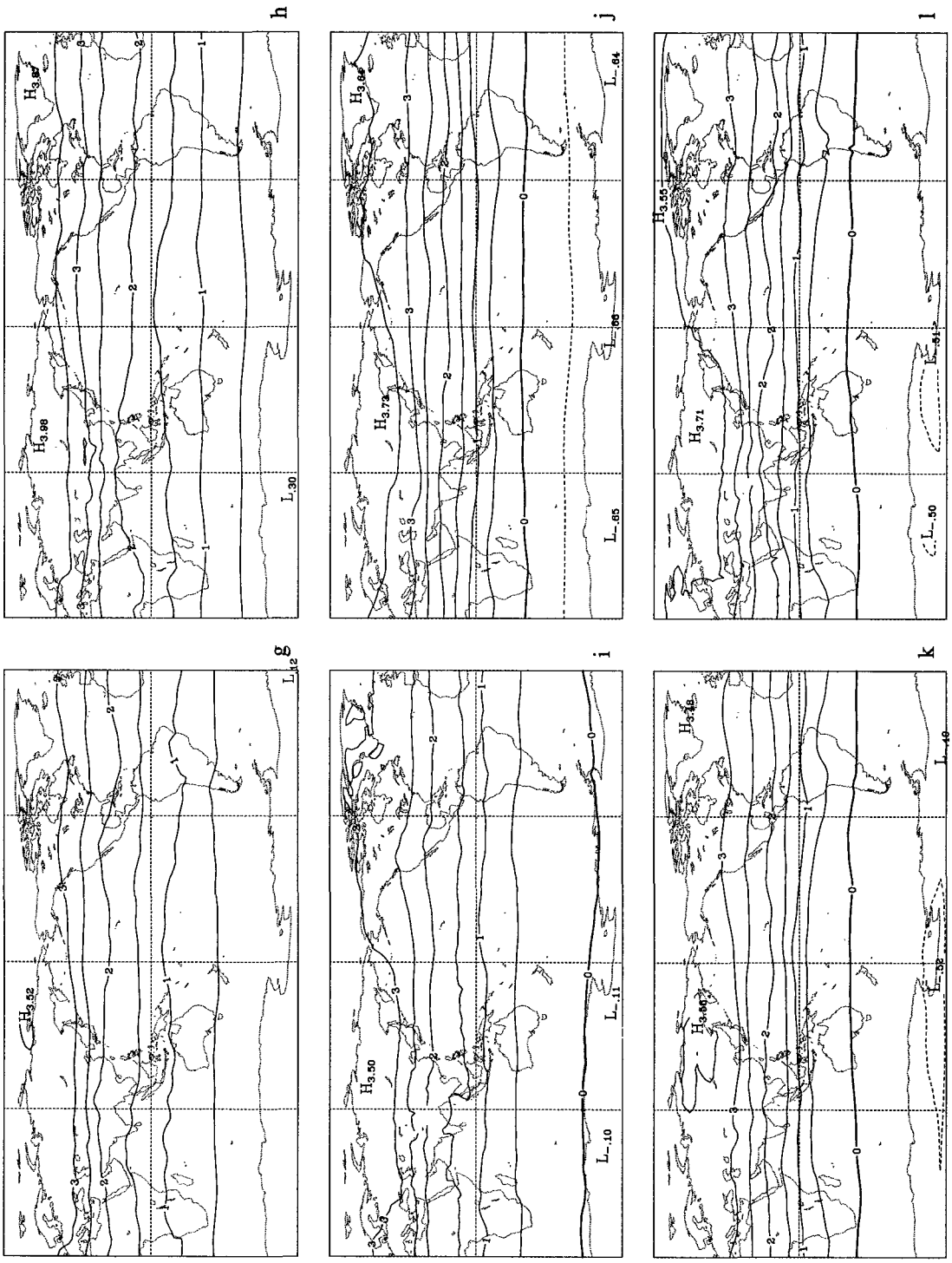

Fig. 3.5: 500 hPa annual mean concentration for the fossil case for (g) MUTM, (h) NCAR, (i) NIRE, (j) TM1, (k) TM2, (l) TM2Z. The contour interval is 0.5 ppmv.

3.3 200 hPa

3.3.1 Zonal, hemispheric and global means

There is a striking variety in the model responses at 200 hPa. The zonal mean is given in Fig. 3.6. Approximately half the models produce maximum concentrations around 0–30°N while the remainder have mid to high northern latitude maxima. In the southern hemisphere the concentration gradients are reasonably similar among models with low gradients at high latitudes and larger gradients through the midlatitudes. An exception is the ANU model which does not show a significant change of gradient through the southern hemisphere.

North of the equator the model results seem to fall into three groups: those with concentrations that continue to increase to 60°N (CSU, GISS, TM1, TM2, TM2Z, also ANU but with a much smaller north-south gradient), those models that produce a small decrease in, or approximately constant concentrations between 0 and 90°N (MUTM, NIRE) and the remaining models (CSIRO9, GFDL, MUGCM, NCAR) which produce large decreases in concentration between the equator and the north pole. The variety of responses at these latitudes is most probably related to each model's representation of the stratosphere. The lower simulated concentrations suggest that these models sample mainly stratospheric air at 200 hPa while the models giving higher concentrations sample mainly tropospheric air at this height.

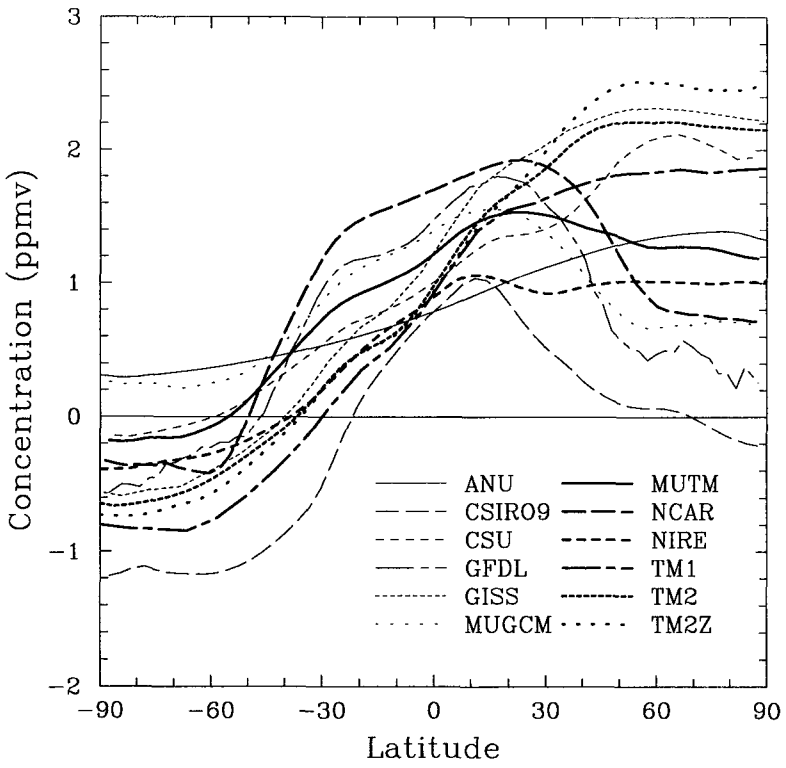

Fig 3.6: Zonal annual 200 hPa mean concentration in ppmv.

Model	Global mean	SH mean	NH mean	IHD
ANU	0.82	0.54	1.11	0.58
CSIRO9	0.08	–0.36	0.52	0.87
CSU	1.01	0.48	1.54	1.06
GFDL	0.97	0.66	1.27	0.62
GISS	1.14	0.30	1.98	1.69
MUGCM	1.00	0.80	1.21	0.41
MUTM	1.00	0.59	1.41	0.81
NCAR	1.21	0.85	1.56	0.71
NIRE	0.61	0.23	0.99	0.77
TM1	0.78	–0.03	1.59	1.62
TM2	0.99	0.16	1.81	1.65
TM2Z	1.02	0.12	1.93	1.81

Table 3.3: Global and hemispheric 200 hPa mean concentration in ppmv.

This variety of northern hemisphere responses is reflected in the interhemispheric differences which range from 0.2–1.8 ppmv (Table 3.3). The range of global means is smaller; 0.6–1.2 ppmv except CSIRO9 which has a global mean of only 0.1 ppmv. This indicates below average vertical mixing with consequent high surface concentrations and low 200 hPa concentrations.

3.3.2 Maps

The annual mean 200 hPa maps (Fig. 3.7) show concentrations that are reasonably zonally uniform in most cases. The standard deviation of concentration at any given latitude (a measure of the zonal uniformity) is generally lower in the mid-high latitudes of the northern hemisphere than at 500 hPa. However in the tropics at least half the models produce higher standard deviations at 200 hPa than at 500 hPa. This may be associated with the rapid mixing of lower tropospheric air (with high concentrations) to this height by convection. Maximum concentrations occur either in the high northern latitudes or between 0 and 30°N. In those models that have low latitude maxima, these tend to occur in the West Pacific / South East Asian region with secondary maxima around Central America. The locations of the maxima are more variable for those models producing high latitude maxima.

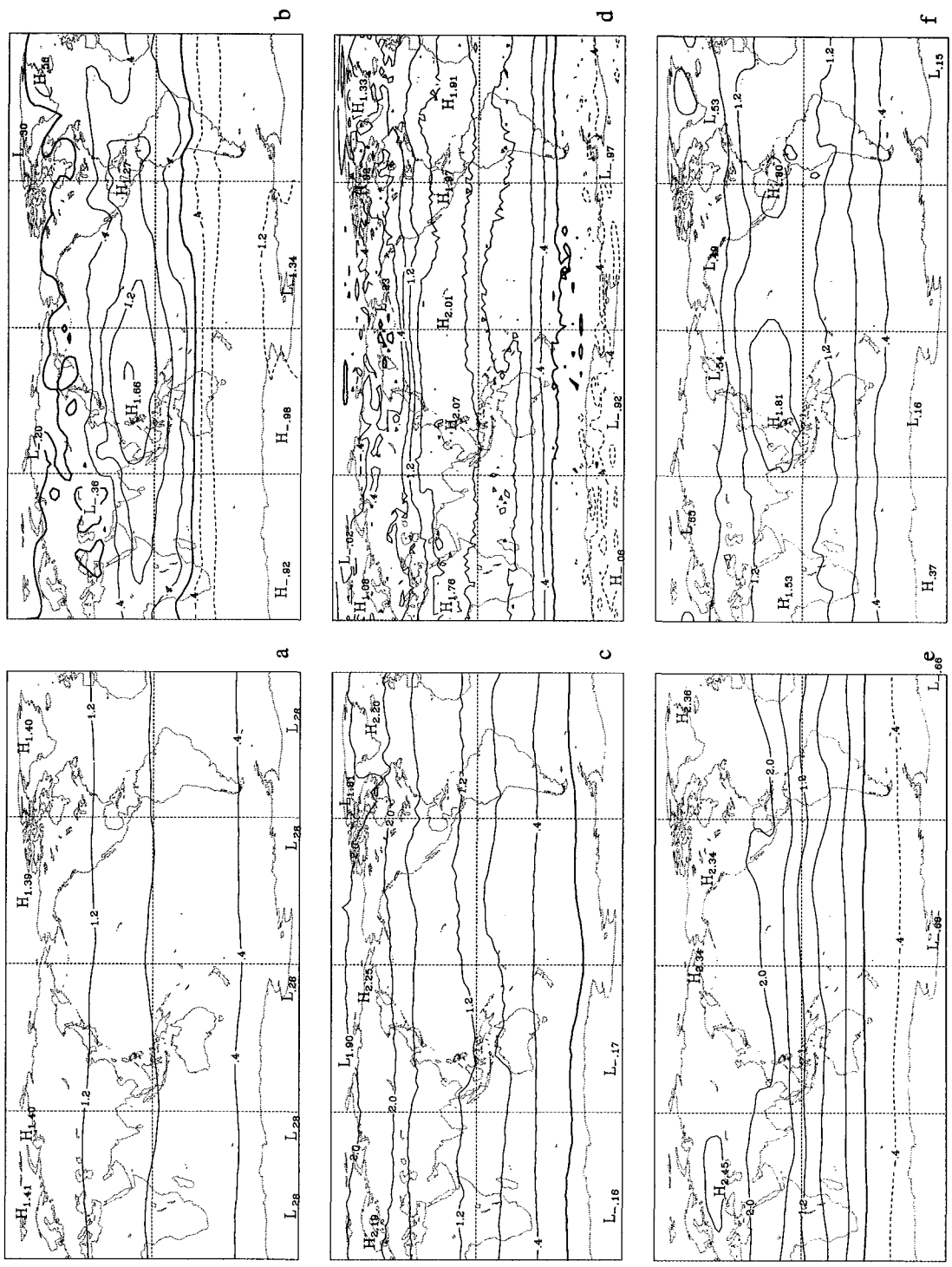

Fig. 3.7: 200 hPa annual mean concentration for the fossil case for (a) ANU, (b) CSIRO9, (c) CSU, (d) GFDL, (e) GISS, (f) MUGCM. The contour interval is 0.4 ppmv.

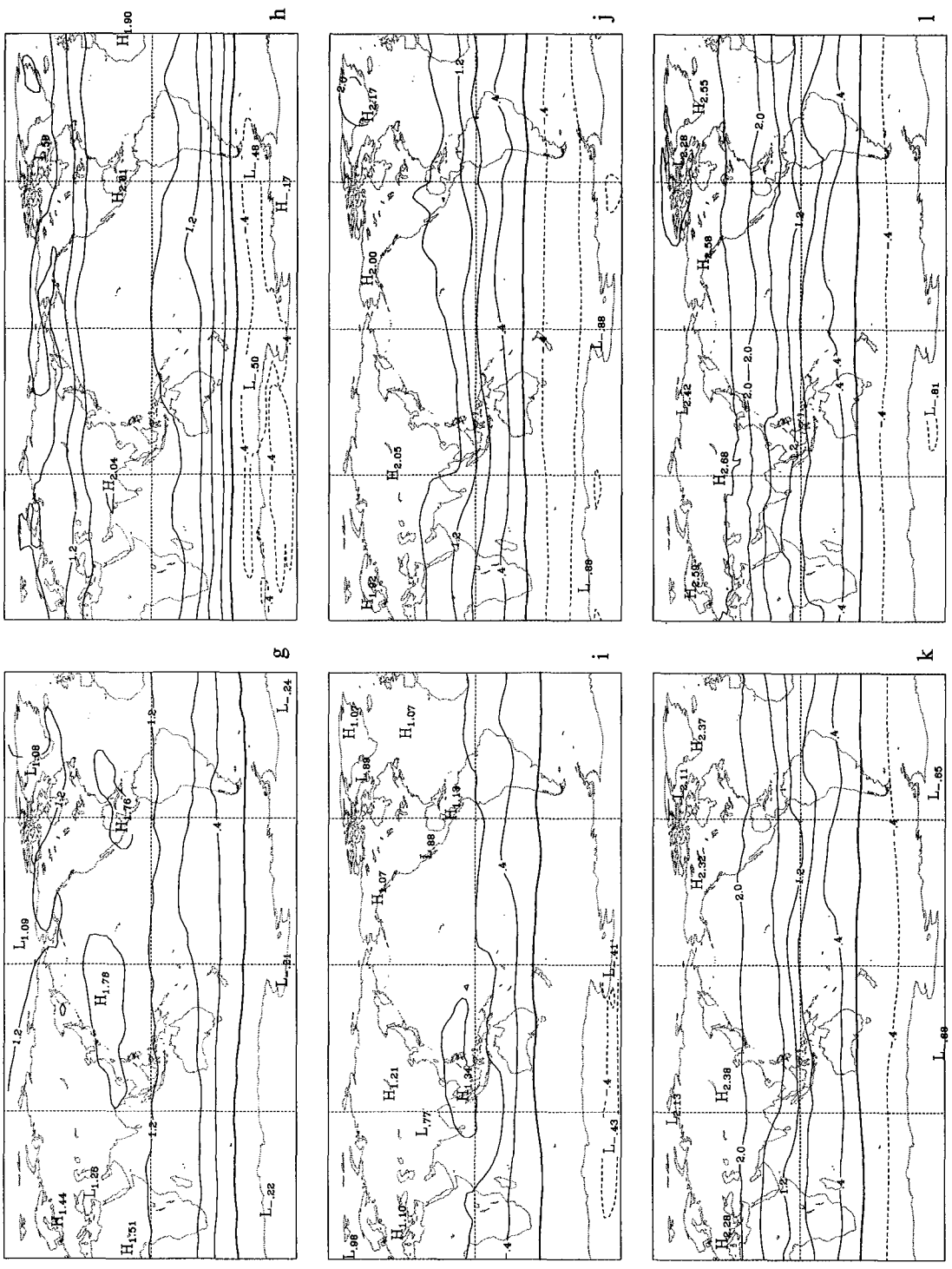

Fig. 3.7: 200 hPa annual mean concentration for the fossil case for (g) MUTM, (h) NCAR, (i) NIRE, (j) TM1, (k) TM2, (l) TM2Z. The contour interval is 0.4 ppmv.

3.4 Vertical structure

3.4.1 Hemispheric mean profiles

Zonal mean concentrations at each model (usually sigma) level were obtained for nine out of the twelve participating models. Note that while sigma is usually defined as the ratio of pressure to surface pressure, this is occasionally modified by different definitions of the top of the model. This manifests itself as a slight stretching of graphs of concentration against height. We present here the hemispheric means plotted against sigma level (Fig. 3.8). The tropospheric gradients in the northern hemisphere vary between models with the CSIRO9 and NIRE models producing larger vertical gradients than the other models. The larger gradients may indicate that less sub-grid scale vertical transport occurs in these models; the NIRE model does not have a parameterisation of convective transport. The GFDL and TM2Z models produce relatively large concentration differences between their first and second model levels but above this region show gradients that are comparable to the majority of models.

In the southern hemisphere vertical gradients are relatively small throughout the troposphere. There is a slight increase in concentration with height in all models. This indicates transport of the northern hemisphere source into the upper troposphere of the southern hemisphere. This increase is larger than average in the lowest levels of the GFDL model. The maximum concentration occurs between about σ=0.5 (CSIRO9) and σ=0.2 (TM1, TM2Z). The concentrations at the top of the models vary substantially with most models producing a rapid decrease in concentration with height above σ=0.2. This is also seen in the northern hemisphere results and indicates some consistency with observations although the above caveat about interpreting σ coordinates should be borne in mind. Nakazawa et al. (1991) found that lower stratospheric CO_2 concentrations in the northern mid-latitudes were typically 1.4–2.1 ppmv lower than the upper tropospheric concentrations.

3.4.2 Meridional cross-sections

The meridional cross-sections (Fig. 3.9) show the same basic features for all models. Maximum values occur around 50°N at the surface and decrease with height through the northern troposphere. It is apparent that CO_2 is transported into the southern hemisphere through the upper troposphere resulting in higher concentrations in the southern mid and low latitudes at this altitude than at the surface. The cross-sections also suggest that in some models this region of increasing concentration with height extends throughout the southern hemisphere.

Most models produce a stratosphere with similar concentrations in the northern and southern high latitudes and maximum concentrations at the equator. The TM2Z (and to a lesser extent the TM1 and NIRE models) continue to produce higher concentrations in the northern than southern hemisphere in contrast to the other models. This indicates some of the difficulties in trying to represent stratospheric CO_2 with models that have so few levels above σ=0.1. The minimum concentrations (-5.3 to -1.3 ppmv) occur at these stratospheric levels while the maximum concentrations (3.9 to 6.8 ppmv) occur at the surface in the northern mid-latitudes. It is worth noting that the GFDL maximum (which is at the high end of the range) is confined to the surface layer and the concentrations through the rest of the troposphere are more consistent with those from other models.

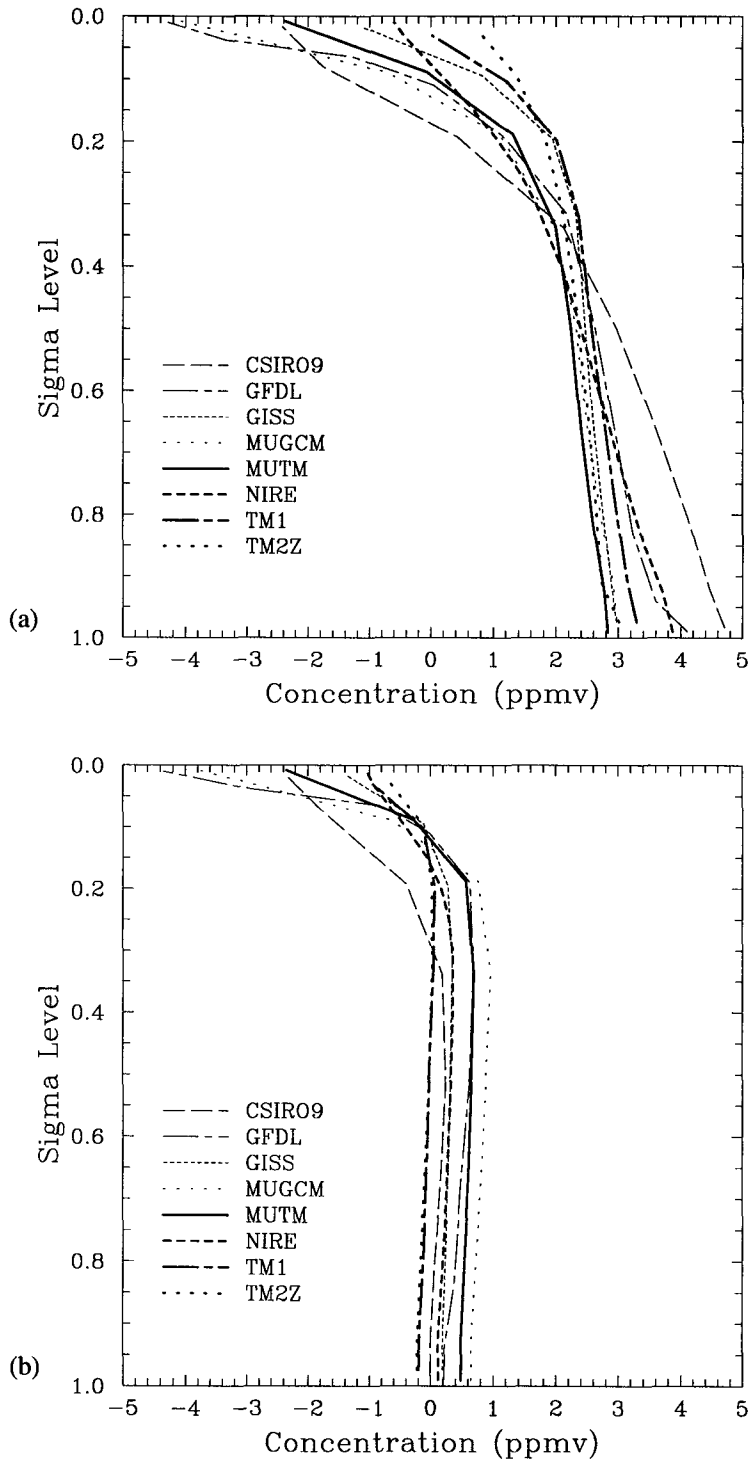

Fig. 3.8: Annual northern hemisphere (a) and southern hemisphere (b) mean concentration for the fossil case in ppmv.

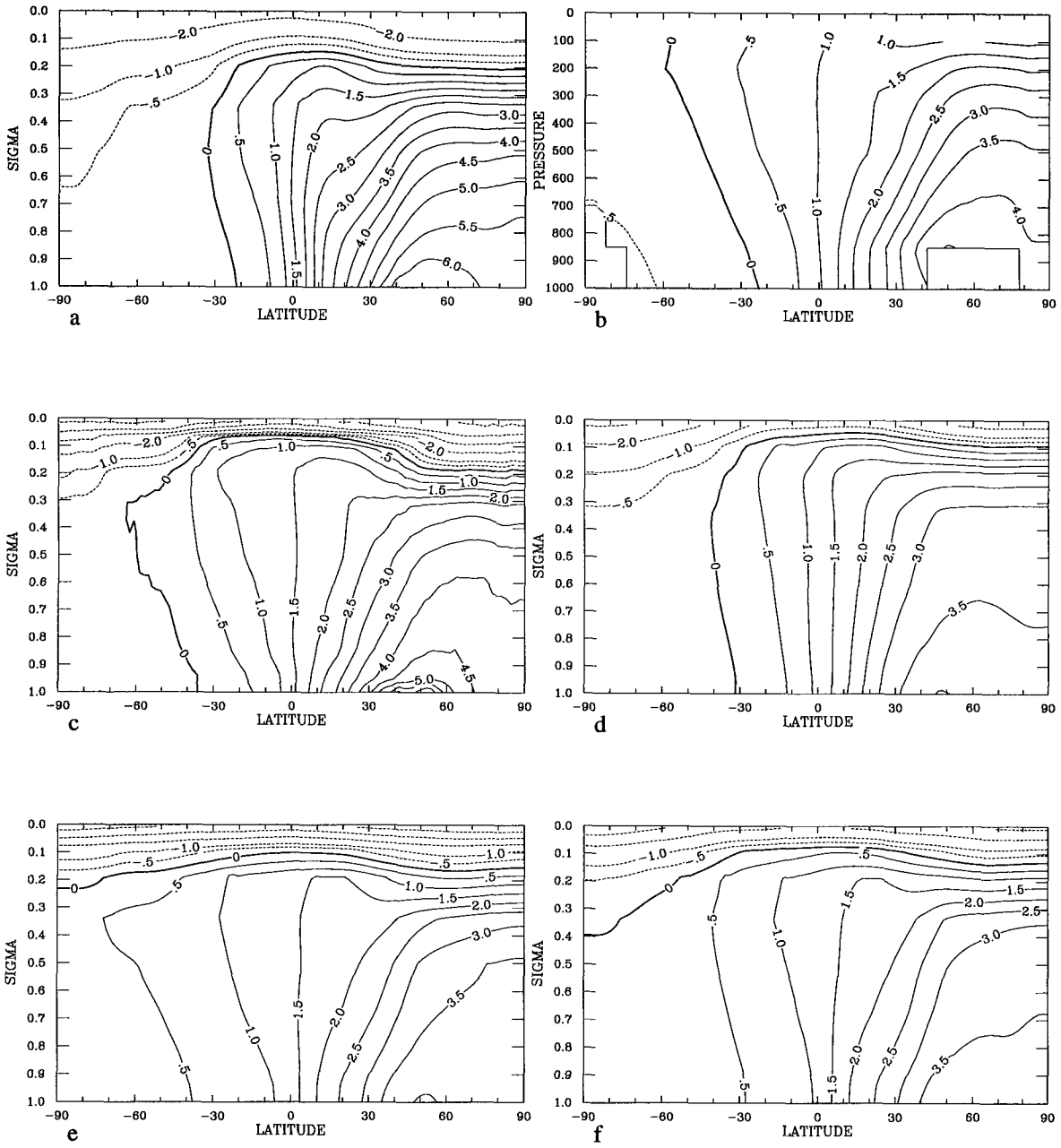

Fig. 3.9: Zonal annual mean concentration for the fossil case for (a) CSIRO9, (b) CSU, (c) GFDL, (d) GISS, (e) MUGCM, (f) MUTM. Note that the CSU figure has pressure as the vertical co-ordinate rather than sigma level. The contour interval is 0.5 ppmv above -1.0 ppmv and 1.0 ppmv below -1.0 ppmv.

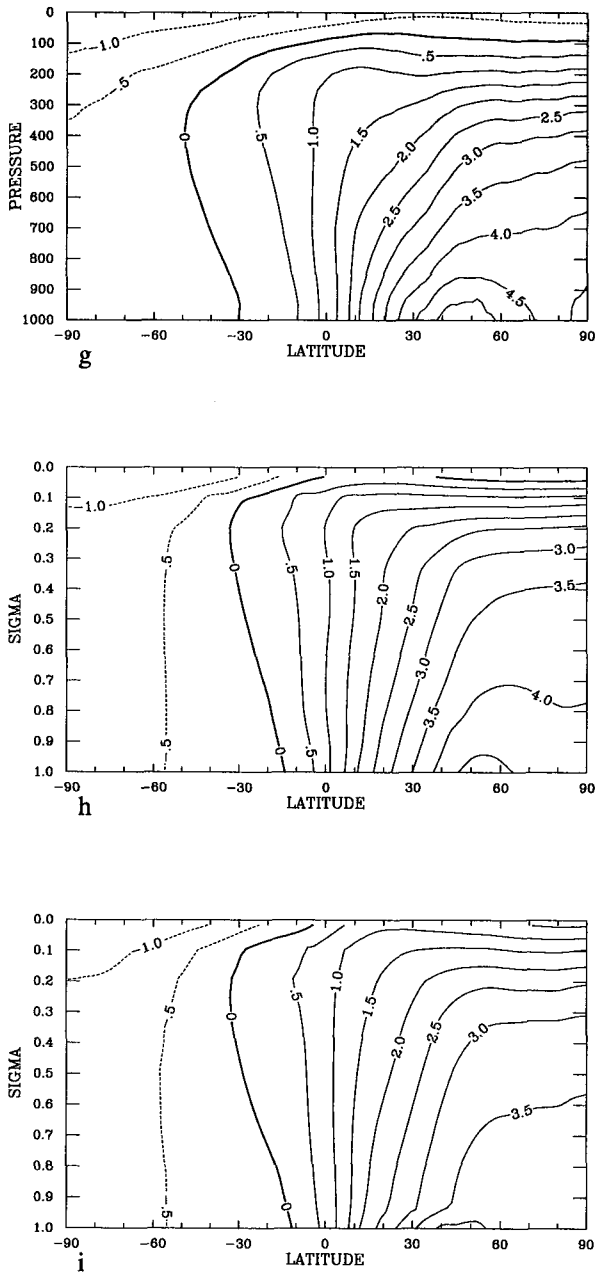

Fig. 3.9: Zonal annual mean concentration for the fossil case for (g) NIRE, (h) TM1, (i) TM2Z. The contour interval is 0.5 ppmv above -1.0 ppmv and 1.0 ppmv below -1.0 ppmv.

4 Biosphere experiment results

The biosphere experiment is characterised by a large seasonal cycle of sources and sinks in the northern hemisphere and a smaller seasonality in the southern hemisphere with opposite phase. The combination of varying sources and seasonality in transport means that there are numerous possibilities for presenting the results. We have chosen to focus on the amplitude of the seasonal cycle but also present the monthly variation of concentration on a hemispheric scale and at a small number of surface locations. We also examine the surface annual mean response.

4.1 Surface

4.1.1 Hemispheric means

The change in the hemispheric mean with time is largely controlled by the monthly variation in sources but also gives some indication of how the interhemispheric transport on a seasonal scale varies between the models. The northern hemisphere mean concentration reaches a maximum in May and a minimum in August-September (Fig. 4.1a). The May maximum occurs at the same time as the maximum source in the northern mid-latitudes. By contrast, the minimum concentrations occur somewhat later than the largest sink at 60°N, indicating the contribution from the northern low-latitudes where the sink continues through to October (Fig. 2.4). There is good agreement between models for the phase of this seasonal cycle.

The amplitude of the response varies substantially (from 3.2 to 7.6 ppmv for the maxima and −4.6 to −7.8 ppmv for the minima). The models with the largest annual northern hemisphere surface means for the fossil case also tend to be those which produce large amplitude seasonal cycles (CSIRO9, GFDL, NIRE, NCAR). The ANU result is interesting in that most models with above average maxima have below average minima whereas the ANU model produces a below average maximum and minimum. This could indicate more rapid vertical mixing during March-May than during July-September.

The southern hemisphere mean varies from approximately −1 ppmv in March to +1 ppmv in August-September (Fig. 4.1b). This is close to the timing of the maximum sources and sinks in the southern low-latitudes (Fig. 2.4). Three models (ANU, CSIRO9 and NIRE) have substantially lower March minima (−1.5 to −1.9 ppmv) than the other models which all lie within about 0.2 ppmv. The March zonal mean concentration (not shown) indicates that the three models tend to have lower concentrations than the other models at almost all latitudes. In August-September there is more variation between the models (about 0.5 ppmv) but no models show extreme values. In the first half of the year the different models produce southern hemisphere means that are in phase but from September the TM models show a noticeable lag compared to the other models.

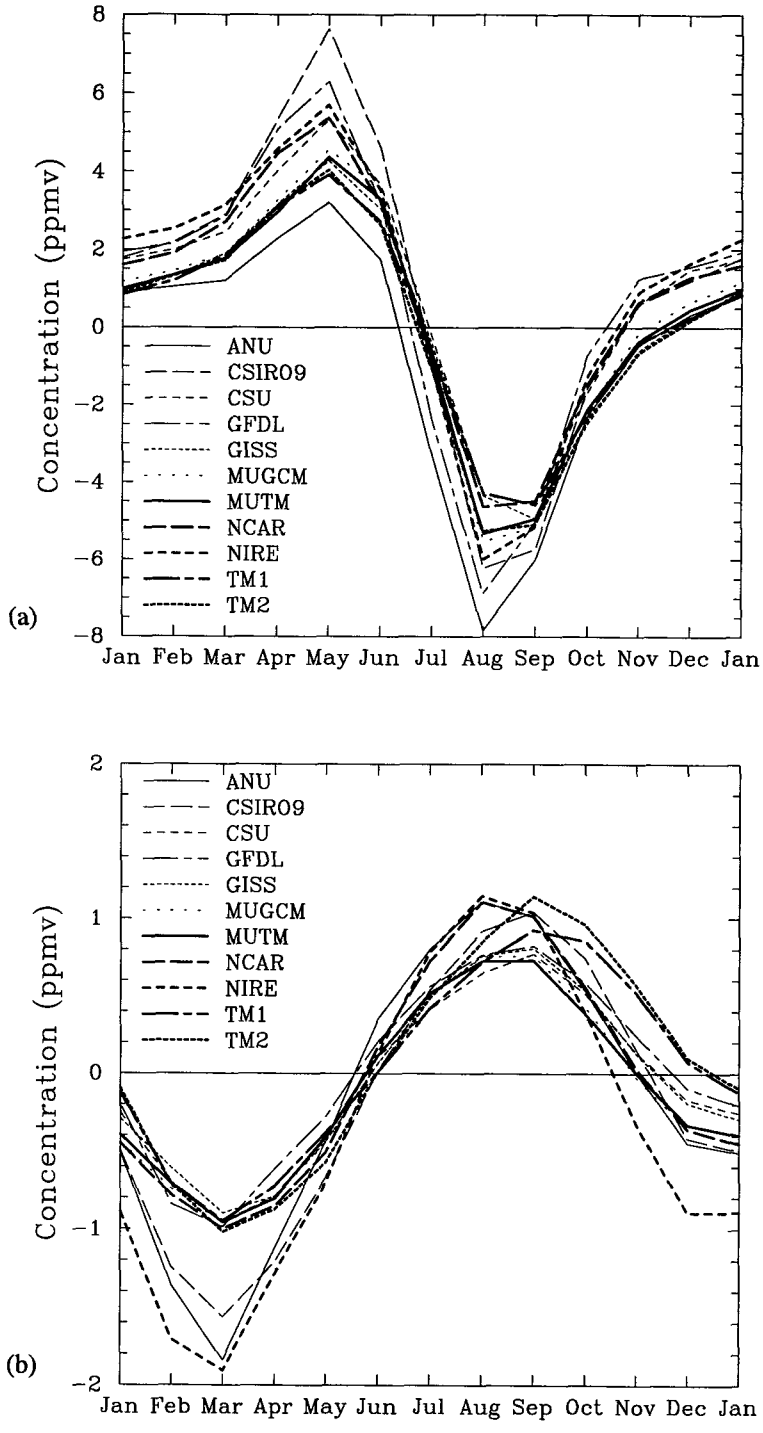

Fig. 4.1: Surface mean concentration for (a) the northern hemisphere and (b) the southern hemisphere for the biosphere case in ppmv.

4.1.2 Zonal mean peak-to-peak amplitude

The peak-to-peak (ptp) amplitudes are calculated as the difference between the maximum and minimum monthly mean concentration at each grid point. The zonal mean ptp amplitude increases from around 1–2 ppmv at the South Pole to between 22 and 52 ppmv around 65°N (Fig. 4.2). There is substantial variability between models at all latitudes north of 15°S; at any given latitude amplitudes generally range over at least 4 ppmv. The maximum amplitudes produced by the CSIRO9 and GFDL models are much larger than produced by the other models whose maxima range from 22–32 ppmv. This is probably due to slow vertical mixing out of the surface layer. While it is to be expected that the zonal mean ptp amplitude would be larger than the amplitudes observed at remote sites, the higher maximum values shown here are many times larger than those observed. This discrepancy will be discussed later when some more direct comparisons are made with the observed seasonal cycles.

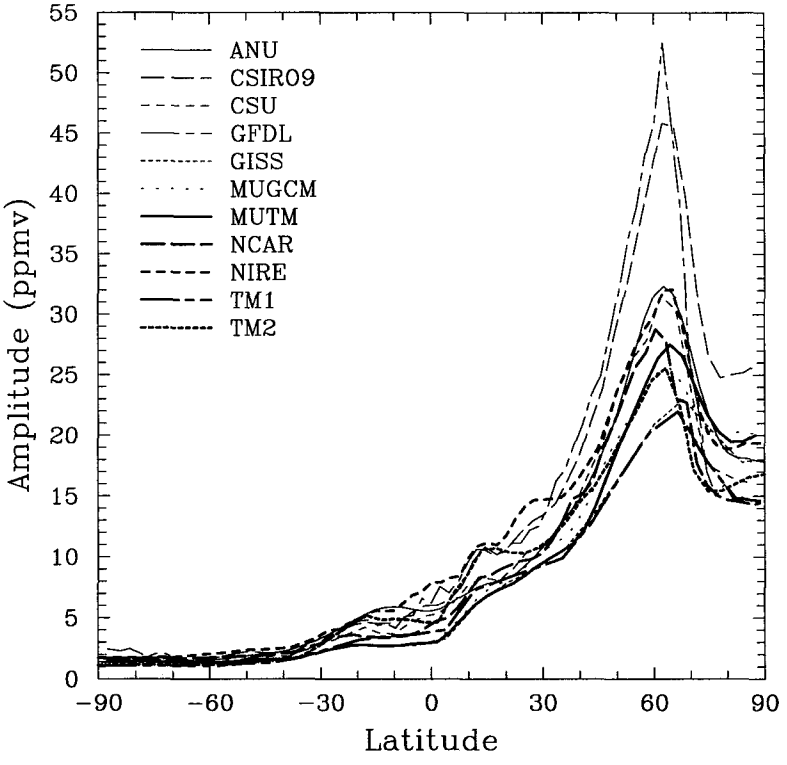

Fig 4.2: Surface zonal mean peak-to-peak amplitude for the biosphere case in ppmv.

While the CSIRO9 and MUTM models do not give the extreme values here as they did for the fossil surface zonal mean concentration, we have again run MUTM with the CSIRO9 GCM winds to understand the differences between these two model results. In this case the resulting zonal mean ptp amplitude was almost identical to that produced by MUTM through the northern mid-latitudes. This suggests that the sub-grid scale parameterisations control the amplitude of the seasonal cycle at these latitudes.

4.1.3 Peak-to-peak amplitude maps

Most models produce amplitude distributions that are broadly similar (Fig. 4.3). Land regions have higher amplitudes than ocean regions at the same latitude (except North Africa). Maximum amplitudes occur through northern Eurasia (especially around 60°N, 110°E), Alaska and Canada, China, India, tropical Africa and South America (0–40°S). This is to be expected, as these are regions where the sources have a large seasonality as seen in Fig. 2.3. For most models the Eurasian amplitudes are largest but the relative magnitude of the high amplitude regions varies between models. For example, TM2 produces maxima that are approximately the same magnitude in Eurasia, China, India and Africa whereas in the MU models the Eurasian amplitude is significantly larger than amplitudes in these other regions. In the NIRE model the maximum around China is larger than the Eurasian values.

The maximum amplitudes vary by a factor of four (30.0 ppmv for GISS compared to 127 ppmv for GFDL). As in the fossil experiment, the model resolution is apparently one factor contributing to these differences. In this case, the horizontal resolution may be less important as the original source fields are smoother (being defined on a $4° \times 5°$ grid rather than the $1° \times 1°$ grid of the fossil source). For example, the maximum source amplitude used with the GISS model is 2722 $gCm^{-2}yr^{-1}$ compared to 3170 $gCm^{-2}yr^{-1}$ for the GFDL model. These values are much closer than the almost factor of two difference in the peak value in the fossil case.

Taguchi (pers. comm.) has investigated the sensitivity to vertical diffusion strength in the vicinity of the surface in the NIRE model by changing the depth of the PBL. When the PBL depth was increased by 50 hPa the ptp amplitude over China dropped from 94 to 43 ppmv. This may also give some indication of the impact of vertical resolution on ptp amplitudes.

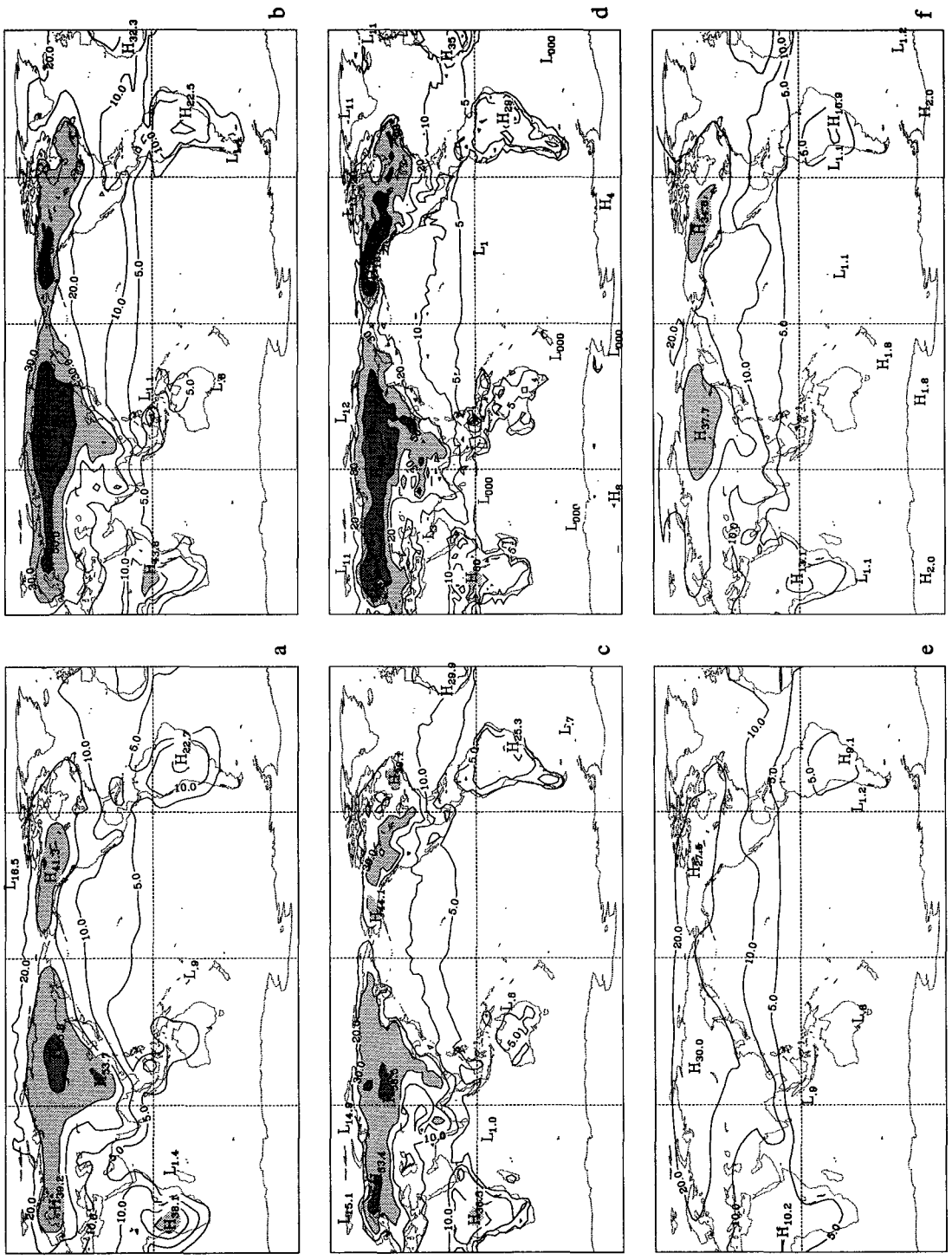

Fig. 4.3: Surface peak-to-peak amplitude for the biosphere case for (a) ANU, (b) CSIRO9, (c) CSU, (d) GFDL, (e) GISS, (f) MUGCM. The contours are 5, 10, 20, 30, 50, 75 and 100 ppmv and values greater than 30 and 50 ppmv are shaded in light and dark grey respectively.

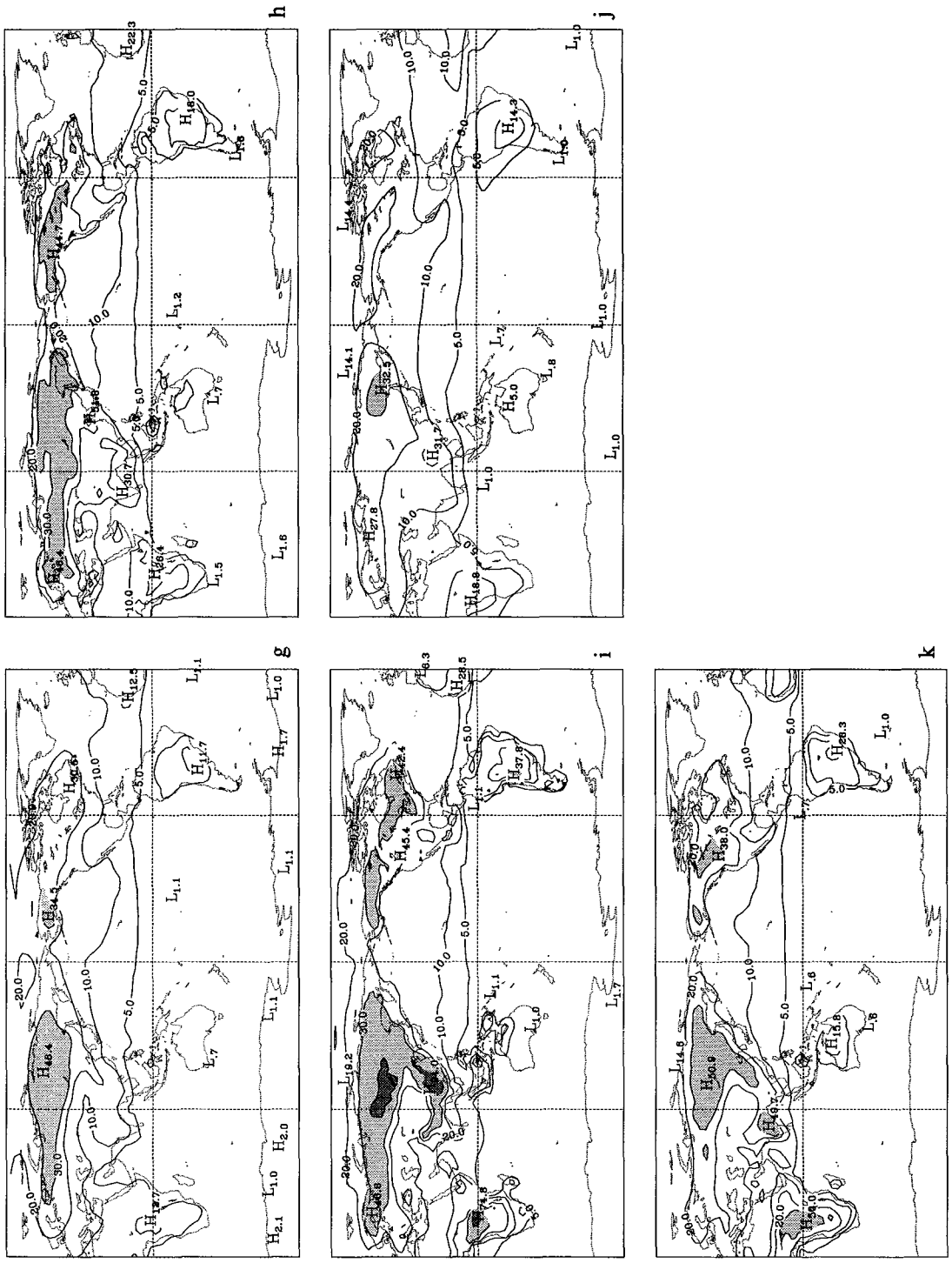

Fig. 4.3: Surface peak-to-peak amplitude for the biosphere case for (g) MUTM, (h) NCAR, (i) NIRE, (j) TM1, (k) TM2. The contours are 5, 10, 20, 30, 50, 75 and 100 ppmv and values greater than 30 and 50 ppmv are shaded in light and dark grey respectively.

4.1.4 Amplitude at monitoring sites

While there are difficulties associated with comparing modelled and observed amplitudes, such comparisons can assist in model evaluation especially in the northern extra-tropics where the biosphere is the major contributor to seasonality. As each model uses a different grid, the four nearest grid points to a monitoring site are used to interpolate to the actual location. This method does not take any account of the practice at coastal sites of measuring CO_2 from marine air, so comparison with the observations at these sites must be done with caution. Twenty-five of the NOAA/CMDL sites have been used and these are listed in appendix D. The amplitude of the seasonal cycle has been calculated as the difference between the maximum and minimum interpolated monthly mean concentration. These have been plotted in Fig. 4.4. Also shown in the figure are dashed lines indicating the ± one standard deviation range of observed amplitudes taken from Fig. 10 of Conway et al. (1994). Lines have been used only for clarity in the figure not because it is realistic to connect the values from different sites. Also for clarity the Kumakahi (KUM) and Ragged Point (RPB) data have been shifted slightly to the north and south respectively so that they do not overlay the neighbouring data.

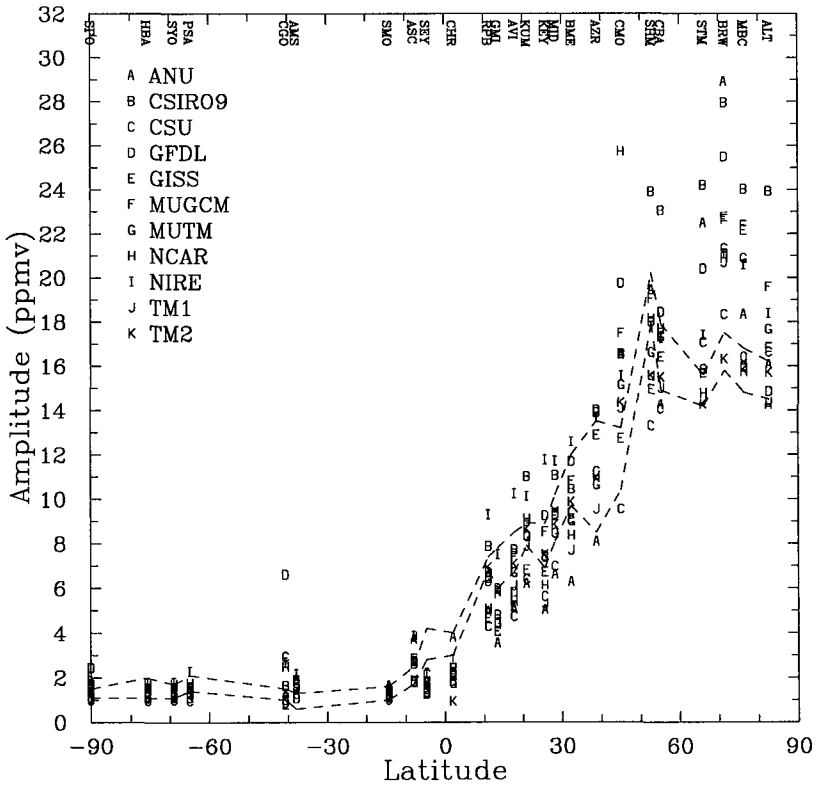

Fig 4.4: Peak to peak amplitude in ppmv at monitoring sites in the NOAA/CMDL network. The dashed lines represent the ± one standard deviation spread of the observed values which were taken from Conway et al. (1994).

The different models produce reasonably similar amplitudes in the southern hemisphere but vary quite substantially in the northern hemisphere, particularly at high latitudes. The range at these high latitudes (up to 15 ppmv) is, however, significantly smaller than the range in the zonal mean at these latitudes (up to 30 ppmv). With the exception of TM2, all models overestimate the amplitude (taken here to mean that they lie above the upper observations curve) at one or more of the four northernmost sites. Some sites are close to land and this may have an impact since we are comparing model data for all times with observed data selected for 'background' conditions. Analysis with MUTM suggests that selecting the model data for recent land content could reduce the modelled amplitude at Barrow by about 2 ppmv which would account for about half this model's difference from the observations. However, at Mould Bay and Alert a similar analysis suggested that data selection had little impact on the amplitude. It appears, then, that the tendency for most models to produce larger than expected amplitudes at these locations either indicates a potential problem with the input source or some serious problems with the modelling of tracer transport at these latitudes. We show later that source error is the more probable cause of the amplitude discrepancy.

The models perform reasonably well for Cold Bay; with the exception of the CSIRO9 model all the amplitudes are within about 1 ppmv of the observed range. At Shemya most models underestimate the amplitude while at Cape Meares the modelled amplitude is generally greater than that observed. This site is also one at which data selection could be expected to reduce the modelled amplitude. At the mid and low latitude sites of the northern hemisphere the models normally span the observations. The NIRE model is typically near the top of the range of model results while the ANU and CSU models are at the low end of the range.

Comparisons with observations are more difficult at low latitudes and in the southern hemisphere as other CO_2 sources and sinks contribute significantly to the seasonality. Thus around the equator (Christmas Island and Seychelles) all the models (except ANU at Christmas Island) produce amplitudes that are too low. This may be due to the seasonal shift of the inter-tropical convergence zone (ITCZ); each site sees air from each hemisphere at different times of the year. Since sources, such as those due to fossil fuel use, produce a significant concentration gradient between hemispheres, this will introduce an extra contribution to the seasonality at these stations. For Seychelles, the impact of fossil seasonality on the amplitude varies between models; in some cases the amplitude is doubled while in others it is virtually unchanged. In general, the addition of the fossil seasonality brings the amplitudes closer to those observed. Total agreement is not expected because contributions to the seasonality from ocean sources and sinks are still neglected. It is also worth noting that an increase in amplitude will only be achieved if the seasonalities of different sources are in phase; otherwise a reduction in amplitude may occur.

With the exception of Cape Grim, most models reproduce the observed amplitudes for the southern hemisphere sites reasonably well. We note, however, that this is without contributions to the seasonality from other sources that might be expected to be important for these low amplitude sites. The large amplitudes produced at Cape Grim by some models (especially GFDL) are almost certainly related to the influence of the Australian continent and data selection might therefore improve the results. This would tend to be confirmed by the fact that the models which give the larger amplitudes at Cape Grim all have relatively high resolutions. It would appear that the lower resolution models average out the influence of the Australian continent compared to the high resolution models.

4.1.5 Seasonal cycle at selected sites

Four locations are presented here: Barrow (71°N, 203°E), Kumakahi (20°N, 205°E), Samoa (14°S, 189°E) and South Pole (89.98°S, 335.20°E). Fig. 4.5 shows the surface monthly mean concentration for each model and the observed seasonal cycle. This is the sum of the first two harmonics of the seasonal cycle representing detrended data for 1987 and is taken from Enting et al., 1995. Before discussing each location, it is worth noting that it is not immediately obvious what constitutes good agreement between models; the large amplitude seasonality in the northern hemisphere will mask differences between models which would appear large in the southern hemisphere where the amplitudes are small. We also note that while we might expect to reproduce the observed seasonal cycles in the northern hemisphere reasonably well, this is not the case in the tropics and southern hemisphere where other processes make significant contributions to the seasonality.

The seasonal cycle simulated at Barrow is reasonably consistent among models. Concentrations are low throughout winter and increase rapidly from March to May. Maximum concentrations occur between May and June and minimum concentrations in August and September. The qualitative agreement of the models is not matched by quantitative agreement. This is particularly evident at the peaks of the cycle where concentrations span over 10 ppmv. In comparison with the observed seasonal cycle at Barrow, all models produce a maximum value which is too large and occurs too late. The winter concentrations are too low but the August-November period is reasonably simulated. Since all the models are producing similar errors, this suggests an error with the input sources rather than with the model transport, particularly as similar discrepancies are seen at most of the high northern latitude sites. Fung (pers. comm.) has indicated that low light and long pathlengths result in errors in the NDVI (and hence CO_2 fluxes) at high latitudes in spring. This illustrates the potential extra information that can be gained by running a range of transport models: had only one result been available it would be more difficult to distinguish between source and transport errors.

At Kumakahi the models produce maximum concentrations in June and minimum concentrations in September-October. The range of concentrations is largest at these times of extreme concentration. The models generally reproduce the observations reasonably well especially through the latter half of the year. In the earlier part of the year the model results tend to lag the observations. This is consistent with the errors seen at Barrow with the maximum concentrations occurring too late in the year.

The seasonal cycle at Samoa is small and somewhat variable between model results. Maximum concentrations occur between July-September (Nov for TM2) and most models produce two minima, in April and November-January. The April minimum is usually lower than the November minimum. No model comes close to representing the observed seasonal cycle because other sources contribute to the seasonality. Adding the seasonal cycle due to transport of the fossil emissions has some impact but does not clearly improve the comparison with the observations, presumably because Samoa is remote from the fossil source. It is apparent, then, that the oceans make a major contribution to the seasonal cycle at Samoa.

There is reasonable agreement between models for the South Pole with minima between February and May and maxima between September and November. There appears to be some tendency for the models to lag the observations but the magnitude of concentrations is approximately correct. The GFDL model produces a very large February concentration and the MU models are also somewhat erratic in concentration from one month to the next. This may indicate problems with polar tracer transport.

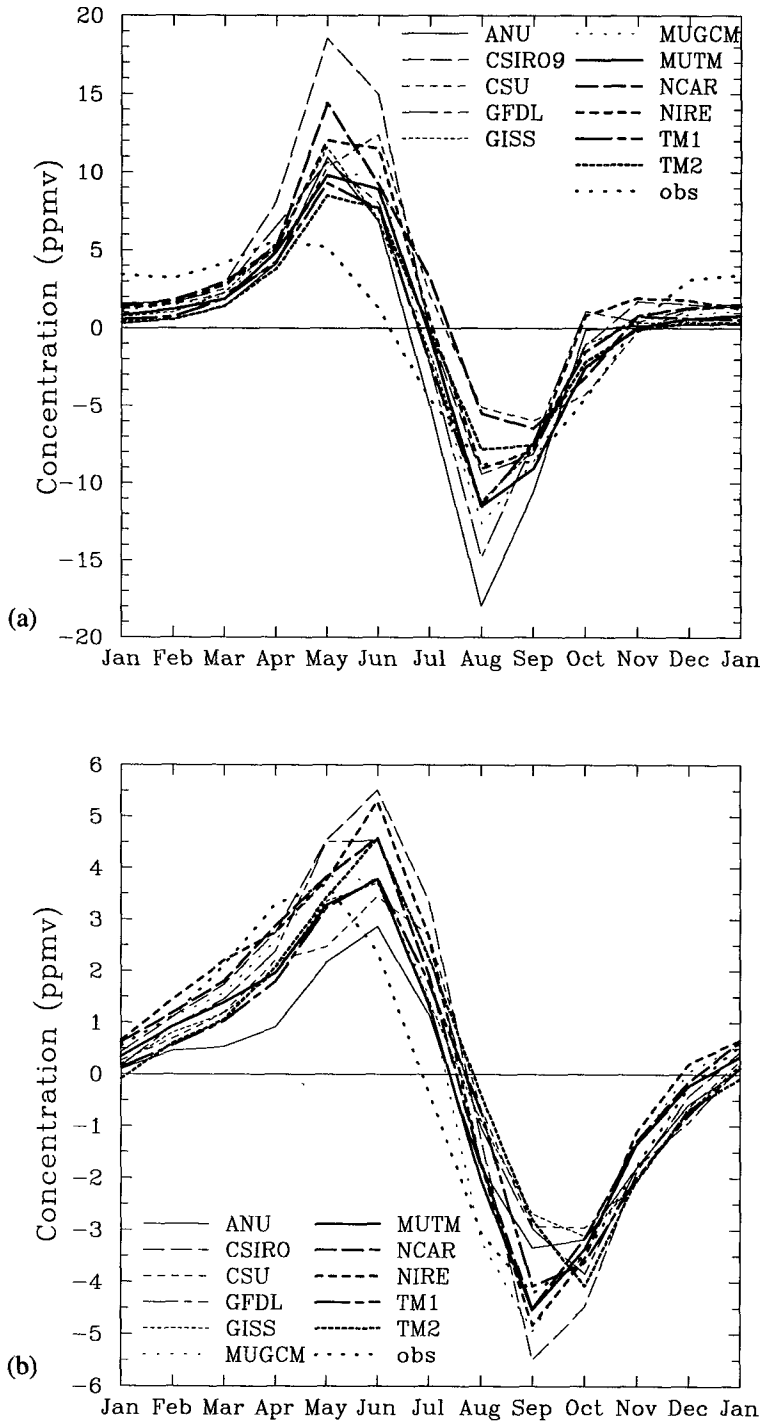

Fig. 4.5: Monthly surface mean concentration at (a) Barrow and (b) Kumakahi in ppmv.

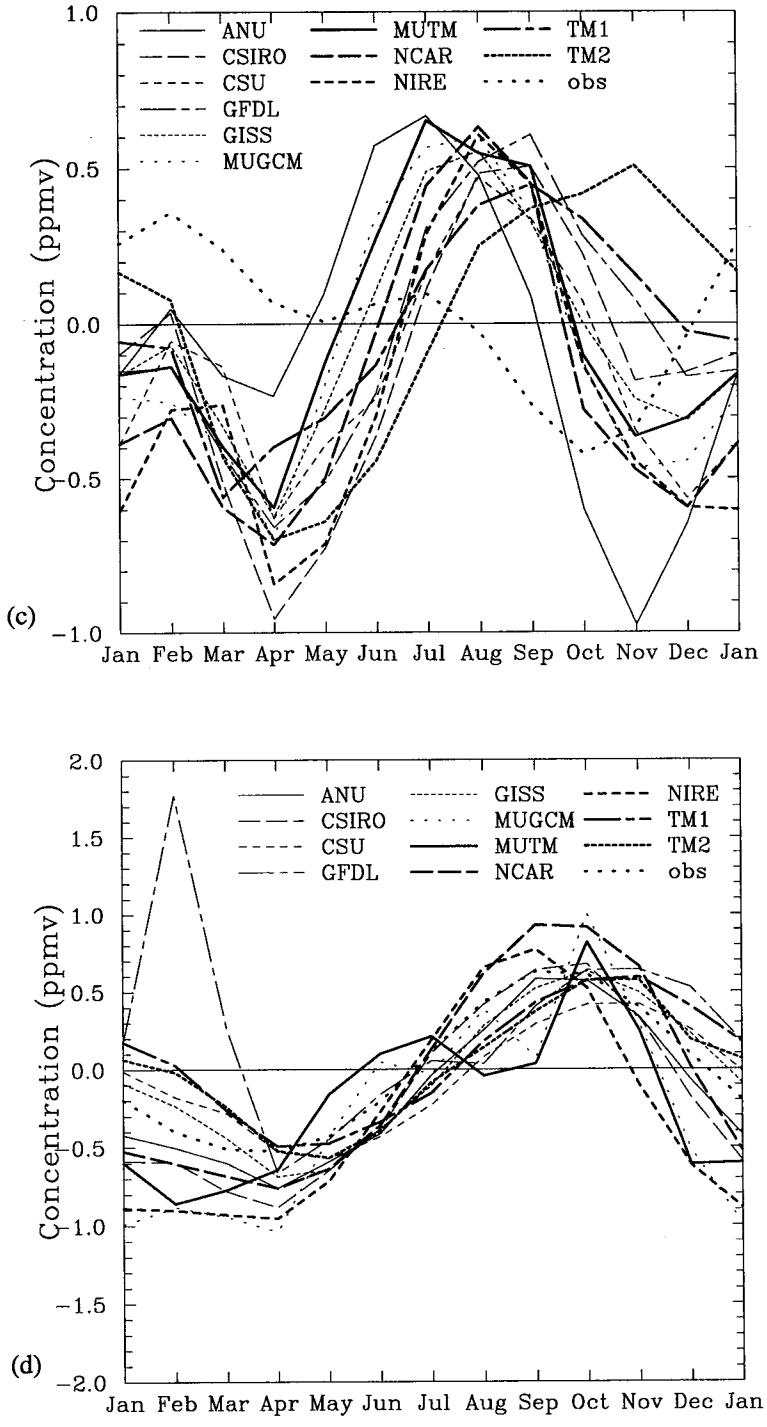

Fig. 4.5: Monthly surface mean concentration at (c) Samoa and (d) South Pole in ppmv.

4.1.6 Zonal Annual Mean

Given that the annual mean source is zero at all locations, it might have been expected that the annual mean concentration would also have been zero at all locations. However the seasonal cycle of sources combined with seasonal variations in transport results in non-zero annual mean concentrations. Fig. 4.6 shows that for some models a significant north-south CO_2 gradient is found in the annual mean. The model results tend to fall into three groups; those with relatively large northern high latitude concentrations (CSIRO9, CSU, GFDL, NCAR and NIRE), those with small concentrations through this region (GISS, MU and TM models) and the ANU model which gives moderate negative concentrations through the northern mid-latitudes. Taylor (pers. comm.) has suggested that the negative concentrations result from the use of 1980 winds at only 7 levels in the ANU model experiments reported here; small positive concentrations were obtained in subsequent experiments when winds from the 1990s at 14 or 15 levels were used. Most models also show a small local maximum near the equator.

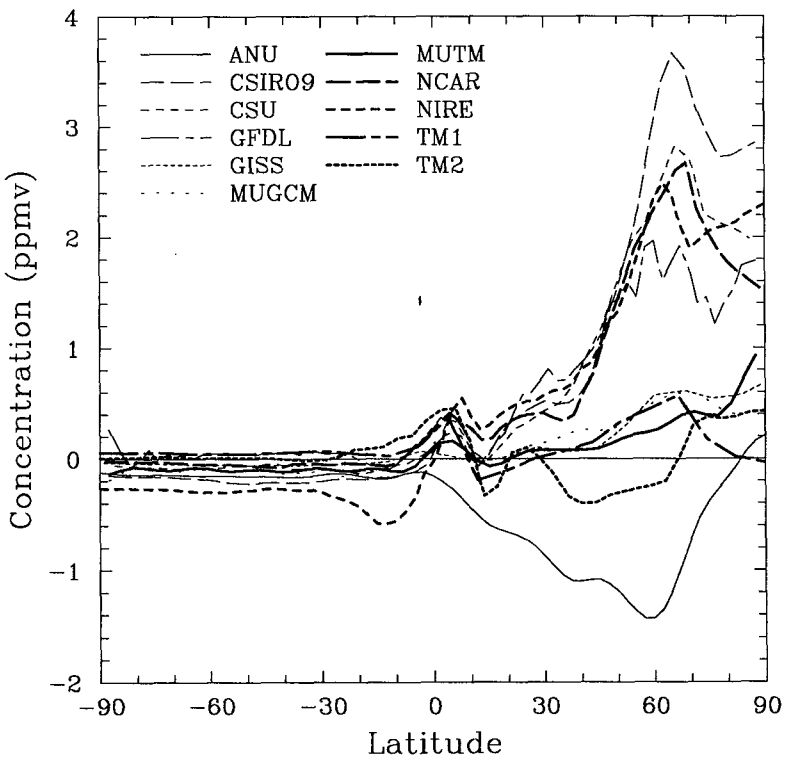

Fig 4.6: Zonal annual mean concentration in ppmv for the biosphere experiment.

Experiments with MUTM suggest that the equatorial feature is due to advection: the shift of the ITCZ means that the equator tends to see northern hemisphere air when the northern hemisphere land surfaces are a source and southern hemisphere air when the southern land surfaces are a source. Hence a positive annual mean results.

The mid-latitude behaviour appears to be dominated by vertical sub-grid scale mixing. For example, in MUTM, convection is rare over land in winter so little convective mixing

of the land sources occurs and high concentrations result. In summer convection is common over land and so the impact of the CO_2 sink at this time is mixed vertically. Thus the surface impact of the source is larger than that of the sink and a small positive concentration results in the annual mean. The opposite result produced by the ANU model is consistent with the suggestion made earlier (Sec. 4.1.1) that in the northern hemisphere the ANU model has more rapid mixing during winter/spring than during summer (which is opposite to the seasonality expected due to convection).

It is not clear whether the same process is also responsible for the large concentrations produced by the first group of models. Three of the models in this group have explicit planetary boundary layer formulations and it may be that seasonality of the PBL depth combined with seasonality in the sources and sinks contributes to the positive annual mean. This has been shown by Denning et al. (1995) for the CSU model and is confirmed by Taguchi (pers. comm.) who found that the NIRE north-south gradient was reduced when the model's PBL depth was increased by 50 hPa. A variable PBL depth is likely to have most impact in winter when a shallow PBL would result in high concentrations. This is seen in Fig. 4.1a where between November and May the 'large annual mean gradient' models give northern hemisphere concentrations that are at least 0.5 ppmv higher than the other models. The ability to resolve changes in vertical mixing due to the diurnal cycle may also be important.

4.2 500 hPa

4.2.1 Hemispheric means

Monthly mean concentrations for the northern and southern hemispheres at 500 hPa are shown in Fig. 4.7. In the northern hemisphere the seasonality is similar to that found at the surface but with reduced amplitude and a lag of up to a month. The reduction in amplitude from the surface is typically by about 40% but varies from 20–55%. There is less variability between models at 500 hPa than at the surface as was seen previously in the fossil case. The two models that are most different are the ANU model with smaller than average amplitude and the GISS model with larger than average amplitude.

In the southern hemisphere the maximum concentration occurs approximately one month earlier at 500 hPa than at the surface. The minimum concentration however occurs during the same month or slightly later than at the surface. The amplitude decrease produced by the models is not as large as in the northern hemisphere (typically 30% rather than 40% with a range of 10–60%). The largest variation among models is in the southern spring and summer; the TM models lag the other results with maxima in September and October rather than August. These models also produce only one minimum whereas most other models give minima in March-April and December.

4.2.2 Zonal mean peak-to-peak amplitude

All models produce a similar latitudinal distribution of zonal mean ptp amplitude at 500 hPa (Fig. 4.8). In the southern hemisphere amplitudes range between about 1 and 3 ppmv with a slight increase in amplitude around 20°S (except ANU). Between the equator and 60°N, amplitudes increase rapidly while north of 60°N, the amplitudes continue to rise but more slowly. In this Arctic region the model results (except ANU) form two clusters (the CSU, GFDL, GISS and MU models; the CSIRO9, NCAR, NIRE and TM models).

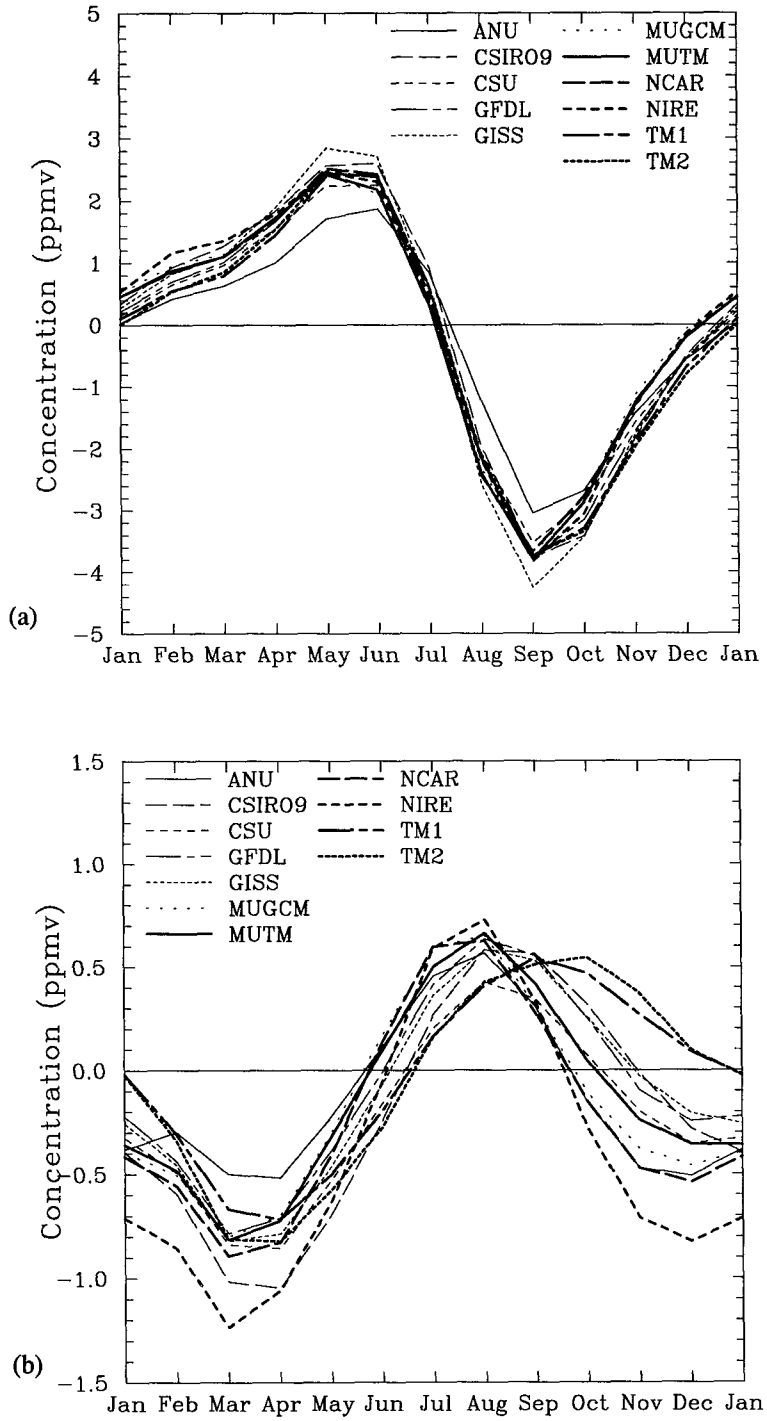

Fig. 4.7: 500 hPa mean concentration for (a) the northern hemisphere and (b) the southern hemisphere for the biosphere case in ppmv.

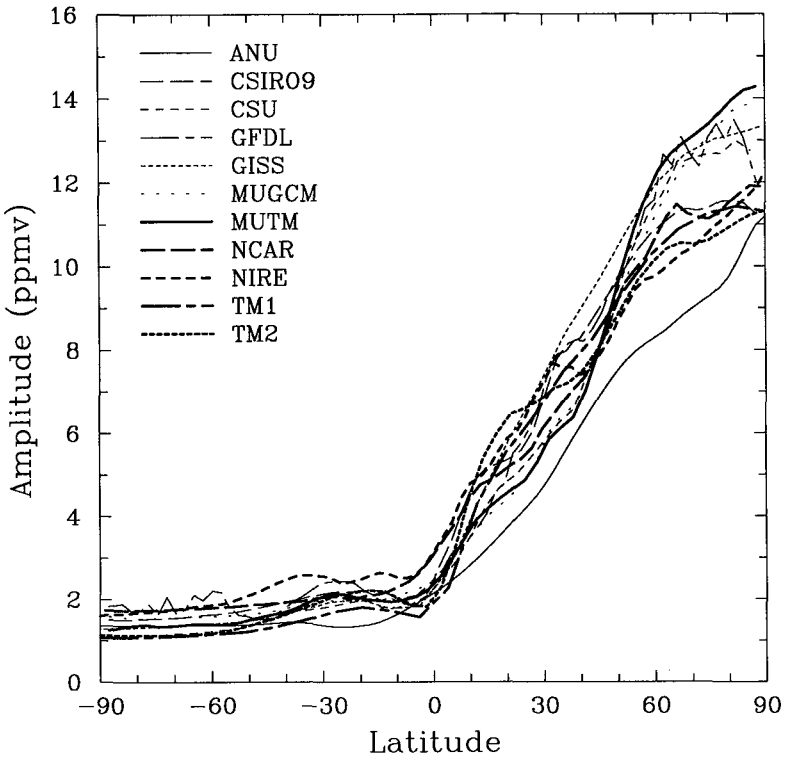

Fig 4.8: 500 hPa zonal mean peak-to-peak amplitude

The ratio of 500 hPa to surface amplitude (not shown) gives some indication of how rapidly the amplitude decreases with height at different latitudes. South of 30°S the ratio is close to one for almost all models and then drops rapidly. At the equator the models are divided into two groups; the GISS, MU and NCAR models produce a ratio of about 0.7 while the other models give a ratio of around 0.4. All models give their lowest ratio around 60°N (ranging from 0.25 to 0.55) which would be expected since this is where the surface amplitudes are largest. The smallest ratios are produced by the models that give the largest amplitudes at this latitude. The ANU ratio is significantly smaller than the other models between 10 and 40°S. An anomalous result was also seen for this model in the fossil experiment for the surface to 500 hPa difference in this region.

4.2.3 Maps of peak-to-peak amplitude

A number of common features are evident in the maps of 500 hPa ptp amplitude which are worth noting (Fig. 4.9). The Tibetan Plateau region is an area of above average amplitude for that latitude. This is particularly noticeable in the CSIRO9, MUGCM, NCAR and NIRE models. The higher amplitudes may be due to the close vicinity of 500 hPa to the surface in this region. High amplitudes are not seen in this region in the ANU model possibly because that model uses constant pressure surfaces rather than the σ surfaces used by the other models. A second feature common to many of the model results is the higher amplitudes extending towards the east from the southern African and South American continents. This gives some indication of the extent of the influence of continental air on the surrounding region.

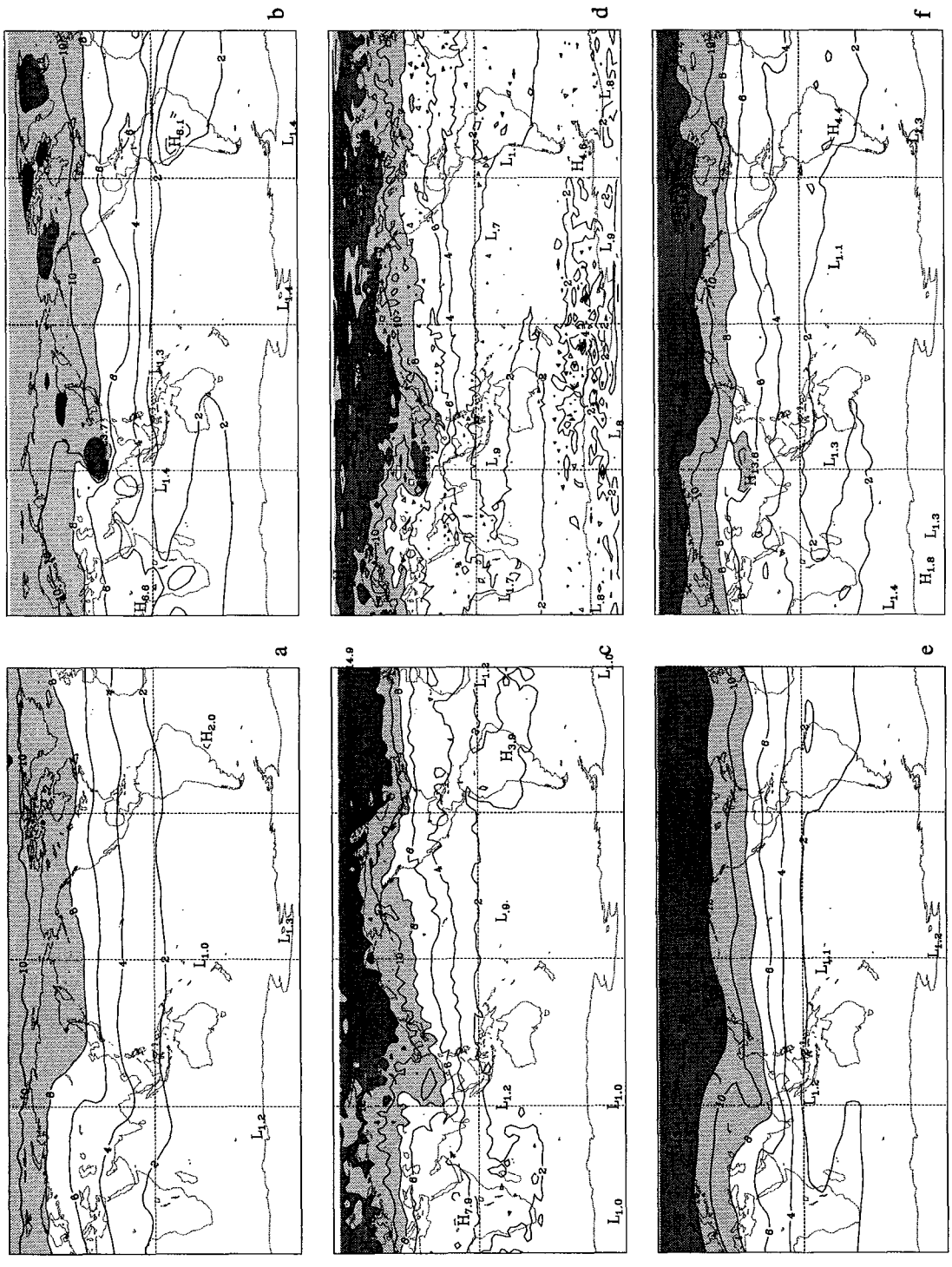

Fig. 4.9: 500 hPa peak-to-peak amplitude for the biosphere case for (a) ANU, (b) CSIRO9, (c) CSU, (d) GFDL, (e) GISS, (f) MUGCM. The contours are 1, 2, 4, 6, 8, 10, 12, 16, 20, and 24 ppmv and values greater than 8 and 12 ppmv are shaded in light and dark grey respectively.

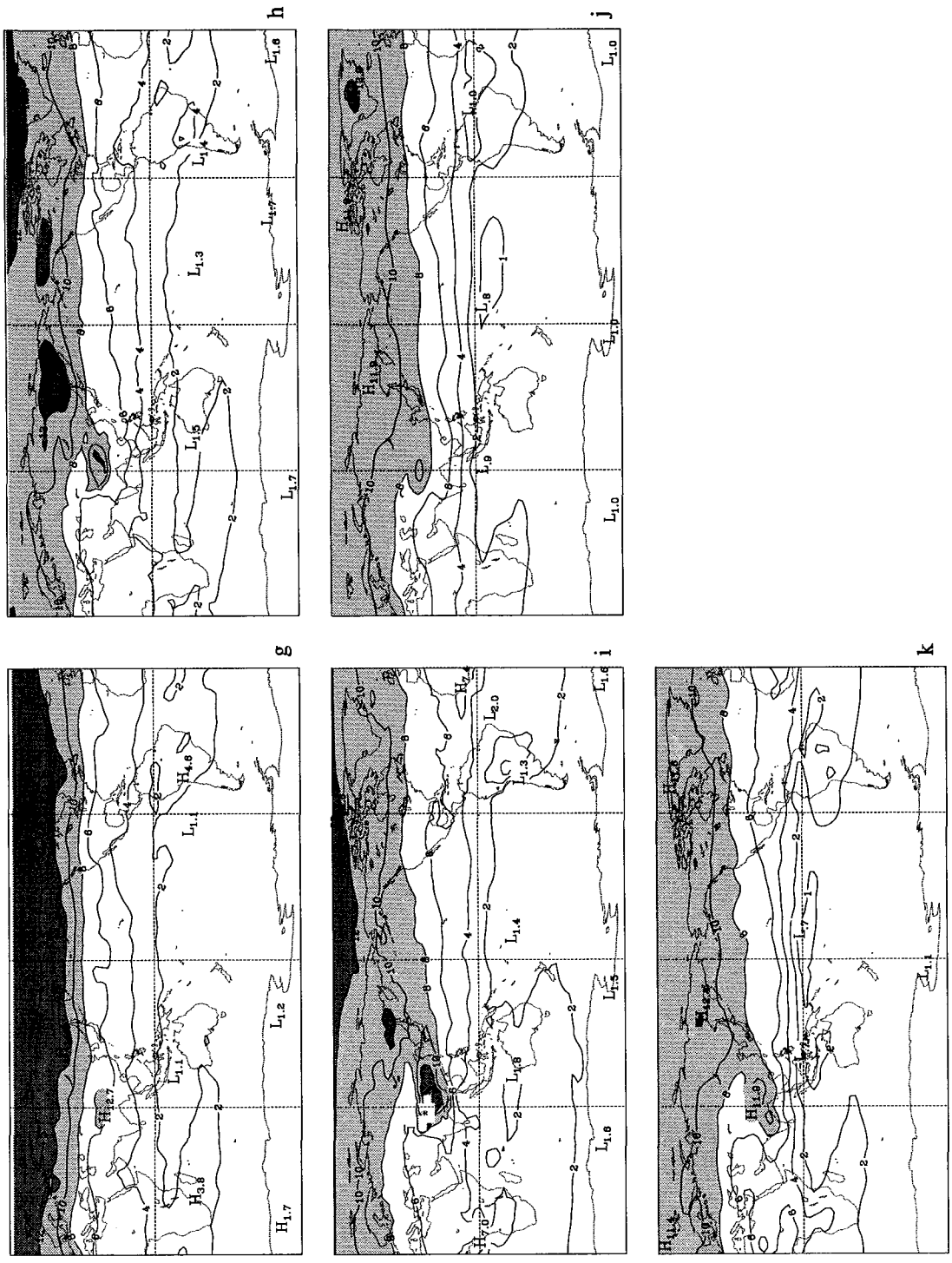

Fig. 4.9: 500 hPa peak-to-peak amplitude for the biosphere case for (g) MUTM, (h) NCAR, (i) NIRE, (j) TM1, (k) TM2. The contours are 1, 2, 4, 6, 8, 10, 12, 16, 20, and 24 ppmv and values greater than 8 and 12 ppmv are shaded in light and dark grey respectively.

4.3 200 hPa

4.3.1 Hemispheric means

The hemispheric means at 200 hPa are shown in Fig. 4.10. In the northern hemisphere there is some phase lag from 500 hPa and a continued decrease in amplitude. The models show a larger spread of results than at 500 hPa. As at 500 hPa the GISS model produces larger extremes than the other models while the CSIRO9, GFDL and MUGCM models produce below average amplitudes.

The two minima seen at 500 hPa in the southern hemisphere means are more pronounced at 200 hPa with only the GISS and TM2 models not showing a November-December minimum. An experiment with MUTM using only southern hemisphere biosphere sources produces minimum concentrations in April and maximum concentrations in November. This indicates that the southern hemisphere means at 200 hPa are being significantly influenced by the northern hemisphere sources; the maximum concentrations around August and minimum concentrations around November seen in Fig. 4.10b occur only one to two months later than the maxima and minima in the northern hemisphere. This suggests that transport between the hemispheres is relatively fast at this altitude.

The decrease in amplitude between 500 and 200 hPa in the southern hemisphere varies amongst the models, some (ANU, CSU, GISS) produce almost no decrease while others (CSIRO9, GFDL, NIRE) give decreases of around 50%.

4.3.2 Zonal mean peak-to-peak amplitude

As for the fossil 200 hPa annual mean, the ptp amplitude at 200 hPa (Fig. 4.11) shows reasonable agreement amongst models in the southern hemisphere but a wide range of responses in the northern hemisphere. Through the southern hemisphere, the amplitudes are small, increasing slowly between 30°S and the equator. The GFDL model produces relatively high amplitudes over Antarctica which are believed to be related to known problems with tracer transport around Antarctica in this model.

In the northern hemisphere, most models give a maximum around 15–30°N with either approximately uniform or decreasing amplitudes north of this region. The exceptions are the CSU model which produces a maximum around 50°N and the ANU and GISS models which give increasing amplitudes through to 90°N. Thus at the North Pole, amplitudes vary from 1.8 (MUGCM) to 8.6 ppmv (GISS). The most probable cause of this difference is whether the 200 hPa surface is more often in tropospheric or stratospheric air in any given model (since amplitudes in the lower stratosphere are expected to be substantially smaller than in the upper troposphere).

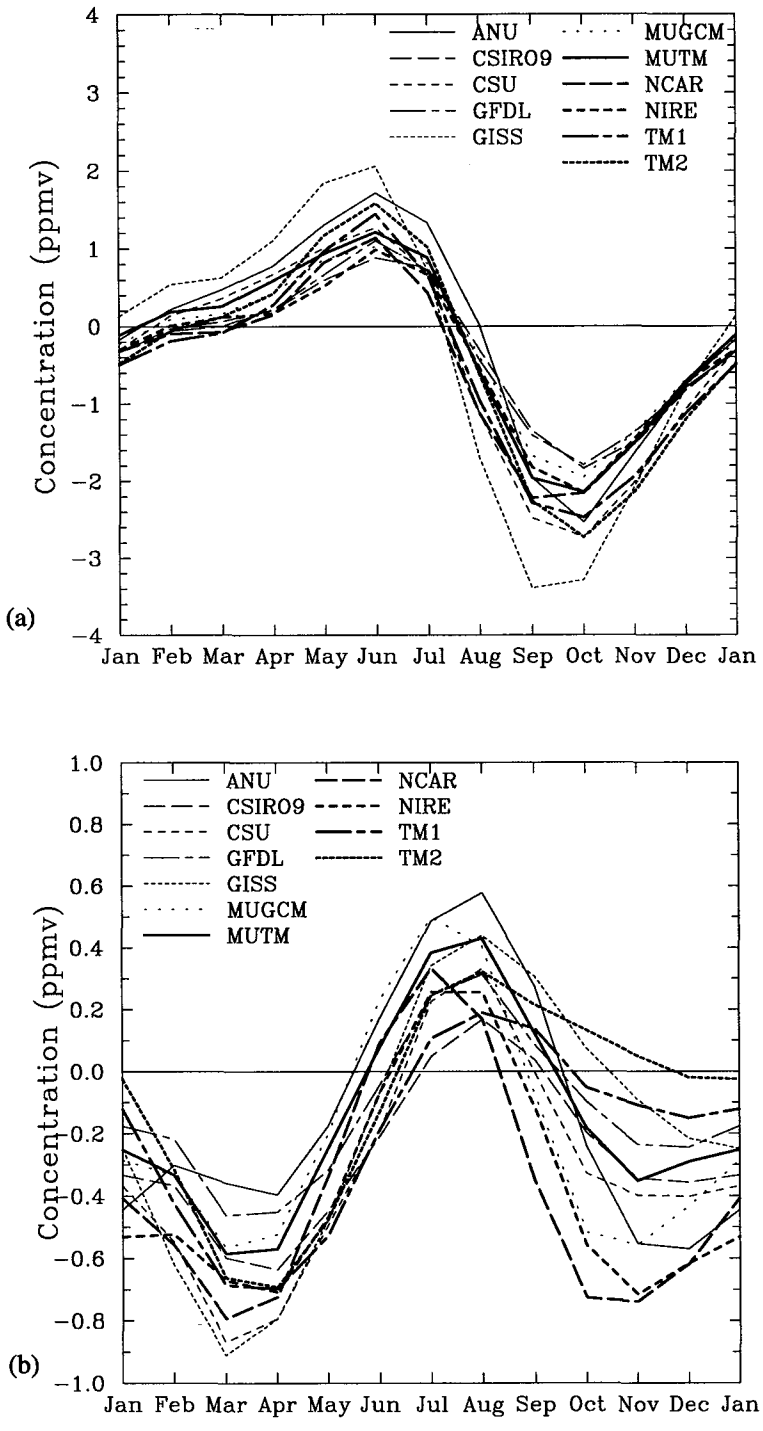

Fig. 4.10: 200 hPa mean concentration for (a) the northern hemisphere and (b) the southern hemisphere for the biosphere case in ppmv.

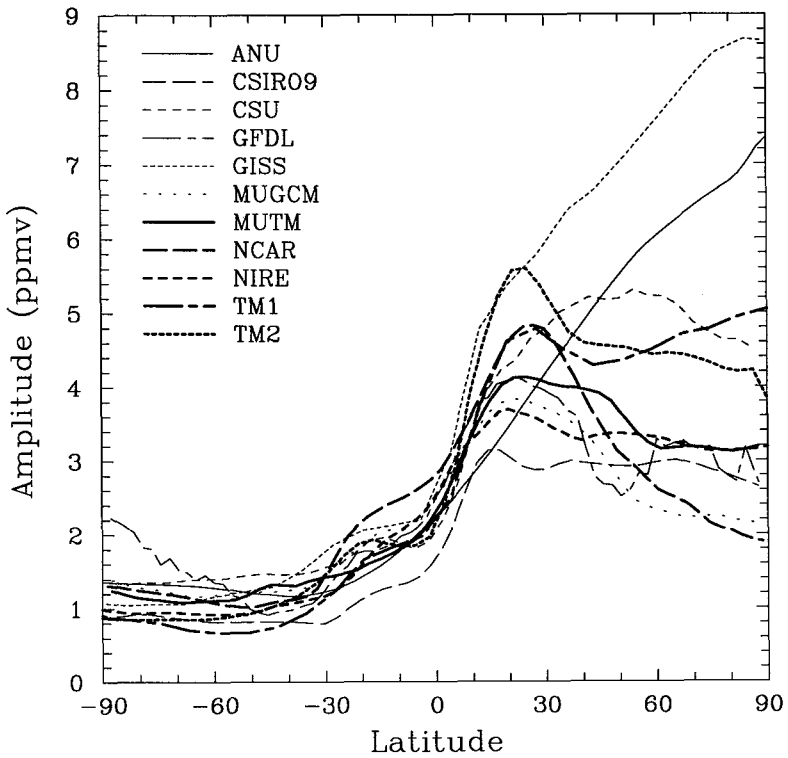

Fig 4.11: 200 hPa zonal mean peak-to-peak amplitude in ppmv.

4.3.3 Maps of peak-to-peak amplitude

The range of results seen in the zonal mean is accentuated in the maps of 200 hPa ptp amplitude (Fig. 4.12). The location of maximum amplitude varies between models but common regions of locally higher amplitudes include China to north India, tropical Africa and tropical South America. It is possible that lower tropospheric air with high amplitudes is lifted to these regions by convection. All models give some regions, predominantly tropical, where the amplitudes are higher at 200 hPa than at 500 hPa. Some models produce large amplitudes at high latitudes perhaps due to a relatively high (or weakly defined) tropopause.

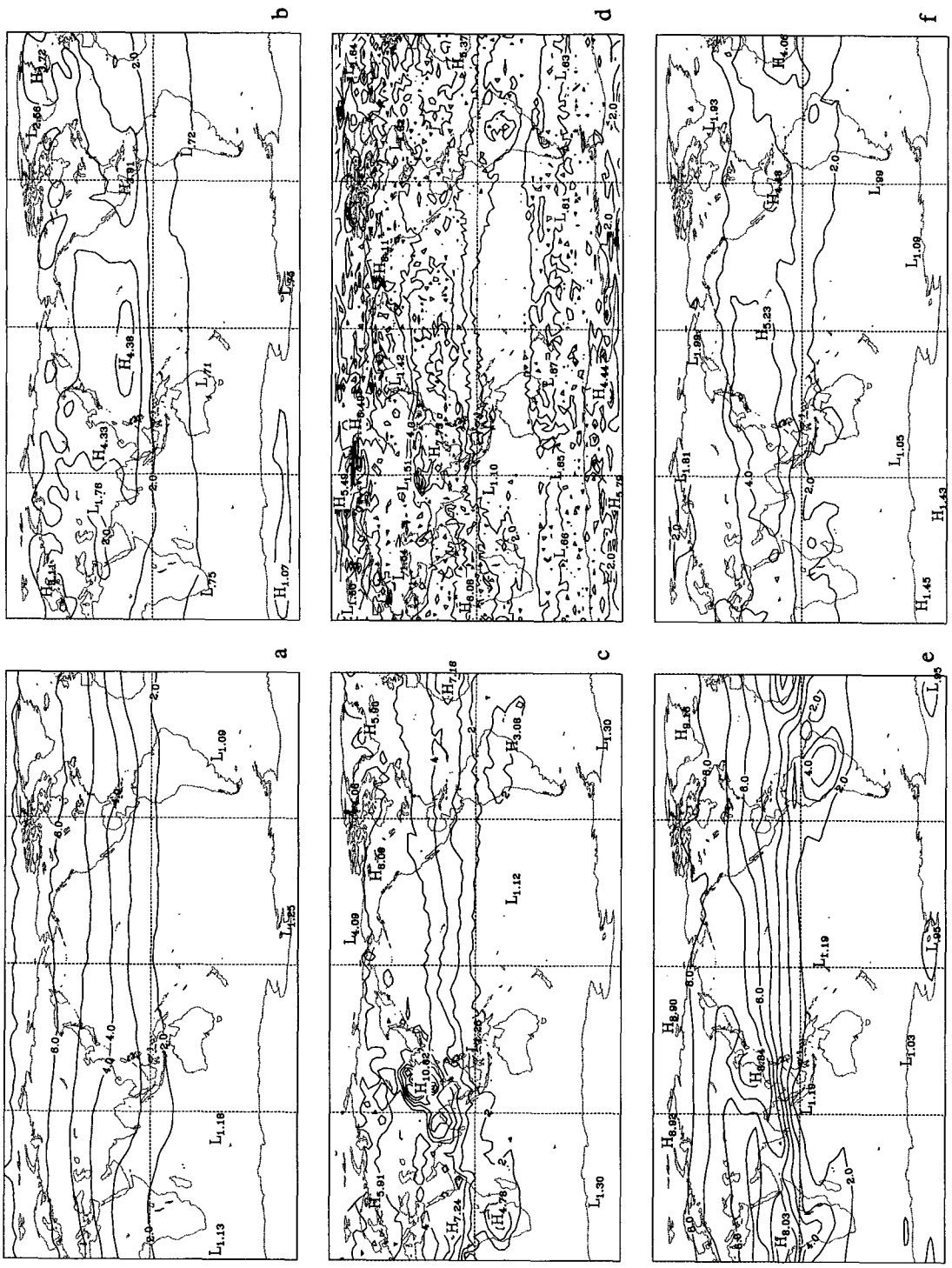

Fig. 4.12: 200 hPa peak-to-peak amplitude for the biosphere case for (a) ANU, (b) CSIRO9, (c) CSU, (d) GFDL, (e) GISS, (f) MUGCM. The contour interval is 1 ppmv.

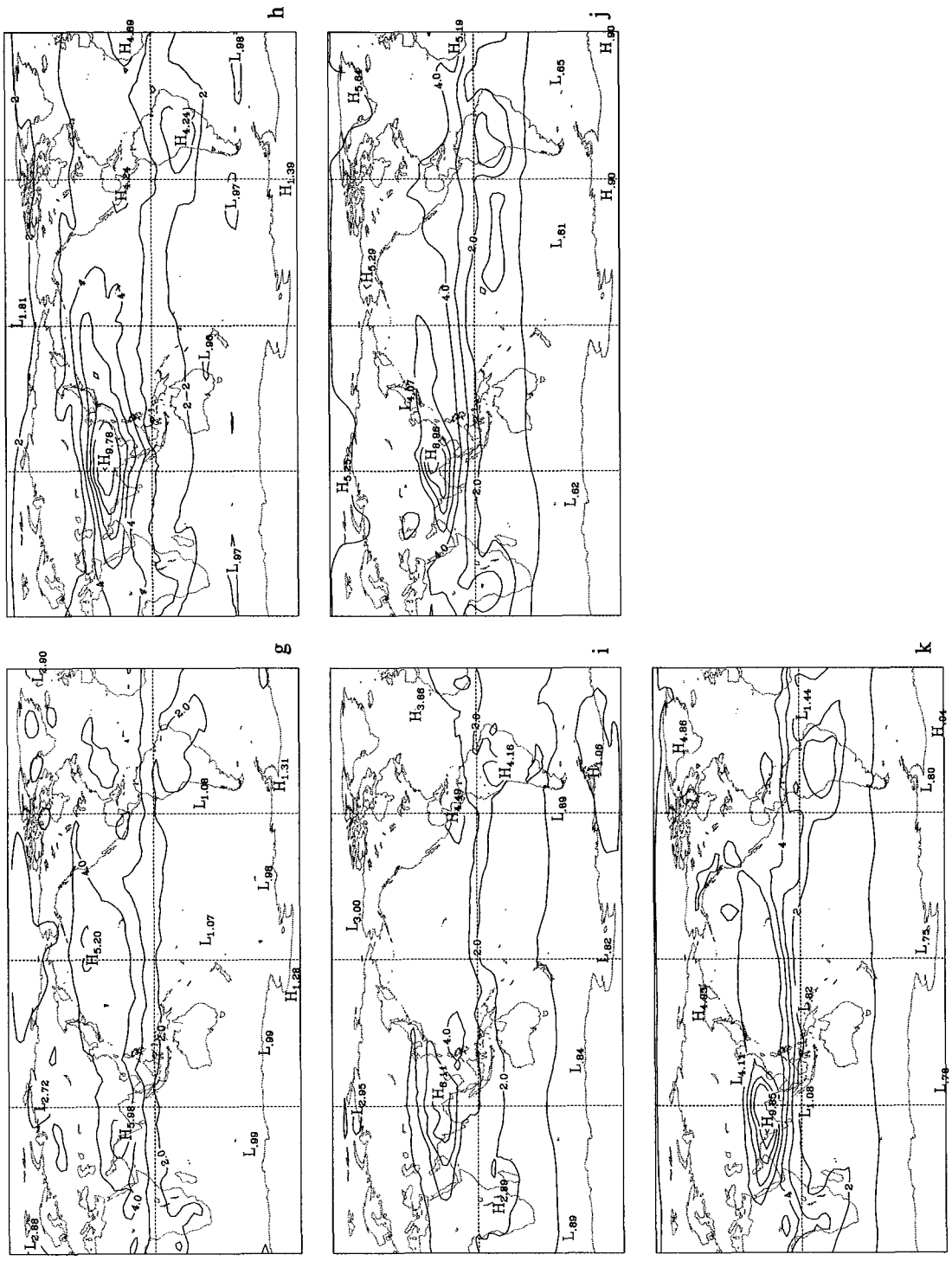

Fig. 4.12: 200 hPa peak-to-peak amplitude for the biosphere case for (g) MUTM, (h) NCAR, (i) NIRE, (j) TM1, (k) TM2. The contour interval is 1 ppmv.

4.4 Peak-to-peak amplitude cross-sections

Cross-sections of ptp amplitude are shown in Fig. 4.13 for the eight models for which data were available. Note that the amplitudes are calculated from zonal mean concentrations which slightly underestimates the zonal mean of amplitudes calculated at each longitude. Maximum amplitudes occur at the surface around 60°N in all models. At this latitude the amplitudes decrease relatively uniformly through the low and mid-troposphere. In the tropics the amplitudes show little decrease with height. A noticeable feature of all the cross-sections is that the 2 and 3 ppmv amplitude contours do not extend into the southern upper troposphere. This contrasts with the annual mean fossil cross-sections where a number of contours did extend into this region from the northern hemisphere. The monthly southern hemispheric means at 200 hPa have already shown that there is significant transport of northern hemisphere air into the southern hemisphere at these altitudes. Thus, it would appear that the lack of penetration of high ptp amplitudes into the southern hemisphere is due to some 'cancellation' between the different seasonalities of the two hemispheres. It is worth noting in this context that Nakazawa et al. (1991) found seasonal amplitudes of 2–3 ppmv between the equator and 30° S for upper tropospheric aircraft observations on flights between Japan and Australia. These are significantly larger than produced by any of the models. Seasonality from the fossil experiment does not appear to make a significant contribution in this region.

The southern hemisphere distributions produced by the models suggest that the biospheric signal from the southern low latitude continents is being transported upwards and southwards. The magnitude of this feature varies between models and may be at least partly resolution dependent; the NIRE model gives large areas of the southern troposphere with amplitudes above 2 ppmv compared with relatively small regions in the GISS and TM1 models.

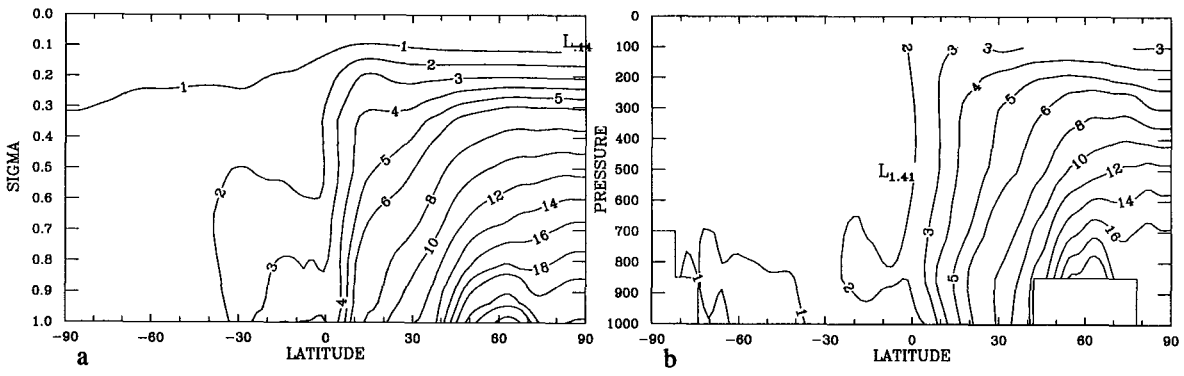

Fig. 4.13: Zonal mean peak-to-peak amplitude for the biosphere case for (a) CSIRO9 and, (b) CSU. The contours are 1, 2, 3, 4, 5, 6, 8, 10, 12, 14, 16, 18, 20, 25, 30, and 40 ppmv.

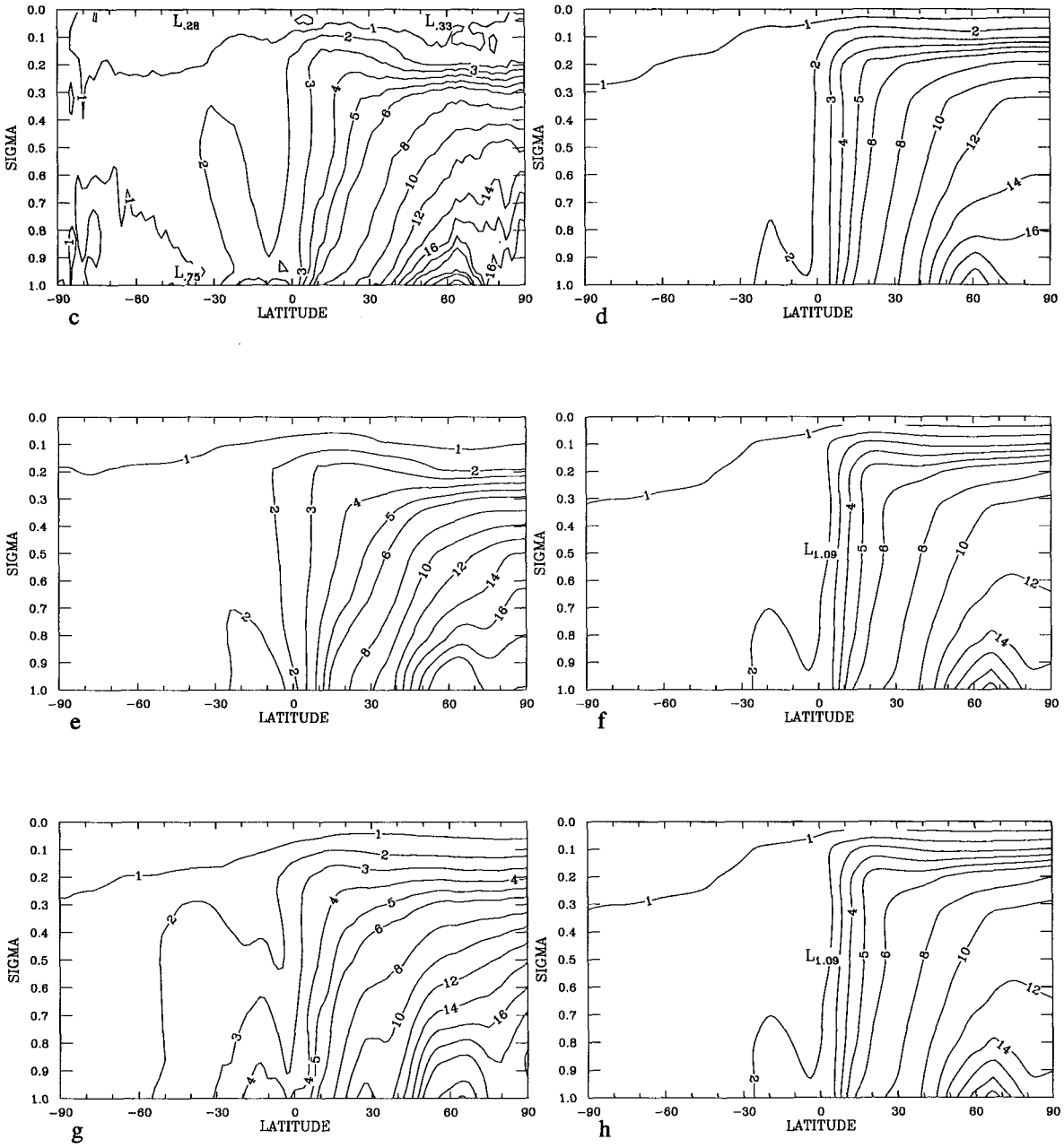

Fig. 4.13: Zonal mean peak-to-peak amplitude for the biosphere case for (c) GFDL, (d) GISS, (e) MUGCM, (f) MUTM, (g) NIRE and (h) TM1. The contours are 1, 2, 3, 4, 5, 6, 8, 10, 12, 14, 16, 18, 20, 25, 30 and 40 ppmv.

5 Discussion

In this section we attempt to distill some of the information presented in the previous two sections. We do not seek an explanation of the transport characteristics of each model in terms of its dynamics and physics. Such an explanation is beyond the scope of this report and requires complete access to model codes and data. In many cases our discussion will be necessarily qualitative although we will endeavour to support the conclusions with simple quantities derived from the submitted data.

The general qualitative similarity of the modelled responses to prescribed sources is not surprising. Transport is generally down gradient which produces maxima in the vicinity of the sources decreasing in all directions. This is seen in both horizontal and vertical planes in Figs. 3.2 and 3.9. Different efficiencies for the transport in different models mean that, remote from the sources, even the qualitative agreement may break down. This is seen in Fig. 3.9 (at the upper levels) and more clearly in Fig. 3.6.

5.1 Measures of large-scale transport

It is difficult to characterize simply the range of behaviour evident in the results of sections 3 and 4. Also our chosen sources are relatively complex for this kind of analysis. We show here (Table 5.1) the exchange time as a measure of large-scale exchange. We define the exchange time as the steady-state difference between concentrations in two boxes divided by half the difference in source strength between the boxes. Note that we are using concentration rather than loading so that sources are expressed in concentration trends per year for the relevant box. This time is closely related to the relaxation time of the concentration difference between the two boxes. In the case of boxes of equal size (such as for interhemispheric exchange) this is the classical exchange time as used, for example, by Weiss et al. (1983).

It is common to use fluxes as measures of efficiency of transport. In this steady state experiment, where sources and growth rates are in equilibrium, model fluxes are identical. The exchange time reveals what gradient is necessary to produce such a flux.

There is a wide variety of partitions of the atmosphere available for a calculation of exchange times. In this case we choose hemispheric surface means, hemispheric three-dimensional means and vertical exchange across the σ=0.2 level. All times are derived from the fossil experiment and use annual mean concentration differences. The calculation requires a difference in annual mean source between the boxes and so is meaningless for the biota case which has an annual mean source of zero everywhere. Note that all quantities are only available for the models which submitted cross-section data in a form allowing calculation of vertical integrals.

It is clear from a comparison of Fig. 3.9 and Table 5.1 that the large-scale exchange times are useful summary quantities for the large-scale structure of the model response. Evident from Table 5.1 is not only a large range of exchange times (already obvious from the measures of large-scale differences) but also great differences in the relationships of different rates within the same model. For example, the GFDL model, which shows the second slowest exchange between surface boxes has the third quickest exchange between vertically integrated hemispheric boxes. Also, among the three models which supplied cross-section data and used analyzed winds from ECMWF, the surface exchange times are more closely grouped than the vertical mean exchanges.

Vertical exchange rates across σ=0.2 are even more variable than between hemispheres.

Model	inter-hemispheric		across
	surface	vertical	$\sigma = 0.2$
ANU	1.16	-	-
CSIRO9	2.14	1.16	1.82
CSU	1.54	0.99	-
GFDL	1.76	0.82	2.02
GISS	1.26	0.9	0.84
MUGCM	1.06	0.58	1.54
MUTM	1.06	0.66	1.1
NCAR	1.38	-	-
NIRE	1.50	0.92	1.0
TM1	1.58	1.2	0.72
TM2	1.52	-	-
TM2Z	1.46	1.06	0.42

Table 5.1: Exchange times in years for transport between various atmospheric boxes in the fossil experiment. The exchange time is defined as the difference between the means in the relevant boxes divided by half the difference in source strength between them.

This is a confirmation of the apparent differences shown in Fig. 3.9. While it is tempting to associate these differences with different rates of stratosphere-troposphere exchange, the choice of an arbitrary σ value rather than some attempt to define the tropopause makes this difficult.

Models with relatively coarse vertical resolution in the stratosphere like those used in TRANSCOM are unlikely to be used for detailed studies of stratosphere-troposphere exchange or any stratospheric process. However the wide difference in vertical transport efficiency even at this level is an important determinant of large-scale horizontal structure. Models with slow vertical exchange must necessarily conduct most of their horizontal transport lower in the atmosphere since horizontal gradients will be suppressed aloft.

5.2 Comments on model performance

It was never the aim of TRANSCOM to provide a detailed assessment of relative model performance among submitted models: CO_2 is clearly the wrong tracer for this purpose. This is fortunate since the results of Sections 3 and 4 and the summary results in Table 5.1 do not give strong guidance. In a following section, we shall use what consensus *is* available from the submitted results as a guide in reducing the apparent range of responses. We shall also make an attempt to interpret the large departures of some models or groups of models from this consensus.

We should stress at the outset that no model lies at the extremes in all cases. Indeed, agreement in one field is no indication of agreement in others, e.g. models which produce quite similar structure at the surface may vary away from it. The ANU model surface exchange time lies comfortably within the range of most of the models. Yet, at 500 hPa it produces a north-south gradient considerably weaker than any other model (see Fig. 3.5). For

surface exchange time, it is CSIRO9 and GFDL which are outliers, contributing almost an extra 50% in the range. The same phenomenon of relatively similar behaviour in one aspect and large differences in another has already been commented on with the TM models. These produced similar exchange times between hemispheric surface boxes but different exchange times for vertically integrated boxes.

While the broad range of results and lack of clear relationship among them poses serious problems, the similarity of two sets of results is encouraging. These are the MUGCM and MUTM results. These results are very similar in almost all aspects and, in the context of the model-model differences in other cases, almost identical. The similarity confirms that it is possible to build an offline model which accurately mimics its online counterpart. This has practical implications for building computationally inexpensive tracer models. More importantly it suggests that, with the use of good analyses, and improved understanding of the role of physical processes in transport, offline models may be good analogues for the real atmosphere.

5.2.1 Behaviour of differences with height

Comparison of Figs. 3.5 and 3.7 (the 500 and 200 hPa fossil distributions) yields a result which is, at first glance, quite surprising. There is a greater variety of model response at 200 hPa than at 500 hPa. This is surprising since the structure of most modelled fields becomes more washed out with height. Hence the behaviour of model-model differences is opposite to that of the models themselves. The ramifications of the different behaviour at these two levels depend entirely on the use to which any potential future data would be put. If the aim is to use such data in inversion studies then data may well be more useful at 500 hPa. This follows from the assumption that, in the absence of data against which to calibrate models and directly quantify model error, model-model differences are the best measure we have of model uncertainty. Thus fields which display relatively little model-model difference are perhaps best suited for use in inversions. On the other hand, if there is a desire to differentiate the behaviour of one model from another the 200 hPa field (which shows more of this difference) will be more useful. As mentioned, the individual models do not show correspondingly more detailed structure at 200 hPa so the model-model differences should be more easily detectable.

5.3 Understanding some differences

In this section we will comment on some of the differences displayed in earlier sections. Our comments are necessarily partial. In particular, we rely on some auxiliary experiments either performed locally or reported to us but not part of the TRANSCOM archived data. Some of these have already been mentioned in sections 3 and 4 but it is worthwhile to focus on them here.

5.3.1 Control by large-scale wind or physical processes

To understand some of the large differences between the CSIRO9 and MUTM results, we repeated the two TRANSCOM experiments using a hybrid model in which MUTM was forced with CSIRO9 winds rather than its usual MUGCM winds.

The results can be summarized as follows. The surface IHD for the fossil hybrid was midway between that for CSIRO9 and MUTM. The vertically integrated IHD was within 0.1 ppmv of CSIRO9. The ptp amplitude in the biosphere case resembled that of MUTM at its maximum values in the northern hemisphere.

The vertically-integrated IHD result quoted above is quite striking. It suggests that, in a vertically and hemispherically integrated sense, the hybrid model behaves like CSIRO9. This is despite the fact that the advection algorithm is that of MUTM (spectral versus semi-Lagrangian) and that the vertical processes which transport tracer from the source regions to the regions of most active interhemispheric transport are those of MUTM. This suggests that the large-scale horizontal wind (vertical wind is diagnosed separately by each model) is the dominant controlling influence on large-scale horizontal transport. At the surface it appears to explain about half the difference between the models.

There is further partial support for the suggestion that the large-scale wind may play a dominant role in the large-scale horizontal transport from four of the models using ECMWF analyses. As we already noted these produce a fairly narrow clustering of results for surface IHD. This is only partial support since their vertically integrated behaviour is not so tightly grouped. Even for the vertically integrated IHD the three models for which we had data (NIRE, TM1 and TM2Z) occupy only half the range of results despite spanning the full range of resolution and using very different specifications for advection and physical processes.

These results are encouraging since they suggest that model-model differences are not merely numerical artifacts but may well result from differences in large-scale wind forcing. The result should be contrasted with the case of the GISS model used by Prather et al. (1987) in which a horizontal diffusion parameterisation, keyed to deep convection, played a major role in horizontal transport.

The second experiment, in which the hybrid model was run with the vegetation source, is equally instructive. It suggests that the processes for redistributing tracer vertically (in this case vertical diffusion, and dry and moist convection) play the dominant role in controlling the amplitude of the response to seasonal forcing, at least in the mid-latitudes. Neither model has an explicit representation of the PBL so the role of different PBL formulations cannot be assessed with such an experiment.

5.3.2 Effect of resolution on peak values

We have already noted that the maximum surface fossil values and particularly the maximum peak-to-peak amplitudes varied even more widely than most other fields. It appears that this is highly resolution dependent; the more highly resolved a model the higher its peak values. This appears to hold for both vertical and horizontal resolution.

For vertical resolution the case is reasonably obvious for the ptp amplitudes at least. The supplied sources are specified in terms of tracer mass so if these are injected into a thinner layer (smaller volume) the resulting concentration fluctuations will be larger. This is confirmed by Taguchi (pers. comm.) who, in a companion experiment to his TRANSCOM case increased the thickness of his planetary boundary layer by 50 hPa. His ptp amplitudes decreased considerably.

For horizontal resolution the case is less clear. The differences caused by resolution are as likely to be a result of different aggregations of the sources and outputs as effects on the dynamical behaviour of the model. To test this we aggregated one of the higher resolution models (GFDL) which had the highest peak values onto the GISS grid. The resultant map (Fig. 5.1), while still showing more structure than the GISS model was much less of an outlier. It is worth noting here that the selection of observing sites to represent large-scale conditions will tend to make their observations resemble more closely those of low resolution models.

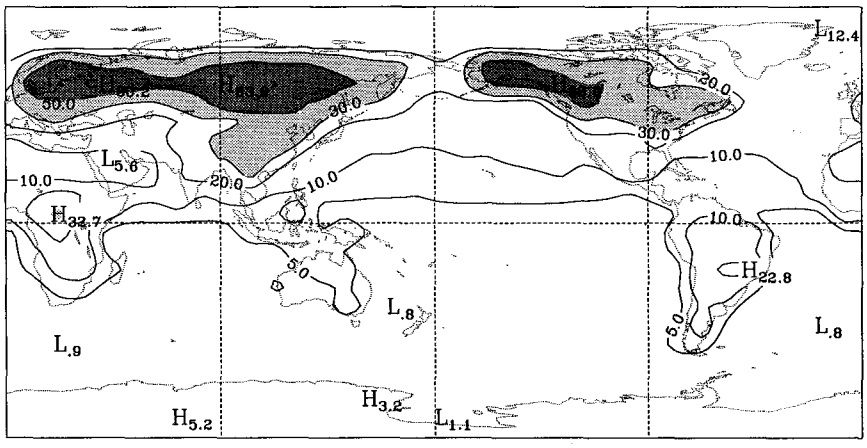

Fig 5.1: Surface peak to peak amplitude for the GFDL model aggregated onto the GISS $8 \times 10°$ grid. The contours are 5, 10, 20, 30, 50, 75 and 100 ppmv and values greater than 30 and 50 ppmv are shaded in light and dark grey respectively.

5.4 Implications for carbon budgets

It is worth relating the differences in large-scale horizontal exchange rates evident in Table 5.1 to carbon budgets derived from such models. At the simplest and broadest level we can write a first order two box model such as

$$\frac{\partial Q_n}{\partial t} = S_n - \frac{Q_n - Q_s}{\tau}$$
$$\frac{\partial Q_s}{\partial t} = S_s - \frac{Q_s - Q_n}{\tau}$$

where Q refers to mixing ratios, S to sources, τ is the exchange time and the subscripts refer to northern and southern hemisphere.

Differencing these two equations and assuming steady state yields

$$S_- = \frac{2Q_-}{\tau}$$

where the subscript refers to interhemispheric differences.

Since the measured concentrations are at the surface, the mixing ratios and exchange times are those for the surface boxes. Calculating τ from the fossil experiment as enumerated in Table 5.1 and then applying the range of values to a nominal observed IHD of 2 ppmv gives a range in the distribution of the net source of 1.9–3.8 $GtCyr^{-1}$. This represents an extra uncertainty in the difference in sources between hemispheres so that for each hemisphere separately there is an uncertainty of ± 0.5 $GtCyr^{-1}$. This is comparable to the uncertainties quoted in Schimel et al. (1995). This result gives further weight to the finding of Enting et al. (1995) who noted that the spatial structure of CO_2 was not a strong constraint on global carbon fluxes in their synthesis inversion. The spatial structure enters their calculation through the use of a tracer transport model. They propagate uncertainties in concentration measurements to uncertainties in source estimates. The extra uncertainty due to model error would further weaken the constraint.

5.5 Reducing uncertainties

Given the large range of model results displayed in the previous sections and the implications for inversions suggested above it is clear that some effort should be made to reduce the uncertainty associated with transport. Three reasonably clear and non-exclusive paths appear to lead in this direction.

The first, and most problematic, is to look for those elements on which models generally agree and weight the results of other models less heavily. Considering the fossil fuel results, and taking the surface interhemispheric exchange time (column 1 of Table 5.1) as a guide we see that the GFDL and CSIRO9 results lie some distance from the other models. These two models also have a large ratio of surface to three-dimensional exchange times suggesting weaker vertical transport than most other models. This suggestion is supported by the large vertical gradients in the lower troposphere for both experiments in these two models. (For GFDL this seems to involve mainly strong trapping near the surface while for CSIRO9 the weak vertical transport extends through more of the troposphere.) By removing these two models from the range, the spread of exchange times is cut by half. The GISS result, from a model calibrated against other tracers, lies at the centre of the range of the reduced set of results.

Consensus is less clear for the biosphere experiment although the spread of annual mean gradients (Fig. 4.6) makes it equally important to narrow the range for this quantity. One model, ANU, has a gradient opposite in sign to the others. Taylor (pers. comm.) has pointed out that this result depends strongly on the source of winds and vertical resolution used to drive the model, with the gradient changing sign when ECMWF winds from the 1990s with higher vertical resolution are used rather than from 1980 in TRANSCOM. For the other models we have already noted the tendency of GFDL and CSIRO9 to trap signals at low levels. Removing these two models leaves an interesting grouping with CSU, NIRE and NCAR producing large gradients and the remaining models producing small gradients. The three models with high gradients all have some explicit formulation of the PBL. This strongly supports the contention of Denning et al. (1995) that the PBL has an important influence on CO_2 surface concentrations from diurnal to annual time scales. It suggests the possibility that the annual mean response of surface CO_2 concentrations in the real atmosphere to a source with the seasonality of the terrestrial biosphere may be towards the high end of the TRANSCOM range.

A less arbitrary approach than establishing consensus is model calibration. This involves the use of tracers with relatively well-known distributions and net sources so that the performance of models can be assessed. Such calibrations should usually be part of the development of a tracer model e.g. Jacob et al. (1987), Prather et al. (1987), Heimann et al. (1989). The species most commonly used have been CFCs and krypton-85 to evaluate interhemispheric exchange and radon to evaluate vertical transport, particularly on the sub-grid scale.

Accurate simulation of both vertical and horizontal transport is necessary for realistic tracer transport. The different properties of the species needed for calibration of each process mean that quite separate experiments with different tracers are required. For the large-scale horizontal transport no species yet fits the three requirements of well known distribution, well known sources and little involvement in complicating chemistry to make it ideally suited for model calibration. The most common choice has been CFCs. There has been a previous comparison of the performance of tracer transport models using various CFC species (Prather, 1992). Prather's work exposed some of the difficulties in using CFCs for

such model calibrations. Firstly it is difficult to deduce a concentration structure which can be easily compared with model output. This is principally because emissions have changed too rapidly to allow equilibrium experiments such as those in TRANSCOM. Prather used a single year of data meaning the experiment required a specified initial condition. Thus, while Prather could compare the synoptic performance of the various models in that comparison, the large-scale and long-term aspects of transport of interest to us were harder to assess. Along with this problem of choosing appropriate data, the CFCs suffer from considerable uncertainty in source strength (e.g. Fisher and Midgley, 1994).

Alternatives are krypton-85 and SF_6 but these are not without there own problems. Krypton has only been sporadically sampled, e.g. Weiss et al. (1983). It also has significant source uncertainty which can be partly reduced by the attribution of the residual in the global inventory to Soviet under-reporting

There is, as yet, no global, intercalibrated network of SF_6 measurements. The species is amenable to precise measurement, e.g. Maiss and Levin (1994) which should provide a strong constraint on the atmospheric inventory. Given the long lifetime of SF_6 the trend in this inventory is a good surrogate for global release. It is more difficult to define the spatial structure of the source which may limit the utility of SF_6 for atmospheric transport calibration. Overall, SF_6 may provide a useful extra constraint although not with the current database of measurements. The use of archival air from sites originally intended for sampling other trace species provides one immediate extension to this sparse measurement set.

Even if the large-scale horizontal transport can be well constrained with calibration tracers, the experiments with the MUTM-CSIRO9 hybrid model mentioned in Section 5.3 suggest this is only half the problem. Fixing the large-scale wind reduced the surface difference by half, the other half is presumably due to differences in vertical processes where sub-grid scale transport plays a major role. The common choice for a calibration tracer for these vertical processes has been radon (e.g. Jacob and Prather, 1990). Radon is emitted from land surfaces and has a relatively short half-life of 3.8 days. An intercomparison of 20 two and three-dimensional model simulations of radon is reported by Prather et al. (1995). They find a good agreement between the 'established' 3d models but comment on the lack of observations available to test the model predictions. It would appear that a radon calibration may be useful to differentiate between some of the extreme cases of vertical transport seen in TRANSCOM but the small number of observations available and uncertainties in the source strength may limit its use in differentiating between those models with relatively similar vertical transport. Also, the scarcity of climatological vertical profiles of radon makes it difficult to calibrate those models not driven by analyzed winds.

Finally, whatever calibration exercise is chosen, there is a need to develop the formalism for the calculation of transport parameters and model error from such calibration experiments. Enting (1985) outlined one strategy for estimating such parameters in a two-dimensional tracer transport model. For model error the case is more difficult. While systematic error is easily calculated, the more comprehensive model statistics needed for introducing model uncertainty into inverse calculations cannot yet be feasibly calculated. This problem could possibly use some of the techniques developed for numerical weather prediction data assimilation.

The other approach to increasing confidence in transport estimates is to isolate and verify those aspects of model performance most influential on CO_2 transport. The discussion of Section 5.3 indicates a start on this kind of work using models locally available to the authors. Other such recent calculations are those of Taguchi (1994).

6 Conclusions

We have performed an intercomparison of various atmospheric tracer transport models used in CO_2 budget studies. We examined the modelled concentrations resulting from input of representations of the fossil fuel and terrestrial biota sources. The main conclusions can be summarized as follows

- There is a large range in the efficiency of transport among the models, with simple measures of transport efficiency varying by a factor of two for large-scale horizontal transport and a factor of five for vertical transport. This range can be significantly reduced by removing a few outlier responses but no one model lies at the extremes in all aspects.
- The large-scale horizontal wind is the dominant influence on vertically integrated transport in the annual mean while column physics controls the amplitude of the response to seasonal sources.
- The representation of the planetary boundary layer plays an important role in controlling the magnitude of the mean response to the terrestrial biotic source.
- The uncertainties in regional carbon budgets caused by the differences in the transport characteristics of various models may be as large as any other uncertainty in these budgets.

Acknowledgements

This study was carried out with support from the Australian Government Cooperative Research Centres Programme. The authors thank I. Enting, T. Hall, P. Monfray and all the model contributors for many constructive comments on the manuscript. P. Rayner wishes to thank the Program in Atmospheric and Oceanic Sciences at Princeton University for support in the early stages of TRANSCOM.

References

Ciais, P., P.P. Tans, J.W.C. White, M. Trolier, R.J. Francey, J.A. Berry, D.R. Randall, P.J. Sellers, J.G. Collatz and D.S. Schimel, 1995: Partitioning of ocean and land uptake of CO_2 as inferred by $\delta^{13}C$ measurements from the NOAA Climate Monitoring and Diagnostics Laboratory Global Air Sampling Network. *J. Geophys. Res.*, **100**, 5051-5070.

Conway, T.J., P.P. Tans, L.S. Waterman, K.W. Thoning, D.R. Kitzis, K.A. Masarie and N. Zhang, 1994: Evidence for interannual variability of the carbon cycle from the National Oceanic and Atmospheric Administration/Climate Monitoring and Diagnostics Laboratory Global Air Sampling Network. *J. Geophys. Res.*, **99**, 22831-22855.

Denning, A.S., I.Y. Fung and D.A. Randall, 1995: Gradient of Atmospheric CO_2 due to Seasonal Exchange with Land Biota. *Nature*, **376**, 220-223.

Enting, I.G., and J.V. Mansbridge, 1989: Seasonal sources and sinks of atmospheric CO_2 : Direct inversion of filtered data. *Tellus*, **41B**, 111-126.

Enting, I.G., and J.V. Mansbridge, 1991: Latitudinal distribution of sources and sinks of CO_2: Results of an inversion study. *Tellus*, **43B**, 156-170.

Enting, I.G., C.M. Trudinger, R.J. Francey and H. Granek, 1993: Synthesis Inversion of Atmospheric CO_2 Using the GISS Tracer Transport Model. CSIRO Div. Atmos. Res. Tech. Paper No. 29, 44pp.

Enting, I.G., C.M. Trudinger and R.J. Francey, 1995: A synthesis inversion of the concentration and $\delta^{13}C$ of atmospheric CO_2. *Tellus*, **47B**, 35-52.

Enting, I.G., 1985: A Strategy for Calibrating Atmospheric Transport Models. CSIRO Div. Atmos. Res. Tech. Paper No. 9, 44pp.

Fisher, D.A., and P.M. Midgley, 1994: Uncertainties in the calculation of atmospheric releases of chlorofluorocarbons. *J. Geophys. Res.*, **99**, 16643-16650.

Fung, I., K. Prentice, E. Matthews, J. Lerner and G. Russell, 1983: Three-dimensional tracer model study of atmospheric CO_2 : response to seasonal exchanges with the terrestrial biosphere. *J. Geophys. Res.*, **88**, 1281-1294.

Fung, I.Y., C.J. Tucker and K.C. Prentice, 1987: Application of Advanced Very High Resolution Radiometer Vegetation Index to Study Atmosphere-Biosphere Exchange of CO_2. *J. Geophys. Res.*, **92**, 2999-3015.

Heimann, M., and C.D. Keeling, 1989: A Three-dimensional Model of Atmospheric CO_2 transport based on observed winds: 2. Model description and simulated tracer experiments. *Aspects of climate variability in the Pacific and the Western Americas, Geophysical Monograph 55*, D. Peterson Ed., AGU, Washington (USA), 237-275.

Heimann, M., C.D. Keeling and C.J. Tucker, 1989: A Three-dimensional Model of Atmospheric CO_2 transport based on observed winds: 3. Seasonal cycle and synoptic time scale variations. *Aspects of climate variability in the Pacific and the Western Americas, Geophysical Monograph 55*, D. Peterson Ed., AGU, Washington (USA), 277-303.

Jacob, D.J., and M.J. Prather, 1990: Radon-222 as a test of convective transport in a general circulation model. *Tellus*, **42B**, 118-134.

Jacob, D.J., M.J. Prather, S.C. Wofsy and M.B. McElroy, 1987: Atmospheric Distribution of ^{85}Kr Simulated With a General Circulation Model. *J. Geophys. Res.*, **92**, 6614-6626.

Keeling, C.D., S.C. Piper and M. Heimann, 1989: A Three-dimensional Model of Atmospheric CO_2 transport based on observed winds: 4. Mean annual gradients and interannual variations. *Aspects of climate variability in the Pacific and the Western Americas, Geophysical Monograph 55*, D. Peterson Ed., AGU, Washington (USA), 305-363.

Keeling, C.D., T.P. Whorf, M. Wahlen and J. van der Plicht, 1995: Interannual extremes in the rate of rise of atmospheric carbon dioxide since 1980. *Nature*, **375**, 666-670.

Law, R., I. Simmonds and W.F. Budd, 1992: Application of an atmospheric tracer model to the high southern latitudes. *Tellus*, **44B**, 358-370.

Maiss, M., and I. Levin, 1994: Global increase of SF_6 Observed in the Atmosphere. *Geophys. Res. Let.*, **21**, 569-572.

Marland, G., T.A. Boden, R.C. Griffin, S.F. Huang, P. Kanciruk and T.R. Nelson, 1989: Estimates of CO_2 emissions from fossil fuel burning and cement manufacturing, based on the U.S. Bureau of Mines cement manufacturing data. ORNL/CDIAC-25, NDP-030, Carbon Dioxide Information Analysis Center, Oak Ridge National Laboratory.

Nakazawa, T., K. Miyashita, S. Aoki and M. Tanaka, 1991: Temporal and spatial variations of upper tropospheric and lower stratospheric carbon dioxide. *Tellus*, **43B**, 106-117.

Plumb, R.A., and J.D. Mahlman, 1987: The zonally averaged transport characteristics of the GFDL general circulation/transport model. *J. Atmos. Sci.*, **44**, 298-327.

Prather, M., M. McElroy, S. Wofsy, G. Russell and D. Rind, 1987: Chemistry of the Global Troposphere: Fluorocarbons as Tracers of Air Motion. *J. Geophys. Res.*, **92**, 6579-6613.

Prather, M., R. Derwent, D. Ehhalt, P. Fraser, E. Sanhueza and X. Zhou, 1995: Other Tracer Gases and Atmospheric Chemistry. *Climate Change 1994: Radiative Forcing of Climate Change and An Evaluation of the IPCC IS92 Emission Scenarios*, J. Houghton, L. M. Filho, J. Bruce, H. Lee, B. Callander, E. Haites, N. Harris and K. Maskell Eds., Cambridge University Press, 73-126.

Prather, M.J. Ed.., 1992: *WCRP Workshop on Long-Range Transport of Trace Gases; 1990, Bermuda. Special Numerical Experiment: Simulation of CFC13 as a Test for 3-D Atmospheric Models*, Vol. 1V. Dept. of Geoscience, University of California, Irvine.

Rood, R.B., 1987: Numerical Advection Algorithms and Their Role in Atmospheric Transport and Chemistry Models. *Rev. Geophys.*, **25**, 71-100.

Russell, G.L., and J.A. Lerner, 1981: A new finite-differencing scheme for the tracer transport equation. *J. App. Meteor.*, **20**, 1483-1498.

Schimel, D., I. Enting, M. Heimann, T. Wigley, D. Raynaud, D. Alves and U. Siegenthaler, 1995: CO_2 and the Carbon Cycle. *Climate Change 1994: Radiative Forcing of Climate Change and An Evaluation of the IPCC IS92 Emission Scenarios*, J. Houghton, L. M. Filho, J. Bruce, H. Lee, B. Callander, E. Haites, N. Harris and K. Maskell Eds., Cambridge University Press, 35-71.

Taguchi, S., 1994: Cross-Tropical Trajectories in the Troposphere. *J. Meteor. Soc. Japan*, **72**, 531-553.

Takahashi, T., J. Olafsson, J.G. Goddard, D.W. Chipman and S.C. Sutherland, 1993: Seasonal variations of CO_2 and nutrients in the high-latitude surface oceans: a comparative study. *Glob. Biogeochem. Cyc.*, **7**, 843-878.

Tans, P.P., T.J. Conway and T. Nakazawa, 1989: Latitudinal Distribution of the Sources and Sinks of Atmospheric Carbon Dioxide Derived From Surface Observations and an Atmospheric Transport Model. *J. Geophys. Res.*, **94**, 5151-5172.

Tans, P.P., I.Y. Fung and T. Takahashi, 1990: Observational constraints on the global atmospheric CO_2 budget. *Science*, **247**, 1431-1438.

Taylor, J.A., 1989: A stochastic Lagrangian atmospheric transport model to determine global CO_2 sources and sinks - a preliminary discussion. *Tellus*, **41B**, 272-285.

Weiss, W., A. Sittkus, H. Stockburger, H. Sartorius and K.O. Münnich, 1983: Large-Scale Atmospheric Mixing Derived from Meridional Profiles of Krypton 85. *J. Geophys. Res.*, **88**, 8574-8578.

Wofsy, S.C., M.L. Goulden, J.W. Munger, S.-M. Fan, P.S. Bakwin, B.C. Daube, S.L. Bassow and F.A. Bazzaz, 1993: Net exchange of CO_2 in a mid-latitude forest. *Science*, **260**, 1314-1317.

A Experimental and data specification

This section contains the experimental specification distributed to the contributing modellers.

A.1 Experiment 1: fossil case

Input is Fung's gridded fossil source interpolated to model grid. The time invariant source is input to the lowest model layer. The input file may be found in the TRANSCOM archive in the 'inputs' directory, file co2ems.dat. It is described in the file read.me in that directory. Note that the units of the sources are $kgCm^{-2}yr^{-1}$.

The model should be run for at least four years with data collected from the fourth year or later.

A.1.1 Required output

Returned data should be in four parts; description, sources, plan fields and cross-sections.

The description should include a brief description of the model used including details such as resolution and any particular features which may strongly impact tracer transport performance. Examples would include explicit boundary layer formulation, Lagrangian transport etc. The description should also include any variation from the experimental protocol used by the particular group. This would include aspects such as multi-year averages in the output etc. Finally the normalization used for both experiments should be included. This is the average mixing ratio through the whole atmosphere for the month of January for the supplied year.

The returned sources should be those actually seen by the model. Note that in a spectral model this means they will be smoother than gridded fields at the resolution implied by the model grid. The format of the files for this field is described under data formats. The units for the sources should be $gCm^{-2}yr^{-1}$(note carbon not CO_2).

The plan fields consist of gridded fields for monthly mean mixing ratio at the surface, 500 hPa and 200 hPa (36 datasets in all). Units are parts per million by volume (ppmv). The surface should generally be taken as the lowest model level unless an explicit boundary layer formulation allows boundary layer values to be returned. The free atmosphere levels should be interpolated from the models' vertical coordinates to pressure surfaces and the special value 99999.9 should be used where topography interrupts the pressure surface. The horizontal grid of the provided model output should be at least regular in longitude and, where possible, should be the grid used by the model.

The data should be normalized by subtracting the monthly mean, global mean mixing ratio for January. This normalization is to correct for drift in mixing ratio due to slightly different source strengths, different starting and archiving times and differences in mass conservation.

Cross-sections should consist of monthly mean zonal mean mixing ratio in ppmv at each model level. These data should be normalized in the same way as the plan fields.

A.2 Experiment 2: vegetation case

Input is the monthly mean 5x4 degree gridded net vegetation exchange from Fung et al. (1987). The source is to be taken as representing mid-monthly values and interpolated linearly

in time between adjacent months. The gridded sources may be found in the 'inputs' directory in the TRANSCOM archive; files 'co2veg.jan', 'co2veg.feb' ... 'co2veg.dec'. These files are described in file 'co2fung.help' in the same directory. Note that the units for these sources are currently $kgCm^{-2}s^{-1}$ and the numbers have been multiplied by 10^{10} in the file. The model should be run for at least four years with data collected from the fourth year or later.

The required fields are as for experiment 1. The normalization is as for experiment 1.

A.3 Data format

Plan fields should be provided in the following format

record no.	contents	comment
1	nlats	number of latitudes
2	lats(i),i=1,nlats	list of latitudes (increasing)
3	nlons	number of longitudes
4	lons(i),i=1,nlons	list of longitudes (increasing)
5	head	80 character heading
6	field(i,j),i=1,nlons,j=1,nlats	data stored by latitude in same order as lat and lon lists

Data may be provided in either formatted or unformatted form. If unformatted the data should be readable by a routine such as the provided 'getmap.f' in the 'routines' directory of the TRANSCOM archive. These files can be read directly on, at least, Sun and SGI workstations and on a Cray with the -F f77.nonvax -N ieee options to the 'assign' statement. The routine 'putmap.f' will produce a file in the correct format. 'fgetmap.f' and 'fputmap.f' are equivalent routines for formatted data for those using machines with incompatible unformatted file structures.

Cross sections are in a similar form.

record no.	contents	comment
1	nlats	number of latitudes
2	lats(i),i=1,nlats	list of latitudes (increasing)
3	nlevs	number of levels
4	levs(i),i=1,nlevs	list of levels (increasing)
5	head	80 character heading
6	field(k,j),k=1,nlevs,j=1,nlats	data stored by latitude in same order as lat and lev lists

These fields can be read and written with the same routines as for plan fields substituting level for longitude.

B Data access

All the submitted data for TRANSCOM have been made available by the contributing modellers and are centrally archived. The archive is stored in a privately accessible ftp area. Access details are available from the authors, contact pjr@dar.csiro.au by electronic mail.

A larger subset of the results as well as a document based on this report is available on the World-Wide Web at Universal Resource Locator

http://www.monash.edu.au/met/research/programb/transcom.html

On the ftp area, results for each modeller are archived by user-id under a results directory. A README directory in the results area explains the mapping between user names and models.

The routines mentioned in Appendix A are available in a routines directory from the main area. Electronic copies of this report and other results arising from the project are available in the text subdirectory and the figures on the WWW pages are available directly from the figures subdirectory.

C Model descriptions and contact information

ANU

CONTACT

Modeller	J.A. Taylor
Address	Centre for Resource and Environmental Studies Australian National University Canberra ACT 0200 Australia Phone: +61 6 249 2635 Fax : +61 6 249 0757 Email: taylorj@cres.anu.edu.au

MODEL HISTORY

Author	J.A. Taylor
Institution	Australian National University
Citation	Taylor, J.A., 1989: A stochastic Lagrangian atmospheric transport model to determine global CO_2 sources and sinks - a preliminary discussion. Tellus, 41B, 272-285.

MODEL DETAILS

Type	Offline
Horizontal resolution	2.5 degree
Vertical resolution	7 pressure levels
Timestep	Variable (set at 24 hours for TRANSCOM)
Advection scheme	Lagrangian
Subgrid processes	Vertical mixing
Wind data source	European Centre for Medium-range Weather Forecasting, 1980 analyses
Wind frequency	Data have been reduced to bimonthy means and variances

EXPERIMENT DETAILS

Year submitted	5
Normalisation	Fossil 360.0, biosphere 350.2

CSIRO9

CONTACT

Modeller Ian Watterson
Address CSIRO Division of Atmospheric Research
Private Bag No. 1
Mordialloc
Victoria 3195
Australia
Phone: + 61 3 9239 4544
Fax: +61 3 9239 4444
Email: igw@dar.csiro.au

MODEL HISTORY

Authors H.B. Gordon, J.L. McGregor, M.R. Dix, I.G. Watterson, L.D. Rotstayn
Institution CSIRO Division of Atmospheric Research
Citation Watterson I.G., Dix M.R., Gordon H.B., McGregor J.L. (1995) The CSIRO 9-level atmospheric general circulation model and its equilibrium present and doubled CO_2 climates. Aust. Meteorol. Mag. (in press)

MODEL DETAILS

Type Online
Horizontal Resolution R21, 5.625°long, 3.2°lat
Vertical Resolution 9 sigma levels
Timestep 30 minutes
Advection Scheme Semi-lagrangian
Subgrid processes Cumulus and shallow convection
Stability dependent vertical diffusion
Boundary layer mixing

EXPERIMENT DETAILS

Year submitted 3-12 average
Normalisation Fossil 15.41, biosphere 0.2623

CSU

CONTACT

Modeller A. Scott Denning
Contact Department of Atmospheric Science
Colorado State University
Fort Collins
CO 80523-1371
USA
Phone: +1 970 491 2134
Fax: +1 970 491 8428
Email: scott@abyss.atmos.colostate.edu

MODEL HISTORY

Authors D.A. Randall and A.S. Denning
Institution Dept. of Atmospheric Science, Colorado State University
Citations Denning, A. S., I. Y. Fung, and D. A. Randall, 1995: Latitudinal gradient of atmospheric CO_2 due to seasonal exchange with land biota. Nature, 376, 240-243

Denning, A. S., 1994: Investigations of the transport, sources, and sinks of atmospheric CO_2 using a general circulation model. Atmospheric Science Paper 564, Colorado State University, Fort Collins, CO 80523-1371, USA.

MODEL DETAILS

Type Online
Horizontal Resolution 5°lon × 4°lat
Vertical Resolution 17 sigma levels
Timestep 6 minutes
Advection Scheme 2nd order finite-difference
Subgrid processes Prognostic PBL depth and turbulence kinetic energy
Dry and cumulus convection

EXPERIMENT DETAILS

Year submitted 4 (after 10 years low resolution initialisation)
Normalisation Fossil 359.14, biosphere 350.16

GFDL

CONTACT

Modeller	Peter Rayner
Address	CSIRO Division for Atmospheric Research Private Bag No. 1 Mordialloc Victoria 3195 Australia Phone: + 61 3 9239 4563 Fax: +61 3 9239 4444 Email: pjr@dar.csiro.au

MODEL HISTORY

Authors	J.D. Mahlman and W.J. Moxim
Institution	Geophysical Fluid Dynamics Laboratory
Citation	Mahlman, J.D. and W.J. Moxim, 1978: Tracer Simulation Using a Global General Circulation Model: Results from a Midlatitude Instantaneous Source Experiment. J. Atmos. Sci., 35, 1340-1374.

MODEL DETAILS

Type	Offline
Horizontal resolution	265 km
Vertical resolution	11 sigma
Timestep	26 min
Advection scheme	2nd order horizontal, 4th order vertical
Subgrid processes	horizontal and vertical diffusion + extra vertical keyed on precipitation to simulate convection
Wind data source	GFDL Zodiac model
Wind frequency	6 hours

EXPERIMENT DETAILS

Year submitted	3.5 (run started on Oct 1)
Normalisation	Fossil 355.66, biosphere 351.37

GISS

CONTACT

Modeller Cathy Trudinger
Address CSIRO Division of Atmospheric Research
Private Bag No. 1
Mordialloc
Victoria 3195
Australia
Phone: + 61 3 9239 4593
Fax: +61 3 9239 4444
Email: cxt@dar.csiro.au

MODEL HISTORY

Authors I.Y. Fung
Institution Goddard Institute for Space Studies
Citation Fung I., K. Prentice, E. Matthews, J. Lerner, G. Russell, 1983. Three-dimensional tracer model study of atmospheric CO_2: Response to seasonal exchanges with the terrestrial biosphere, J. Geophys. Res., 88, 1281-1294

MODEL DETAILS

Type Offline
Horizontal Resolution 8°lat, 10°long
Vertical Resolution 9 sigma levels
Timestep 4 hours
Advection Scheme Slopes scheme (Russell and Lerner, 1981)
Subgrid processes Convection
Horizontal diffusion
Wind data source GISS GCM
Wind frequency 4 hours

EXPERIMENT DETAILS

Year submitted 4
Normalisation Fossil 7.633, biosphere 0.171

MUGCM

CONTACT

Modeller Rachel Law
Contact CRC for Southern Hemisphere Meteorology
Monash University
Wellington Rd
Clayton
Victoria 3168
Australia
Phone: +61 3 9905 9660
Fax : +61 3 9905 9689
Email: rml@vortex.shm.monash.edu.au

MODEL HISTORY

Authors I. Simmonds and others, tracer code R. Law
Institution University of Melbourne
Citation Simmonds, I., G. Trigg, R. Law, 1988: The climatology of the Melbourne University General Circulation Model. Pub No. 31, Department of Meteorology, University of Melbourne, 67pp. [NTIS PB 88 22749]

MODEL DETAILS

Type Online
Horizontal resolution R21, 5.625°long, approx. 3.3°lat
Vertical resolution 9 sigma
Timestep 15 min
Advection scheme Spectral
Subgrid processes Convection
Vertical diffusion (lowest 4 layers only)
Horizontal diffusion

EXPERIMENT DETAILS

Year submitted 3
Normalisation Fossil 4.971, biosphere 0.220
Note Biosphere sources were fixed throughout month

MUTM

CONTACT

Modeller	Rachel Law
Address	CRC for Southern Hemisphere Meteorology Monash University Wellington Rd Clayton Victoria 3168 Australia Phone: +61 3 9905 9660 Fax : +61 3 9905 9689 Email: rml@vortex.shm.monash.edu.au

MODEL HISTORY

Authors	R. Law
Institution	University of Melbourne / CRC for Southern Hemisphere Meteorology
Citation	Law, R., I. Simmonds and W.F. Budd, 1992: Application of an atmospheric tracer model to the high southern latitudes. Tellus, 44B, 358-370.

MODEL DETAILS

Type	Offline
Horizontal resolution	R21, 5.625°long, approx. 3.3°lat
Vertical resolution	9 sigma
Timestep	15 min
Advection scheme	Spectral
Subgrid processes	Convection based on daily statistics Vertical diffusion (lowest 4 layers only) Horizontal diffusion
Wind data source	Melbourne University GCM
Wind frequency	Daily (no diurnal cycle)

EXPERIMENT DETAILS

Year submitted	4
Normalisation	Fossil 7.402, biosphere 0.239
Note	Biosphere sources were fixed throughout month

NCAR

CONTACT

Modeller	David Erickson
Contact	NCAR P.O. Box 3000, Boulder, CO 80307 USA Phone: +1 303 497 1424 Fax: +1 303 497 1400 email: erickson@ucar.edu

MODEL HISTORY

Authors	David Erickson
Institution	National Center for Atmospheric Research
Citation	Erickson, D.J., P.J. Rasch, P.P Tans, P. Friedlingstein, P. Ciais, G.P. Brasseur, E. Maier-Reimer, K. Six, C.A. Fischer and S. Walters: The seasonal cycle of atmospheric CO2: A study based on the NCAR Community Climate Model (CCM2). (Submitted to JGR).

MODEL DETAILS

Type	Online (CCM2)
Horizontal resolution	T42, 2.8° × 2.8°
Vertical resolution	18 sigma levels
Timestep	15 min
Advection scheme	Semi-lagrangian
Subgrid processes	Convection Vertical diffusion PBL

EXPERIMENT DETAILS

Year submitted	5

NIRE

CONTACT

Modeller	Shoichi Taguchi
Address	CSIRO Division of Atmospheric Research Private Bag No. 1 Mordialloc Victoria 3195 Australia Phone: +61 3 9239 4585 Fax: +61 3 9239 4444 Email: sxt@dar.csiro.au
From February 1997	National Institute for Resources and Environment Environmental Assessment Division 16-3, Onogawa Tsukuba Ibaraki 305 Japan Phone: +81 298 58 8384 Fax: +81 298 58 8358 Email: p1871@nire.go.jp

MODEL HISTORY

Authors	Shoichi Taguchi
Institution	National Institute for Resources and Environment
Citation	Taguchi, S.: A three-dimensional model of atmospheric CO_2 transport based on observed winds: Model description and simulation results for TRANSCOM. (submitted to JGR)

MODEL DETAILS

Type	Offline
Horizontal resolution	2.5°
Vertical resolution	15 sigma
Timestep	6 hours (interpolation of winds at each 30 minutes to get departure point for semi-Lagrangian scheme)
Advection scheme	Semi-lagrangian
Subgrid processes	Linear interpolation among grids, Uniform mixing ratio in the planetary boundary layer estimated by bulk-Richardson number at each grid point
Wind data source	European Centre for Medium-range Weather Forecasting, TOGA/ADVANCED 1992 analyses
Wind frequency	6 hours

EXPERIMENT DETAILS

Year submitted	Fossil 2, biosphere 5
Normalisation	Fossil 352.584, biosphere 350.043

TM1

CONTACT

Modeller Stephen C. Piper
Contact Scripps Institution of Oceanography A-020
La Jolla,
CA 92093-0220
USA
Phone: +1 619 534 4230 ext. 12
Email: scpiper@ucsd.edu

MODEL HISTORY

Authors M. Heimann and C.D. Keeling
Institution Max Planck Institut für Meteorologie, Hamburg and Scripps Institution of Oceanography
Citations Heimann, M. and C.D. Keeling, 1989: A three-dimensional model of atmospheric CO_2 transport based on observed winds: 2. Model description and simulated tracer experiments, in D.H. Peterson, ed., Aspects of Climate Variability in the Pacific and Western Americas, Geophysical Monograph No. 55, American Geophysical Union, Washington, D.C.,237-275.
Keeling, C.D., S.C. Piper, and M. Heimann, 1989: A three-dimensional model of atmospheric CO_2 transport based on observed winds: 4. Mean annual gradients and interannual variations, in D.H. Peterson (Ed.), Aspects of Climate Variability in the Pacific and Western Americas, Geophysical Monograph No. 55, American Geophysical Union, Washington, D.C.,305-363.

MODEL DETAILS

Type Offline
Horizontal resolution 7.83°lat (3.91°at poles) by 10°long
Vertical resolution 9 sigma layers (surface layer averages 400 m thick)
Timestep 240 minutes
Advection scheme Slopes scheme (Russell and Lerner 1981)
Subgrid processes Monthly-averaged vertical convection and horizontal diffusion from GISS GCM
Wind data source ECMWF (Global Weather Experiment period, Dec 1978-Nov 1979)
Wind frequency 720 minutes

EXPERIMENT DETAILS

Year submitted 4
Normalisation Fossil 7.885, biosphere 0.468

TM2

CONTACT

Modeller	Martin Heimann
Address	Max Planck Institut für Meteorologie Bundesstrasse 55 D-20146 Hamburg Germany Phone: +49 40 41173 240/293 Fax: +49 40 41173 293/298 Email: heimann@dkrz.d400.de

MODEL HISTORY

Authors	M. Heimann
Institution	Max Planck Institut für Meteorologie
Note	The TM2 tracer model originated from the tracer model code developed at the Goddard Institute for Space Studies (Russell and Lerner, 1981). This original model was based on the meteorology and monthly vertical convection statistics of the GISS general circulation climate model. A revised model version, TM1, included the preprocessing packages for arbitrary meteorological fields (Heimann and Keeling, 1989). The present version, TM2, represents a largely rewritten code with additional new packages for the calculation of the subgridscale vertical transport by convective clouds and turbulent diffusion.
Citations	Heimann, M., 1995. The global atmospheric tracer model TM2. Technical Report No. 10, Deutsches Klimarechenzentrum, Hamburg, Germany (ISSN 0940-9327), 51pp. Rehfeld, S. and M. Heimann, 1995. Three-dimensional atmospheric transport simulation of the radioactive tracers ^{210}Pb, ^{7}Be, ^{10}Be and ^{90}Sr. J. Geophys. Res. (Atmospheres), (in press).

MODEL DETAILS

Type	Offline
Horizontal resolution	5°lon × 4°lat
Vertical resolution	9 sigma layers
Timestep	60 minutes
Advection scheme	Slopes scheme
Subgrid processes	Stability dependent vertical diffusion Simplified Tiedtke mass-flux cumulus scheme
Wind Data Source	ECMWF analyses for 1986
Wind frequency	12 hours

EXPERIMENT DETAILS

Year submitted	4
Normalisation	Fossil 7.54, biosphere 0.153

TM2Z

CONTACT

Modeller	Michel Ramonet
Address	NOAA/CMDL Carbon Cycle Group R/E/CG1 325 Broadway Boulder CO 80303 USA Phone: +1 303 497 6180 Fax: +1 303 497 6290 Email: michel@ccg2.cmdl.noaa.gov

MODEL HISTORY

Authors	M. Ramonet, P.Bousquet, M.Heimann
Institution	Centre des Faibles Radioactivites Laboratoire Mixte CNRS/CEA Avenue de la Terrasse F-91198 Gif-sur-Yvette Cedex, France
Citation	Ramonet M., Le Roulley J.C., Bousquet P., Monfray P., Radon-222 measurements during the TROPOZ II campaign and comparison with a global atmospheric transport model, J.Atm.Chem., (in press)

MODEL DETAILS

Type	Offline
Horizontal resolution	2.5° lat by 2.5° lon
Vertical resolution	9 sigma levels
Timestep	60 minutes
Advection Scheme	Slopes scheme
Subgrid Processes	Cumulus convection (Tiedtke 1989) Stability-dependent vertical diffusion (Louis 1979)
Wind data source	ECMWF analyses for 1990/1991
Wind frequency	12 hours

EXPERIMENT DETAILS

Year submitted	4
Normalisation	Fossil 7.6243
Note	The biosphere experiment was not performed. Analysis is of run with 1990 winds. 1991 winds were used for the 5th year after 4 years running with 1990 winds.

D NOAA/CMDL station locations used in Figure 4.4

Code	Station	Latitude	Longitude
ALT	Alert	82.50°N	297.67°E
AMS	Amsterdam Is	37.95°S	77.53°E
ASC	Ascension Is	7.92°S	345.59°E
AVI	St Croix	17.75°N	295.25°E
AZR	Azores	38.75°N	332.92°E
BME	Bermuda East	32.36°N	295.35°E
BRW	Barrow	71.32°N	203.40°E
CBA	Cold Bay	55.20°N	197.28°E
CGO	Cape Grim	40.68°S	144.73°E
CHR	Christmas Is	2.00°N	202.70°E
CMO	Cape Meares	45.00°N	236.00°E
GMI	Guam	13.43°N	144.78°E
HBA	Halley Bay	75.67°S	334.50°E
KEY	Key Biscayne	25.67°N	279.83°E
KUM	Kumakahi	19.52°N	205.18°E
MBC	Mould Bay	76.23°N	240.67°E
MID	Sand Is	28.22°N	182.62°E
PSA	Palmer	64.92°S	296.00°E
RPB	Ragged Point	13.16°N	300.57°E
SEY	Seychelles	4.67°S	55.17°E
SHM	Shemya	52.75°N	174.08°E
SMO	Samoa	14.25°S	189.43°E
SPO	South Pole	89.98°S	335.20°E
STM	Station M	66.00°N	2.00°E
SYO	Syowa	69.00°S	39.58°E

Technical Paper Series.
Division of Atmospheric Research, CSIRO, Australia

No. 1 Galbally, I. E.; Roy, C. R.; O'Brien, R. S.; Ridley, B. A.; Hastie, D. R.; Evans, W. J. F.; McElroy, C. T.; Kerr, J. B.; Hyson, P.; Knight, W.; Laby, J. E. *Measurements of trace composition of the Austral stratosphere: chemical and meteorological data.* 1983. 31 p.

No. 2 Enting, I. G. *Error analysis for parameter estimates from constrained inversion.* 1983. 18 p.

No. 3 Enting, I. G.; Pearman, G. I. *Refinements to a one-dimensional carbon cycle model.* 1983. 35 p.

No. 4 Francey, R. J.; Barbetti, M.; Bird, T.; Beardsmore, D.; Coupland, W.; Dolezal, J. E.; Farquhar, G. D.; Flynn, R. G.; Fraser, P. J.; Gifford, R. M.; Goodman, H. S.; Kunda, B.; McPhail, S.; Nanson, G.; Pearman, G. I.; Richards, N. G.; Sharkey, T. D.; Temple, R. B.; Weir, B. *Isotopes in tree rings.* 1984. 86 p.

No. 5 Enting, I. G. *Techniques for determining surface sources from surface observations of atmospheric constituents.* 1984. 30 p.

No. 6 Beardsmore, D. J.; Pearman, G. I.; O'Brien, R. C. *The CSIRO (Australia) Atmospheric Carbon Dioxide Monitoring Program: surface data.* 1984. 115 p.

No. 7 Scott, John C. *High speed magnetic tape interface for a microcomputer.* 1984. 17 p.

No. 8 Galbally, I. E.; Roy, C. R.; Elsworth, C. M.; Rabich, H. A. H. *The measurement of nitrogen oxide (NO, NO_2) exchange over plant/soil surfaces.* 1985. 23 p.

No. 9 Enting, I. G. *A strategy for calibrating atmospheric transport models.* 1985. 25 p.

No. 10 O'Brien, D. M. *TOVPIX: software for extraction and calibration of TOVS data from the high resolution picture transmission from TIROS-N satellites.* 1985. 41 p.

No. 11 Enting, I. G.; Mansbridge, J. V. *Description of a two-dimensional atmospheric transport model.* 1986. 22 p.

No. 12 Everett, J. R.; O'Brien, D. M.; Davis, T. J. *A report on experiments to measure average fibre diameters by optical fourier analysis.* 1986. 22 p.

No. 13 Enting, I. G. *A signal processing approach to analysing background atmospheric constituent data.* 1986. 21 p.

No. 14 Enting, I. G.; Mansbridge, J. V. *Preliminary studies with a two-dimensional model using transport fields derived from a GCM.* 1987. 47 p.

No. 15 O'Brien, D. M.; Mitchell, R. M. *Technical assessment of the joint CSIRO/Bureau of Meteorology proposal for a geostationary imager/sounder over the Australian region.* 1987. 53 p.

No. 16 Galbally, I. E.; Manins, P. C.; Ripari, L.; Bateup, R. *A numerical model of the late (ascending) stage of a nuclear fireball.* 1987. 89 p.

No. 17 Durre, A. M.; Beer, T. *Wind information prediction study: Annaburroo meteorological data analysis.* 1989. 30 p. + diskette.

No. 18 Mansbridge, J. V.; Enting, I. G. *Sensitivity studies in a two-dimensional atmospheric transport model.* 1989. 33 p.

No. 19 O'Brien, D. M.; Mitchell, R. M. *Zones of feasibility for retrieval of surface pressure from observations of absorption in the A band of oxygen.* 1989. 12 p.

No. 20 Evans, J. L. *Envisaged impacts of enhanced greenhouse warming on tropical cyclones in the Australian region.* 1990. 31 p. [Out of print]

No. 21 Whetton, P. H.; Pittock, A. B. *Australian region intercomparison of the results of some general circulation models used in enhanced greenhouse experiments.* 1991. 73 p.

[Out of print]

No. 22 Enting, I. G. *Calculating future atmospheric CO_2 concentrations.* 1991. 32 p.

No. 23 Kowalczyk, E. A.; Garratt, J. R.; Krummel, P. B. *A soil-canopy scheme for use in a numerical model of the atmosphere - 1D stand-alone model.* 1992. 56 p.

No. 24 Physick, W. L.; Noonan, J.A.; McGregor, J.L.; Hurley, P.J.; Abbs, D.J.; Manins, P.C. *LADM: A Lagrangian Atmospheric Dispersion Model.* 1994. 137 p.

No. 25 Enting, I. G. *Constraining the atmospheric carbon budget: a preliminary assessment.* 1992. 28 p.

No. 26 McGregor, J. L.; Gordon, H. B.; Watterson, I. G.; Dix, M. R.; Rotstayn, L. D. *The CSIRO 9-level atmospheric general circulation model.* 1993. 89 p.

No. 27 Enting, I. G.; Lassey, K. R. *Projections of future CO_2.* with appendix by R. A. Houghton. 1993. 42 p.

No. 28 [Not published]

No. 29 Enting, I. G.; Trudinger, C. M.; Francey, R. J.; Granek, H. *Synthesis inversion of atmospheric CO_2 using the GISS tracer transport model.* 1993. 44 p.

No. 30 O'Brien, D. M. *Radiation fluxes and cloud amounts predicted by the CSIRO nine level GCM and observed by ERBE and ISCCP.* 1993. 37 p.

No. 31 Enting, I.G.; Wigley, T.M.L.; Heimann, M. *Future emissions and concentrations of carbon dioxide: key ocean/atmosphere/land analyses.* 1994. 120 p.

No. 32 Kowalczyk, E.A.; Garratt, J.R.; Krummel, P.B. *Implementation of a soil-canopy scheme into the CSIRO GCM regional aspects of the model response.* 1994. 59 p.

No. 33 Prata, A.J. *Validation data for land surface temperature determination from satellites.* 1994. 40 p.

No. 34 Dilley, A.C.; Elsum, C.C. *Improved AVHRR data navigation using automated land feature recognition to correct a satellite orbital model.* 1994. 22 p.

No. 35 Hill, R.H.; Long, A.B. *The CSIRO dual-frequency microwave radiometer.* 1995.

Contact information

Mailing Address: CSIRO Division of Atmospheric Research
Private Bag No.1, Mordialloc, Victoria 3195, Australia

e-mail: chief@dar.csiro.au

phone: +61 3 9239 4400

fax: +61 3 9239 4444